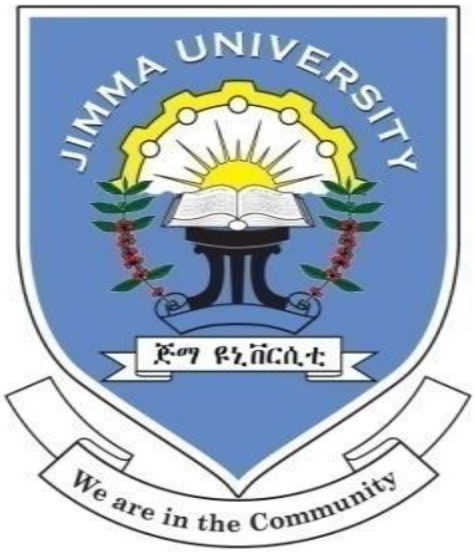

JIMMA UNIVERSITY

SCHOOL OF GRADUATE STUDIES

JIMMA INSTITUTE OF TECHNOLOGY

FACULTY OF CIVIL AND ENVIROMENTAL ENGINEERING

STRUCTURAL ENGINEERING STREAM

Non-Linear Finite Element Analysis of Circular Bamboo Fiber Tube Concrete-Filled Composite Column

A Thesis Submitted to School of Graduate Studies of Jimma University in Partial Fulfillment of the Requirements for the Degree of Masters of Science in Structural Engineering

BY:

MULETA EJETA FILATE

May, 2024

JIMMA, ETHIOPIA

JIMMA UNIVERSITY

SCHOOL OF GRADUATE STUDIES

JIMMA INSTITUTE OF TECHNOLOGY

FACULTY OF CIVIL AND ENVIROMENTAL ENGINEERING

STRUCTURAL ENGINEERING STREAM

Non-Linear Finite Element Analysis of Circular Bamboo Fiber Tube Concrete-Filled Composite Column

A Thesis Submitted to School of Graduate Studies of Jimma University in Partial Fulfillment of the Requirements for the Degree of Masters of Science in Structural Engineering

By:

MULETA EJETA

Advisor: DR. KABTAMU GETACHEW (Ph.D.)

Co-Advisor: ENG. HABTAMU GEBREMEDHIN (MSc)

May, 2024

JIMMA, ETHIOPIA

JIMMA UNIVERSITY

SCHOOL OF GRADUATE STUDIES

JIMMA INSTITUTE OF TECHNOLOGY

FACULTY OF CIVIL AND ENVIROMENTAL ENGINEERING

STRUCTURAL ENGINEERING STREAM

NON-LINEAR FINITE ELEMENT ANALYSIS OF CIRCULAR BAMBOO FIBER TUBE CONCRETE-FILLED COMPOSITE COLUMN

MULETA EJETA

APPROVED BY BOARD OF EXAMINERS

1. Dr. Kabtamu Getachew (Ph.D.).		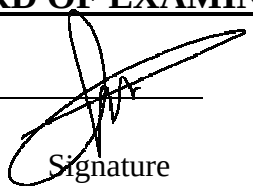	21/05/2024
Main Advisor		Signature	Date
2. Engr. Habtamu Gebremedhin (MSc.).			
Co-Advisor		Signature	Date
3. Dr. Binaya Patnaik (Ph.D.).			21/05/24
External Examiner		Signature	Date
4. Engr. Besukal Befekadu (MSc.)			
Internal Examiner		Signature	Date
5. Engr. Abinet Alemseged (MSc.)			
Chairperson		Signature	Date

DECLARATION

I declare that this Thesis entitled **"*Non-Linear Finite Element Analysis of Circular Bamboo Fiber Tube Concrete-Filled Composite Column***" is my original work and has not been submitted as a requirement for the award of any degree in Jimma University or in any other university. Where ever contribution of others is involved, every effort is made to indicate this clearly, with due reference to the pieces of literature.

Muleta Ejeta Filate	_____	_____
NAME	SIGNATURE	DATE

As research adviser, I hereby certify that I have read and evaluated this thesis paper prepared under my guidance, by Muleta Ejeta Filate entitled "***Non-Linear Finite Element Analysis of Circular Bamboo Fiber Tube Concrete-Filled Composite Column***" and recommend and would be accepted as a fulfilling requirement for the Degree Master of Science in Structural Engineering.

Dr. Kabtamu Getachew (Ph.D.).	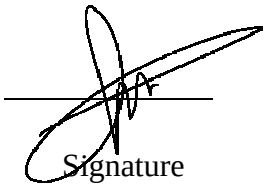	21/05/2024
Advisor	Signature	Date

Eng. Habtamu Gebremedhin (MSc)	_____	_____
Co-Advisor	Signature	Date

ABSTRACT

The structural composite construction techniques find increasingly wide applications in bridges, ramp, buildings and other different area throughout the world focusing on the composites systems. Composite structures are created by combining two or more structural elements to act as a single combined structural unit, where each element behaves in structurally efficient manner. Due to their superior confining effect, concrete-filled tube columns have been widely used in building construction. Bamboo fiber tube is suggested to replace steel and fiber-reinforced polymer tube as the confining jacket acting on concrete due to renewable material, low carbon content and economical in building construction.

The existing research on the replacement of steel tubes with bamboo fiber tubes in a concrete-filled composite column is insufficient and cannot address all behavioral aspects of the column. So, additional investigation is important to narrow this gap by adding other parameters to the bamboo fiber tube concrete-filled composite column. This study investigates the non-linear finite element analysis of bamboo fiber tube concrete-filled composite columns. The results obtained from finite element analysis were carried out and verified with the experiment results to validate the finite element analysis software known as ABAQUS 2023. The effects of the parameters investigated are eccentric loading value, bamboo fiber tube diameter, load application, and bamboo fiber tube thickness.

As a result of the parametric investigation of this study, the efficiencies of bamboo fiber tube confinement increase with an increasing eccentricity of the axial load of the bamboo fiber tube concrete-filled composite column. The axial stress capacity enhancement ratio of the bamboo fiber tube concrete-filled composite column decreases with increasing the diameter of the bamboo fiber tube. The axial load capacity of the bamboo fiber tube concrete-filled composite column increases when the load is applied to the bamboo fiber tube concrete-filled composite column compared to the core concrete column. The ductility behavior of the column increases when bamboo fiber tube thickness increases for the bamboo fiber tube concrete-filled composite column.

***Key words**: Enhancement ratio, Bamboo fiber tube, Finite element method, Axial stress capacity, ductility behavior, Eccentric loading, diameter of bamboo fiber tube.*

ACKNOWLEDGEMENT

First of all, my heartfelt thanks are extended to Almighty God for his unending helping and blessings for every success in my life and satisfactory accomplishment of this Thesis. Next, I would to express my deepest gratitude to my main advisor, **Dr. Kabtamu Getachew (Ph.D.)** and my co-advisor **Eng. Habtamu Gebremedhin (MSc.)** for their continuous support, guidance and encouragement over the past years of my master candidate and thesis performing.

My special heartfelt gratitude goes to my family and friends, for their love, support, and encouragement throughout this research and during the many years of study that preceded it. I also would like to express my thanks to my friend Hababe Mulugeta for her technical and practical supports throughout my work.

Also, my deepest gratitude goes to the Ministry of Education (MoE) and Jimma University (JU) to create this beautiful environment for me and have got the chance of this lovely education.

Finally, my special thanks go to Jimma Institute of Technology (JIT) particularly the Structural Engineering Department for facilitating this program which helps me to upgrade my knowledge and profession.

TABLE OF CONTENT

Contents **page**

LIST OF TABLES

LIST OF FIGURES

ACCRONYM

BST	Bamboo slices twining tube
BCC	Bamboo slices twining tube confined concrete
BST-5	Bamboo slices twining tube 5.8mm thickness
BST-8	Bamboo slices twining tube 9.5mm thickness
BST-10	Bamboo slices twining tube 12mm thickness
BCC-5	Bamboo slices twining tube confined concrete with 5.8mm thickness of BST
BCC-8	Bamboo slices twining tube confined concrete with 9.5mm thickness of BST
BCC-10	Bamboo slices twining tube confined concrete with 12mm thickness of BST
C3D8R	8-node linear brick, reduced integration, hourglass
CDP	Concrete damage plasticity
ES EN	Ethiopian Standard Euro Norm code
FEA	Finite Element Analysis
FEM	Finite Element Method
FRP	Fiber reinforced plastic
JIT	Jimma Institute of Technology
JU	Jimma University
LBL	Laminated bamboo lumber
MoE	Ministry of Education
PC	Plain concrete
SC8R	An 8-node continuum shell, reduced integration with hourglass

LIST OF SYMBOLS

a. Latin upper-case letters

Ac	Cross sectional area of concrete
E_{cm}	Secant modulus of elasticity of concrete
E_o	Initial modulus of elasticity for the undamaged material
G_f	Fracture energy
E_1	Modulus of elasticity of Bamboo slices twining tube in 1-direction
E_2	Modulus of elasticity of Bamboo slices twining tube in 2-direction
E_3	Modulus of elasticity of Bamboo slices twining tube in 3-direction
G	Shear Modulus

b. Latin lower-case letters

d	Effective depth
d_c	Compressive damage
d_t	Tensile damage
e	Eccentricity
f_{cc}	ultimate confined concrete strength (MPa)
f_{co}	ultimate unconfined concrete strength of standard cylinder (MPa)
p_{cc}	Axial load capacity for confined concrete (KN)
p_{co}	Axial load capacity for unconfined concrete (KN)
t_b	Thickness of bamboo fiber tube

c. Greek lower-case letters

ξ	Confinement factor

ψ	Dilation angle
σ_z and σ_θ	Axial and circumferential stresses
ν	Poisson's ratio
ε_{cc}	Confined concrete strain at ultimate strength (mm/mm)
ε_{co}	ultimate unconfined concrete strain of standard cylinder (mm/mm)
ε_{cy}	ultimate unconfined concrete strain of standard cylinder (mm/mm)
ε_t	Total strain
ϵ_{inc}	inelastic strain
ε_x	Strains in the x directions

CHAPTER ONE

1. INTRODUCTION

1.1 Background of the Study

With the advancement of construction technology, the focus has shifted from building a structure that can withstand specific stress to building structures by utilizing the materials to their maximum load capacity. This shifting of focus has made it possible to build lighter structures by eliminating and improving old materials' drawbacks. Concrete filled tubular columns are the results of the advancement in construction technology. Through the elimination and improvement of the shortcomings of older materials, it has become possible to build structures with maximum load capacity that are lighter and more economical. Nowadays, using composite building materials is a common way to solve building problems. Bamboo continues to be of interest in buildings and structures owing to its good mechanical properties and sustainability. In this study, a new method of bamboo use is proposed, which is to twine laminated bamboo lumber (LBL) slices to forma bamboo-fiber-reinforced composite tube known as bamboo slices twining tube.

The axial compressive strength and ductility of concrete are greatly increased when steel tubes and fiber-reinforced polymer material are used as external confinement. Concrete columns made of steel tubes with fiber-reinforced polymer have become a common option for compression members. To clarify the confinement mechanism in Fiber-reinforced polymer-steel tube concrete columns and to further demonstrate their axial compressive behavior, an experimental program was carried out. Test results indicated that increasing the Fiber-reinforced polymer confinement increased the capacities of the axially loaded Fiber-reinforced polymer steel tube concrete specimens. Because of the FRP hoop rupture near their mid-height section, the columns that were subjected to axial compression failed. The additional fiber reinforced polymer wraps could effectively reduce the outward local buckling of the steel tubes in the columns(Wang *et al.*, 2021a).

Natural fibers have several benefits over synthetic fibers, like carbon and fiberglass, including lower cost, lower density, less energy usage, renewability, and biodegradability(Hussain *et al.*, 2020). Because Bamboo has an abundant of bamboo resources and a short natural growth cycle, it makes for an extremely attractive natural fiber. Bamboo is a flowering plant that grows quickly and can be used as a renewable building material. Bamboo has the potential to increase both its long-term carbon fixation capacity and economic benefits when used in building construction. While Bamboo offers many benefits, including better performance, low carbon content, high energy efficiency, and the ability to reduce emissions. Bamboo is an

anisotropic material, which has many factors affecting its material performance, large variability of material performance, lack of systematic research(Shu *et al.*, 2020).

It is expected that bamboo's excellent tensile performance will develop to confine the concrete core if the bamboo is wound into a tube shape and the core is filled with concrete. Thus, a new method of using bamboo was proposed: laminated bamboo lumber slices are twined to form a bamboo-fiber-reinforced composite tube. This is done to verify the viability of using bamboo composite tubes as external confining materials for a concrete core. Bamboo slices twining tubes are suggested to replace steel and fiber-reinforced polymer as the confining jacket acting on concrete due to the high tensile strength of bamboo fiber. The results showed that natural bamboo fiber reinforced composite tubes had excellent confinement properties for structural applications(Kou, Tian and Jin, 2021).

Commonly used codes like the ES EN and Eurocode 4 have simplified techniques for analyzing composite columns using ABAQUS software. The purpose of this study was to implement and verify the Non-Linear Finite Element Analysis of Bamboo Fiber Tube Concrete-Filled Composite Column with ductility behavior, effects of eccentric loading, effects of bamboo fiber tube diameter, load application and BST-Bamboo thickness on the column an action of uniaxial load by using Finite Element method. The simulation result was verifying the ductility properties, effect of eccentric loading, effect of Bamboo fiber tube diameter and load application and BST-Bamboo thickness on the Concrete-Filled Composite Column for the stated loading condition and additionally used as reference for simulation and practice work in the future.

1.2 Statement of the Problem

Due to the continuously increasing demand for building materials across the world, it is necessary to use renewable materials in place of the existing nonrenewable materials in construction projects. Bamboo is a flowering plant with quick growth that can be utilized in building as a renewable resource(Shu *et al.*, 2020). The experimentally investigated various axial compressive parameters of a new type of confined concrete, which is termed bamboo sheet twining tube-confined concrete. This new composite structure was composed of an outer bamboo composite tube jacket and a concrete core. But the existing experimental test on the replacement of steel tube by bamboo fiber tube of concrete-filled composite column is insufficient, and it cannot address all behavioral aspects of the column. so, the additional investigation is important before using bamboo fiber tube use as construction material by adding other parameter effect on the bamboo fiber tube concrete-filled composite column. Limited studies were found on the ductility behavior, effects of

eccentric loading, effects of bamboo fiber tube diameter, load application for Non-Linear properties of Bamboo Fiber Tube Concrete-Filled Composite Column subjected to uniaxial loading conditions.

This study aims to perform extensive numerical investigations on Bamboo Fiber Tube Concrete-Filled Composite Column under concentric axial and eccentric axial loading. Therefore, it is necessary to establish systematic research by finite element program to examine the Non-Linear Finite Element Analysis of Bamboo Fiber Tube Concrete-Filled Composite Column subjected to uniaxial loading. by considering this loading condition non-linear behavior of the concrete-filled composite column was examined and generate information on the effects of controlling parameters through parametric study using a validated numerical model which can adequately predict the Non-Linear Behavior of Concrete-Filled Composite Column.

1.3 Research Question

1. What are the effects of eccentric loading values on non-linear finite element analysis of circular bamboo fiber tube concrete-filled composite column?
2. How the bamboo fiber tube diameter effect on the non-linear finite element analysis of circular bamboo fiber tube concrete-filled composite columns?
3. How does the load application affect the non-linear finite element analysis of circular bamboo fiber tube concrete-filled composite columns?
4. What is the ductility behavior of circular bamboo fiber tube concrete-filled composite column?

1.4 Objectives of the Study

1.4.1 General Objectives of the thesis

The aim of this study was to assess the non -linear finite element analysis of circular bamboo fiber tube concrete-filled composite column.

1.4.2 Specific Objective

1. To determine effects eccentric loading on non-linear finite element analysis of circular bamboo fiber tube concrete-filled composite column.
2. To evaluate the effects of bamboo fiber tube diameter on the non-linear finite element analysis of circular bamboo fiber tube concrete-filled composite column.
3. To determine effects of load application on non-linear finite element analysis of circular bamboo fiber tube concrete-filled composite column.
4. To check the ductility behavior of circular bamboo fiber tube concrete-filled composite column.

1.5 Significance of the Study

The result of this study is to provide data and information that helps for stake holders in construction industry such as designer, architects, contractors and students to know the non-linear finite element analysis of bamboo fiber tube concrete-filled composite column for building structure on the capacity of building. The study motivates those who are interested to conduct further research on non-linear finite element analysis of bamboo fiber tube concrete-filled composite column and the result should be interest to engineers considering the use of such columns in various structural applications. Practical use of bamboo fiber tube concrete -filled composite column requires knowledge of the basic non-linear behavior of the column as well as knowledge of the interrelationship between stress and strain.

An advanced finite element model of bamboo-fiber tube concrete-filled composite column subject to uniaxial load was developed, which show to be valid excellent correlation with the experimental result obtained from the journal. This research also provided new information on the influence of important structural variables on the key response parameters of bamboo-fiber tube concrete -filled composite column. This information can be used to develop guidelines for the safe designs of such columns. Finally, it helps to minimize the gap for other researchers.

1.6 Scope and Limitation of the Study

This study to cover the non-linear finite element analysis of bamboo fiber tube concrete-filled composite column and extend to demonstrate ductility behavior, effects of eccentric loading, effects of bamboo fiber tube diameter, effect of load application and BST-bamboo thickness on the column non-linear behavior.

This thesis was focusing on FEA program ABAQUS©CAE of bamboo fiber tube concrete-filled composite column under uniaxial eccentricity by achieving the above specific objectives of this research. The use of FEM has proposed to model bamboo fiber tube concrete-filled composite column**.** The proposed procedure was to study the non-linear finite element analysis of bamboo fiber tube concrete-filled composite column of different parameters in geometry of the same cross section of column is limited to finite element analysis by Abaqus/CAE.

CHAPTER TWO

2. REVIEW OF RELATED LITERATURE

2.1 General

This chapter provides a review of related literature on the Non-Linear properties of bamboo fiber tube concrete-filled composite column. A literature review is important and central in a study, as it provides the most information on the topic in question. Each portion includes a critical examination of current Literature and explains what has been understood from them. The main purpose of a literature review is to establish the academic and research areas that are relevant to the subject under study.

2.2 Use bamboo as construction material

Bamboo is recognized as a sustainable substitute for green building design, and it has cultural meaning in certain parts of the world. Before bamboo is extensively used, more research is needed to determine its structural strength in various design scenarios. Although the mechanical properties of bamboo and wood are similar, bamboo is more advantageous for construction because it is a versatile, renewable, sustainable, and disaster-resistant material. Global interest in natural bamboo and its derivatives is growing as they are regarded as an extremely popular green and ecologically friendly alternative building material. Its large developing area and fast growth rate make it more useful than a limited supply of timber. On the other hand, natural bamboo has a nonhomogeneous, anisotropic material property that varies in different directions. There is a lack of engineering research and data regarding bamboo material's use in and impacts on construction. Strand7 examined three distinct bamboo models for this study; each model had unique structural characteristics and used a different primary building material. By enhancing the three provided structures, a new model was put forth that maximized the mechanical capacity. A few design guidelines were put forth after various bamboo structures were analyzed and contrasted. The model will use bamboo scrimber, an engineered bamboo derivative with more consistent material properties, in place of natural bamboo.(Tahmasebinia *et al.*, 2021).

Since ancient times, bamboo has been used extensively as a load-bearing material in building construction because of its low density, quick growth, and excellent mechanical performance under load. An in-depth understanding of the relationship between bamboo's morphology and mechanics including how this regularly spaced segmental structure adapts to taking the applied loads is necessary for applications in engineering, architecture, and infrastructure. We discover that one critical failure mode that causes the entire structure to collapse is column buckling. Its strength is found to be significantly influenced by the gradient

fiber distribution pattern along the radial direction. We discover that the strength of bamboo is decreased when fiber deviation occurs at the node region. However, our findings demonstrate that structural elements like the internal diaphragm and external ridge serve as reinforcement, with a greater impact on bamboo than on other plants with comparable node appearances. By creating more exciting uses for bamboo, this research may also help to mitigate the scarcity of non-renewable resources and promote sustainable development(Cui *et al.*, 2020).

Bamboo is a naturally fiber-reinforced material that grows quickly and has good ductility and flexural strength. Although bamboo is being used in more and more applications, its flexural ductility and the techniques for assessing it have not been thoroughly studied. Bamboo's flexural strength and vascular bundle content showed a positive correlation, while the parenchyma content and flexural ductility showed a direct correlation. Bamboo exhibited a contradictory correlation between its flexural strength and ductility. The flexural strength and ductility of bamboo as a sustainable building material are important topics that this work contributes significantly(M. Chen *et al.*, 2020).

Bamboo has become more and more popular as a potential reinforcement material. Bamboo is predicted to serve as a sustainable substitute for more conventional structural materials like concrete, steel, and wood because it is a renewable resource that grows quickly and requires little labor. A replacement building material that is renewable, environmentally friendly, and widely accessible has come to the attention of people all over the world due to the depletion of natural forests and the decreasing availability of wood, especially in tropical regions. Bamboo fiber has the potential to have tensile strength similar to that of steel and an average fracture toughness greater than that of aluminum alloy. Bamboo grows quickly; in a few months, it nearly reaches its maximum size, and in five years, it completes its development. The fastest-growing woody plant on Earth is bamboo. It grows between 7.5 and 40 cm every day, with a world record of 1.2 m in a single day recorded in Japan. Compared to most other species, bamboo grows three times faster. Bamboo species with significant commercial value typically reach maturity in 4 or 5 years (Vijayabanu K and Sivakumar M, 2021).

A brand-new technique for using anchorage structures to strengthen timber beams with bamboo scrimber was put forth. The bottom of the timber beam was covered with bamboo scrimber, which was fastened with wooden pins or carbon fiber-reinforced polymers. The effects of various anchorage methods and thicknesses of bamboo scrimber on the reinforcing effect of timber beams were investigated through bending tests conducted on eight reinforced beams and two control beams. The ultimate load, stiffness, and ductility of

the timber beams were examined, along with their failure characteristics. The findings demonstrate that there are two types of timber beam failure modes: bending failure and bending-shear failure. Additionally, the timber beams clearly display ductile deformation prior to failure. The test results show that bamboo scrimber and carbon fiber-reinforced polymers can stick to each other firmly. As a result, bamboo strengthening timber beams with anchorage structures can significantly increase the member's ultimate bearing capacity, stiffness, and ductility(Chen *et al.*, 2021).

The purpose of this study is to investigate the effects of bamboo species, the presence of bark and nodes, and moisture content on the tensile strength of bamboo strip. It also aims to provide an appropriate cutting shape of the bamboo strip to be used for tensile test. By contrasting the performance of bamboo bars with mild steel bars under a three-point bending test setup, the viability of using bamboo as reinforced bars for concrete beams was investigated. All of the findings suggested that the species Bambusa Vulgaris Vittata and Bambusa Heterostachya could be utilized in place of steel reinforcement in reinforced concrete beams(Al-Fasih *et al.*, 2022).

The construction industry's use of non-renewable resources has a number of negative effects on the environment, including excessive energy use and material loss. As a result, the construction industry is constantly looking for ways to innovate and improve upon current practices, with the goal of using sustainable and alternative materials. Bamboo is a perennial plant that grows quickly, is inexpensive, and has excellent mechanical and physical qualities that guarantee its performance in a building environment. Because bamboo-reinforced beams can be designed using the same techniques as reinforced concrete beams and because they adhere to the Bernoulli-Kirchoff bending theory, the use of bamboo in place of steel in beams has received extensive research. These findings are intended to encourage the use of bamboo as a sustainable building material that can strengthen concrete beams subjected to bending forces(Tokuda *et al.*, 2020).

It is common knowledge that steel reinforcement plays a crucial role in the formation of building structures. However, the primary material used to form steel reinforcement is becoming less common as the community's need for it grows, driving up the cost. Bamboo is recommended as an affordable and readily available substitute for tensile steel reinforcement. The aim of this study was to calculate the bending load that square and circular bamboo reinforcement could withstand as well as the ratio of beam bending using these materials. This study employed an experimental design, carrying out a number of tests including the preservation of bamboo and the evaluation of aggregates as concrete building blocks. The cross sections

made of bamboo reinforcement are 900 mm x 150 mm x 150 mm in diameter, and they are shaped like squares and circles. The findings demonstrated that the flexural strength generated by the steel-reinforcing concrete beam was 11,36 MPa, the bamboo-reinforcing concrete beam with a circular cross section was 8,73 MPa, and the bamboo-reinforcing concrete beam with a rectangle cross section was 9,04 MPa(Ampangallo and Ambali, 2021).

Anisotropic materials that are renewable and have been used for a long time in human society are wood and bamboo. Compared to raw bamboo or original sawn lumber, engineered wood or bamboo that aims to reduce the variability of the natural material can offer better material properties and structural performance. A state-of-the-art review of three novel wood composites, fiber reinforced polymer (FRP) reinforced glulam, cross-laminated timber (CLT), and wood scrimber, and three novel bamboo composites, laminated bamboo lumber (LBL), glued-laminated bamboo, and bamboo scrimber, was carried out in this paper. Special attention was paid to the manufacturing processes, modeling techniques, and mechanical properties of each material. Next, a thorough comparison of the mechanical properties and densities of these innovative engineered wood/bamboo composites was carried out. In conclusion, a number of structural applications were demonstrated, wherein the previously mentioned engineered wood/bamboo composites were utilized as the primary building materials. The feasibility of utilizing these engineered wood/bamboo composites for structural applications was validated, and possible drawbacks were also discussed(Sun, He and Li, 2020).

2.3 Bamboo fiber use for composite column

Because bamboo has good mechanical properties and is sustainable, it is still used in buildings and other structures. This study proposes an innovative method to use bamboo: generate a bamboo-fiber-reinforced composite tube (also known as a bamboo slice twining tube, or BST) by twining laminated bamboo lumber slices. The excellent tensile performance of bamboo should develop to confine the concrete core if the bamboo is wound into a tube form and the core is filled with concrete. Thus, a new method of utilizing bamboo was suggested: combining laminated bamboo lumber slices to produce a bamboo-fiber-reinforced composite tube. This was done to confirm the viability of using bamboo composite tubes as external confining materials for a concrete core. It is suggested that bamboo slices twining tubes be used in place of steel and fiber-reinforced polymer as the confining jacket acting on concrete due to the high tensile strength of bamboo fiber. Axial compressive tests were performed on ten BST and BST-confined concrete (BCC) short columns, with the BST wall thickness serving as a variable. According to the test results, bamboo slices twining tubes have mechanical characteristics that, in both tension and compression, are comparable

to those of engineered bamboo. The BST wall rupturing in the center of the columns is the BCC specimens' failure mode. Concrete can be effectively confined by bamboo slices twining tube. Ultimately, a stress-strain model focused on analysis is put forth for the BCCs, and the model's predictions precisely match the experimental curves. The findings showed that natural bamboo fiber reinforced composite tubes had good confinement properties for structural applications.(Kou, Tian and Jin, 2021).

Figure 2.1: Manufacturing Process of The Bamboo Slices Twining Tube(Kou, Tian and Jin, 2021).

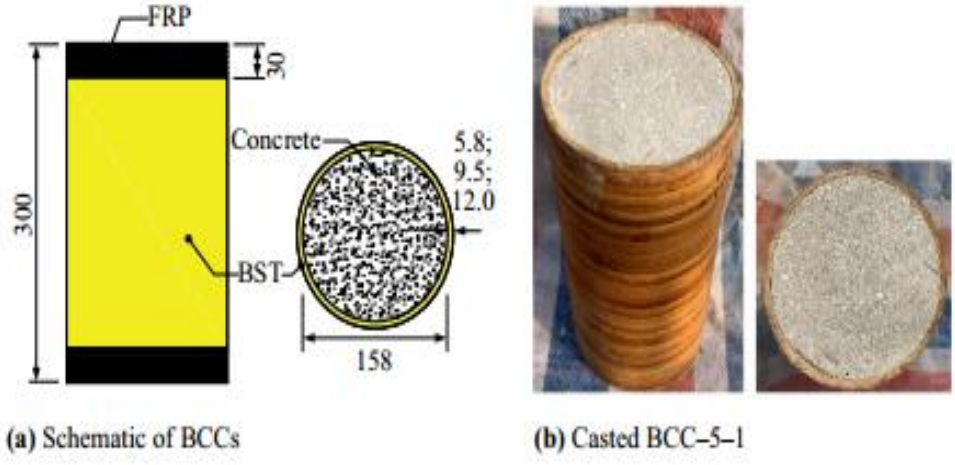

Figure 2.2: Details of The Bamboo Slices Twining Tube Confined-Concrete Columns. (Unit: mm)(Kou, Tian and Jin, 2021).

By substituting the internal steel tube of concrete-filled double skin steel tubular columns with a structural bamboo culm, circular concrete-filled steel tubular columns with an inner bamboo culm encourage the use of natural materials that are less expensive and lighter in weight. It is expected that this kind of composite column will combine the benefits of all three material types. 22 circular stub columns were tested under axial compression. These included 12 hollow circular concrete filled steel tubular columns, 3 circular concrete filled steel tubular columns, 4 concrete-filled double skin steel tubular columns, and 3 circular concrete filled steel tubular columns with an inner bamboo culm. The thickness, diameter, and diameter to thickness ratio of the external steel tubes are among the test parameters for bamboo culms. The columns with an inner bamboo culm had outstanding ductility, according to test results. Additionally, the axial load-displacement curve of the columns with an inner bamboo culm declined initially before exhibiting strain hardening behavior; however, the inner bamboo culm only slightly increased the final load. This study shows that it is possible to use a bamboo culm as the inner core of circular concrete-filled steel tubular columns, particularly if the culms' durability is improved. To reduce the amount of concrete used and achieve between 0.25 and 0.34 of the strength at the maximum loads, the inner bamboo culms can be utilized as a mold. They can greatly increase the ductility of steel tubular columns filled with hollow concrete, indicating excellent energy dissipation capacity(Gan *et al.,* 2020).

2.4 Concrete-filled composite column under axial and uniaxial eccentricity.

In order to predict the behavior of circular, thin-walled concrete-filled double skin steel tubular slender columns loaded eccentrically, a computational modeling method was developed and presented. The fiber-based formulation takes into account all of the significant characteristics of concrete-filled double skin steel tubular slender columns, such as concrete confinement, geometric imperfection, second-order, gradual plasticity of steel, and material and geometric nonlinearities. The computational model's accuracy has been confirmed by the available experimental data. Using computer modeling, the responses of thin concrete-filled double skin steel tubular columns have been determined. The obtained numerical results have shown that the ultimate loads of concrete-filled double skin steel tubular circular columns are significantly reduced by increasing either the member slenderness or the e /Do ratio. As the e/Do ratio rises, the sandwiched concrete's axial load capacity increases noticeably. Conversely, a greater slenderness of the member results in a greater distribution of the axial load onto the outer steel tube. Increasing the Di/Do ratio improves the columns' ultimate load and initial bending stiffness, while increasing the Do/to ratio decreases it. The ultimate loads of concrete-filled double skin steel tubular columns are greatly increased by the use of high-strength materials. But as a member gets thinner, their effects become less noticeable. When the e/Do ratio

is more than 2.5 or the slenderness ratio is more than 60, the impact of concrete confinement on the column strengths can be ignored. It is demonstrated that the design models are capable of accurately predicting the final axial loads of thin concrete-filled double skin steel tubular columns loaded concentrically as well as the strength interaction diagrams of these columns under eccentric loading. These models can be applied in real-world situations(Ahmed *et al.*, 2020a).

The behavior of high strength concrete-filled square spiral-confined steel tube members under combined axial and flexural loading was examined in this work. Under eccentric axial loading, nine specimens with a concrete compressive strength of 111 MPa were tested. Column configuration (without spirals, with normal strength steel, and with high strength steel) and eccentricity ratio were among the test variables. An equivalent uniaxial stress-strain model was developed for the high-strength concrete in concrete-filled steel tube and spiral-confined concrete-filled steel tube columns based on the test results and an existing stress-strain model for the steel tube plate in these columns. In order to study the flexural behavior of spiral-confined concrete-filled steel tube columns and concrete-filled steel tube columns with high-strength concrete under various axial load levels, this stress-strain model was further implemented with a fiber beam-column element. The following is a summary of the primary findings: The primary reason for the axial load capacity degradation was concrete crushing. The first concrete crushing happened either right before or right on top of the peak axial load. Both normal strength and high strength steel ruptured in the post peak stage at eccentricity ratios of 0.14 and 0.32, but high strength steel ruptured significantly sooner. Despite the higher eccentricity ratio of 0.54, the spirals did not break. Large horizontal tensile strain demands at the corners caused the vertical welds on the steel tube's compression side to fracture for the majority of specimens close to the testing's conclusion. The concrete core crushing process was successfully postponed by the spirals. Spiral reinforcement has very little impact on a column's ability to support more weight. Nonetheless, the addition of spiral confinement can significantly increase the ductility of the columns, and this improvement is amplified by a rise in the spiral reinforcement's yield strength. The steel plate strains were essentially distributed linearly along the cross-sectional depth during the initial loading phase. Following local buckling, the measured strains at the locations away from the buckled regions continued to be roughly distributed linearly, but the measured strains in the buckled regions no longer reflected the global deformation. The curvature and the strains on the compression side corresponding to the global deformation were found using a linear strain distribution with the measured strains on the tension side. The bending moment at the critical section essentially peaked when the peak axial load was reached. The moment declined more slowly than the rate at which the axial load dropped because of the second-order effect. Since

the eccentricity ratio has little effect on the equivalent rectangular stress block parameters, the suggested concrete stress-strain relationships can be used to practically simulate the flexural behavior of columns under different axial load levels. The descending branch of the proposed concrete stress-strain relationship is primarily affected by the degree of confinement offered by the spirals. The accuracy of the proposed model is verified by the good predictions made by the fiber beam-column element with the proposed stress-strain relationships for the load-displacement responses of the columns tested in this study and those of square concrete-filled steel tube columns with high-strength concrete tested by other researchers(Hu *et al.*, 2020).

This paper presents the experimental and numerical studies conducted on the behavior of rectangular concrete-filled double skin steel tubular short columns loaded eccentrically. A detailed description of the experimental programs and outcomes on twenty short steel tubular columns with double skin filled with concrete has been provided. A mathematical model that takes into account the local buckling of the outer steel sections has been developed to predict the moment-curvature behavior and strength envelopes of rectangular concrete-filled double skin steel tubular columns. The mathematical model has been used to determine the significance of several key features on the responses of thin-walled concrete-filled double skin steel tubular stub beam-columns. The model has been validated by experimental results. Concrete crushing and outward local buckling of the internal and external steel tubes caused the axially loaded double skin steel tubular columns to fail. After the outer tube gave way and the concrete between it was crushed, the inner tube gave way locally outward. Significant local buckling of the external steel tubes may have contributed to the shear failure of concrete-filled double skin steel tubular columns. Concrete crushing near buckled walls, considerable column bending, and localized buckling of the external steel tube walls in the compression zone were the reasons for the failure of eccentrically loaded concrete-filled double skin steel tubular columns. Increasing the Bo/to ratio dramatically lowers the bending, axial, and curvature ductility of concrete-filled double skin steel tubular columns, according to numerical analyses. On the other hand, the column strengths are somewhat decreased by raising the Bi/ti ratio. Concrete-filled double skin steel tubular columns' ultimate axial and bending strengths are significantly increased by raising the steel yield stress and concrete strength. Pure bending resistance is more significantly impacted by the steel yield stress than pure ultimate axial loads are. Conversely, the pure ultimate axial strength is more influenced by the strength of the concrete than is the pure bending resistance. The concrete-filled double skin steel tubular columns' bending resistance and curvature-ductility are significantly reduced when the axial load ratio is increased. When designing and performing nonlinear analyses of concrete-filled double skin steel tubular

columns, it is important to consider the significant reduction in strength caused by the local buckling of the external steel sections(Ahmed *et al.*, 2020b).

This study described an experimental program on concrete-filled steel tubular columns with various cross-sectional configurations that were subjected to eccentric loads. The findings were then presented and examined. Experimental research on steel tubular columns with two skins filled with concrete that are subjected to eccentric loads—especially when the ends have varying eccentricities—is lacking. In fact, the continuation of the program presented here will include specimens with this type of loading, as the authors firmly believe that more tests along these lines should be conducted. The load-deflection curves for each specimen showed a smooth post-peak branch, indicating global buckling as the mode of failure. The specimen with the smoothest curve and highest ductility index was the steel tubular columns filled with concrete. When exposed to eccentric loads, specimen DS was most frequently used. It was found that the degree of utilization decreased with increasing slenderness. Specimen DS was utilized at a 25% higher rate than the single concrete-filled steel tubular columns. The DT level only went up by 8%. Because DS is less slender, second-order effects take longer to manifest and the column can operate at a higher level of utilization. The DT column is 13% less effective than the DS under the experimental program's conditions. In the first part of the curve, where the response is still linear, the columns' stiffness corresponds with the value of the flexural stiffness provided by the EN1994-1-1 formula. Higher loads result in different values. The concrete-filled steel tubular columns under analysis yielded conservative predictions with a low standard deviation when analyzed using the simplified method from EN1994-1-1. A conservative trend was noted, even though there were not enough tests to draw reliable conclusions. For the method to be conservative, a coefficient for member imperfection must be taken into account. However, because of the current manufacturing processes, the recommended value of this variable assumes an unrealistic level of imperfection(Albero *et al.*, 2021).

This paper presents the test results of eight 3 m long circular beam-columns filled with concrete and subjected to unequal load eccentricities at both ends of the columns. The number of experiments on this loading typology for concrete-filled steel tubular columns that are currently available is increased by this experimental program. In concrete-filled steel tubular beam-columns, the application of unequal load eccentricities increases the maximum resisting load but decreases the column's ductility. For columns with a length-diameter ratio (L/D) of 27.78, this result was noted; however, for columns with a lower L/D ratio (L/D = 13.69), it was not apparent. Based only on the loading eccentricity ratio (r), the current provisions for the equivalent moment factor from Eurocode 4 and AISC 360-16 were found to be inadequate in

accounting for the influence of other parameters, such as column slenderness, which was demonstrated by the test results observation conducted for this paper. Consequently, additional study should be conducted to include additional parameters in order to increase the precision of the existing equations.(Albero *et al.*, 2022).

This study investigates thorough experimental and numerical modeling program designed to asses the behaviors of steel tube stub columns filled with concrete and encased in concrete under uniaxial and biaxial eccentric compression. In the experimentally planned, three uniaxial eccentric compression tests, eleven biaxial eccentric compression tests, and one axial compression test were carried out. We looked at the effects of end moment ratio and loading eccentricity. Under uniaxial and biaxial eccentric compression, it was discovered that the loading eccentricity and end moment ratio generally influenced the ductility and failure modes of concrete-encased concrete-filled steel tube stub columns. Each specimen's axial load-carrying capacity decreased as the outer concrete cracked and split after the peak load was reached. However, the steel tubes filled with concrete inside allowed the bending strength to be preserved. Numerical modeling was done in tandem with the experimental program. First, FE models were created and verified against the test outcomes. Afterward, they were employed in parametric studies to produce additional numerical data across a broad range of end moment ratios and initial loading eccentricities(Ma, Zhao and Tan, 2021).

An experimental study of the structural behavior of ultra-high-performance concrete-filled steel tube columns under eccentric compression is presented in this work. The present study, as reported in this paper, allows for the derivation of the following conclusions. The initial stiffness and load-bearing capacity of the column decreased as the initial eccentricity and slenderness ratio increased, and the bending characteristics gradually became apparent. When the specimen reached its peak strength, the load-deformation curve smoothly decreased and it showed ductile properties as opposed to axial compression. In-plane bending was the primary mode of failure for the ultra-high-performance concrete-filled steel tube under eccentric compression. Multiple transverse cracks on the tension flange and crushing at the steel's buckling point were the hallmarks of the Ultra-high-performance concrete core failure. Under eccentric compression, the deflection curve of an ultra-high-performance concrete-filled steel tube roughly followed a sine half-wave. The circular section series' moment-curvature curve is more shaped, meaning that after the steel yields, the bending moment either stayed constant or gradually increased. In contrast, the bending moment in the square section series decreased as the steel yielded until stress hardening of the steel developed because of the weak confinement effect. ABAQUS was used to create a comprehensive finite element model of an ultra-high-performance concrete filled steel tube column that was subjected to eccentric compression.

Regarding failure mode, axial load-deflection relationship, and ultimate strength, there was a good match between the test results and the FE simulations. This suggests that additional analysis of the performance of ultra-high performance concrete filled steel tubes can be conducted using the currently available finite element model(Zhang *et al.*, 2020).

Under eccentric monotonic compression, square reinforced concrete columns with varying slenderness ratios reinforced by carbon fiber reinforced polymer were put to the test. P-M diagrams of strengthened columns were obtained analytically and compared with P-M diagrams obtained experimentally. The concrete is contained by carbon fiber-reinforced polymer hoop wraps, which also improve the studied columns' strength and deformability. Carbon fiber reinforced polymer hoop wraps have a greater impact on strength in shorter columns, but a more noticeable impact on deformability in slender columns. In comparison to strengthened columns, carbon fiber reinforced polymer strengthened columns generally exhibit much higher axial and flexural deformability, depending upon the slenderness ratio and the quantity of longitudinal and hoop carbon fiber reinforced polymer fibers. The peak load of strengthened columns is increased by the inclusion of longitudinal layers of carbon fiber-reinforced polymer sheets. The 600 mm column experienced the largest increase in peak load, which decreases as column height increases. The P-M diagram in the transition- and compression-control regions is significantly improved when only hoop carbon fiber reinforced polymer sheet is present, but the P-M envelop of the tension-control region (higher moment and low axial load) experiences almost no expansion. All three of the P-M diagrams' regions have a notably high expansion for alternative strengthening schemes. The expansion in the tension-control region is notably greater than that of the other two carbon fiber reinforced polymer gions. The longitudinal carbon fiber reinforced polymer sheets layered two and four times, respectively, increase the control column's flexural capacities by six and ten times. P-M diagram predictions are fairly close and conservative. The failure load for the control specimens was lower than the expected P-M diagram. Nonetheless, the theoretical P-M diagram was conservative for the strengthened specimens. The number of FRP layers and the method of strengthening have a significant impact on the degree of strength and ductility increase. When a single layer of hoop sheet was utilized for reinforcement in 1200 mm columns, the increase in ductility was greatest but the increase in strength was lowest (in comparison to 600- and 900-mm high columns). Nevertheless, when the identical 1200 mm thin columns were reinforced with two or four layers of longitudinal and subsequently one layer of hoop FRP sheet, the improvements in strength and ductility were little(Siddiqui *et al.*, 2020).

2.5 Fiber confinement and ductility behavior Concrete-filled composite column

This investigation uses high strength concrete to study the compressive behavior of FRP-confined steel-reinforced concrete columns. The compressive behavior of FRP-confined steel-reinforced concrete columns was compared with that of concrete-filled FRP tubes and steel-reinforced concrete columns. The effects of concrete strength, types of encased steel section, and thickness of glass fiber reinforced polymer tube were investigated. The most effective way of preventing both local and global buckling of the encased steel section is to increase the thickness of the glass fiber reinforced polymer tube. It is advised to use a Class 1 steel section, such as the I-shaped steel section used in this study, to lessen the negative effects of local buckling. If not, local buckling will lower the axial load capacity of the corresponding FRP-confined steel-reinforced concrete column, such as the one used in this study with a cruciform steel section. FRP-confined steel-reinforced concrete columns using high strength concrete have lower deformation capacities than their counterparts with normal strength concrete because of the smaller axial and lateral strains at failure. Increasing the confining stiffness of the glass fiber reinforced polymer may improve its deformation capacity. The glass fiber reinforced polymer tube's hoop strain distribution becomes less uniform as the concrete strength increases, and the encased steel section's symmetry decreases. The encased steel section exhibits variation in both axial and lateral strains. The variation is particularly noticeable in the thinner steel section (such as the cruciform steel section in the current study), where a sudden increase in strain may be linked to the occurrence of local buckling. Because of the local buckling that occurs in the steel section, the strain distribution is generally more uniform in glass fiber reinforced polymer tubes than in those in the steel section. Higher axial stiffness in the elastic stage but lower ductility in the hardening range are the results of using high strength concrete in fiber-reinforced polymer-confined FRP-reinforced concrete columns. Both axial stiffness and ductility can be improved by increasing the stiffness of the glass fiber reinforced polymer or by encasing the steel section. In the case of glass fiber reinforced polymer tube and concrete-filled FRP tubes column, there is a composite effect between the constituent materials, which is defined as the composite load-carrying capacity at the ultimate limit state of the composite column higher than the superimposed load capacity of its constituent materials; however, this effect does not exist in the case of concrete-filled FRP tubes column and steel column, unless local buckling does not occur in the encased steel section(G. M. Chen *et al.*, 2020).

This article develops a new energy absorption technique for strain estimation. Numerous models for actively and passively confined concrete (like FRP wrapped) have been proposed based on the theoretical analyses presented. The features of confined concretes are further investigated with the help of these suggested

models, which offer precise predictions of the experimental data. A novel technique for energy absorption serves as the foundation for the theoretical analyses. The lateral confinement and the energy absorbed by the concrete column have a transfer factor (k) of 8.2. A peak strain model for actively confined concrete is proposed. There is a connection between the dissipative energy of the confined concrete and the unconfined concrete. Future research on the softening branch of the confined concrete can benefit from this discovery. This paper examines the demarcation point, peak strain, and demarcation confinement of confined concrete. Based on the relationship between lateral strain and axial strain, models are proposed to estimate each characteristic. This paper established the constitutive model for analysis. The proposed model utilized the energy method for strain estimation and the concrete failure criterion for stress estimation. As a result, the theoretical establishment process of the suggested constitutive model is high. In the meantime, the suggested model's accurate prediction could be based on the stress strain curves' verification. Future research is nevertheless required to determine the relationship between the lateral and axial strains as well as to develop a model for estimating the true rupture strain of FRP. Most importantly, the theoretical analyses can be used to establish a model for the stress-strain curves of confined concrete. This new methodology can be further developed to include concrete columns confined with any type of confinement method(Rong and Shi, 2021).

The circular FRP-steel tube concrete stub columns under axial compression are examined experimentally and theoretically in this work. To assess the axial compressive behavior of FRP-steel tube concrete stub columns, tests were conducted on three distinct specimen configurations: FRP-confined concrete specimens, steel tube concrete specimens, and FRP-steel tube concrete specimens. By contrasting the development of the steel confining pressure and the FRP confining pressure, a better understanding of the confinement mechanism in the FRP-steel tube concrete columns was attained. When the FRP hoop ruptured close to their mid-height section, the axially compressed FRP steel tube concrete stub columns failed. The additional FRP wraps could effectively reduce the outward local buckling of the steel tubes in the FRP-steel tube concrete stub columns. Shear failure mode was the cause of the concrete core failure in the FRP-steel tube concrete stub columns. The FRP-steel tube concrete stub columns' axial bearing capacities rose as the FRP confinement level rose and the diameter-to-thickness (D/t) ratio of the steel tube decreased. The disconnected steel tube's axial bearing contribution to the peak loads of the fiber-reinforced polymer steel tube concrete stub columns was negligible, and as such, it could be disregarded and regarded as a safety feature during design. The axial load-strain responses of the inner concrete in the FRP-steel tube concrete specimens showed a bilinear shape that was strikingly similar to the FRP-steel tube concrete stub columns after the steel tube's contribution was subtracted. The FRP confinement stiffness had a greater effect on the

second stiffness of the inner concrete in the FRP-steel tube concrete stub columns than it did on the steel confinement level. The proposed confinement mechanism in the FRP-steel tube concrete stub columns is divided into three stages: domination of steel confinement, domination of FRP-steel dual confinement, and domination of FRP confinement. These stages are based on the different development rates of the steel confining pressure and the FRP confining pressure as different loading stages. The interaction between the outer FRP steel composite tube and the inner concrete is taken into account by the suggested mechanism throughout the entire loading procedure(Wang *et al.*, 2021b).

The behavior of short FRP-confined concrete-encased cross-shaped steel columns under axial compression has been studied in detail in this work, with an emphasis on the effects of combined FRP-steel confinement in the columns. The steel section's flange width, flange thickness, and web thickness in addition to the thickness of the FRP tube were the primary test variables. The corresponding square FRP-confined plain concrete column specimens and square FRP-confined plain concrete column specimens for comparison were also tested as part of the experimental program. The tested FRP-confined concrete-encased cross-shaped steel column specimens feature a variety of steel sections that collectively provide substantial lateral confinement to the concrete, thereby significantly enhancing its strength and ductility. The ultimate axial strain of the tested FRP-confined concrete-encased cross-shaped steel columns is significantly larger than that of the corresponding square FRP-confined plain concrete columns, and can even be larger when the FRP tube thickness is relatively small. This is true despite the large variations in the dimensions of the steel section and the FRP tube thickness. The behavior of the concrete core and the FRP outer tube of FRP-confined concrete-encased cross-shaped steel columns is marginally affected by variations in the cross-sectional dimensions of the steel section within the broad range of parameters chosen for this study. The investigation examined FRP-confined concrete-encased cross-shaped steel columns with a 200 mm column side length. The coated flange widths (B) varied from 60 to 100 mm, flange thicknesses (tf) from 4.5 to 8.0 mm, and web thicknesses (tw) from 3.2 to 6.0 mm were observed for the steel section. The practical design of FRP-confined concrete-encased cross-shaped steel columns may be made simpler by this straightforward but significant conclusion. FRP-confined concrete-encased cross-shaped steel columns with a thicker FRP tube exhibit less of an impact from the steel section's lateral confinement. Consequently, in real-world scenarios, it may be possible to maximize the stiffness of FRP tube in cross-shaped steel columns with FRP-confined concrete encasement. The suggested approach can accurately forecast the axial load capacity of fiber-reinforced polymer-encased cross-shaped steel columns and conservatively forecast the final axial strain of these columns(Huang, Yu and Zhang, 2021).

. The strength and ductility of ultra-high performance concrete cylinders were enhanced by the addition of steel spirals. The improvement in ductility, however, was more noteworthy. The stress-strain curves illustrate the confinement effect of steel spirals in terms of higher plastic deformations, increased stress and strain capacities, and significantly improved energy absorption and dissipation. Three distinct zones could be identified from the observed stress-strain curves for confined ultra-high-performance concrete: post-peak softening, nonlinear hardening, and linear-elastic. Conversely, unconfined ultra-high performance concrete specimens only showed nearly linear behavior up to the strength peak, after which there was a sharp decline. The ultra-high-performance concrete between the spirals in confined cylinders was crushed or spalled, and tiny vertical cracks also contributed to the failure mode. Two parameters, the confinement effectiveness ratio and ultimate strain, were used to quantitatively examine the confined specimens' peak strength and ductility in comparison to the unconfined ones. For instance, for confined 2% fiber ultra-high performance concrete cylinders with 8% steel spirals, the confinement effectiveness ratio and ultimate strain were found to be 1.26 and 1.16%, respectively. When 4% steel fibers are used in specimens with lower steel fiber ratios, the nonlinear pre-peak behavior is more noticeable and the behavior is linearized to nearly 80% of the strength value. Unconfined specimens without any fiber showed a totally brittle behavior with a sharp drop in specimen strength after the peak strength was reached; however, this slope was less for higher ratios of steel fibers. Overall, steel spirals and steel fibers both contribute to confining effects; however, based on all of the tests carried out for this study, the effect of steel spirals is more convincing. Furthermore, this study demonstrates that the additional mechanical and confinement benefits do not outweigh the significant increase in material cost, negating the need to take 4% steel fibers into account for future ultra-high performance concrete column designs(Naeimi and Moustafa, 2021).

The ultrahigh-performance concrete's brittleness is significantly enhanced by the confinement inside steel tubes. The ultrahigh-performance concrete-filled steel tube columns have a small restriction on the shear slip of the ultrahigh-performance concrete core, but there is no discernible effect of the steel fiber volume fraction on the failure modes of the steel tube-confined reinforced and steel tube-confined ultrahigh-performance concrete columns. When the ultimate bearing capacity is reached for reinforced ultrahigh-performance concrete columns, the bearing capacity rapidly drops, making it challenging to capture the descending stage. The reinforced ultrahigh-performance concrete columns, steel tube-confined reinforced concrete columns, and steel tube-confined ultrahigh-performance concrete columns all exhibit a comparable method of confinement between the steel tube and the concrete core. The entire section is loaded, which causes the steel tube to yield prematurely. This has a negative impact on how the steel tube and concrete

core interact. Before the ultimate load is reached, the ultrahigh-performance concrete-filled composite structure experiences a negligible confinement effect. The best compressive ductility is exhibited by steel tube-confined reinforced concrete columns, while the highest bearing capacity is found in these ultrahigh-performance concrete columns. The strength of composite structures is increased by the addition of longitudinal reinforcements. The steel tube can be fully contained when a load is applied to the ultrahigh-performance concrete core. The compressive behavior of steel tube-confined reinforced ultrahigh-performance concrete columns and steel tube-confined ultrahigh-performance concrete columns is only slightly affected by the addition of steel fibers. However, adding 2% steel fibers by volume slightly improves the post peak behavior of the ultrahigh-performance concrete-filled steel tube columns. Furthermore, reinforced ultrahigh-performance concrete columns' compressive behavior can be enhanced by adding steel fibers(Wei *et al.*, 2021).

The axial compressive behavior of square and circular stainless-steel tube confined concrete column piers is investigated in this work. For most stainless square specimens, steel tube fracture is seen, but concrete shear failure is the primary mode of failure for stainless circular specimens. Enhancing the strength and ductility of steel tubes while delaying their fracture is feasible through the use of stiffeners or reinforcement cages in stainless steel square specimens. The concrete strength and tube thickness have an impact on the final strength. In stainless steel circular specimens, the ultimate strength is more clearly influenced by the tube thickness than by the concrete strength; in stainless steel square specimens, the influence is more clearly felt by the concrete strength. The ductility of stainless square specimens can be greatly increased by increasing the tube thickness. The ductility index of concrete specimens with tube thicknesses of 3 and 4 mm is 51.1 and 71.2% higher, respectively, than that of specimens with thicknesses of 2 mm, for square normal strength concrete specimens. The corresponding increasing ratios for square high strength concrete specimens are 23.7 and 280.2%. As the confinement factor ξ increases, the SI of the circular stainless specimens increases as well. The SI for stainless square specimens exhibits a decreasing trend as ξ increases, suggesting that large ξ stainless square columns are not a cost-effective choice in design practice. Square specimen steel tube strains yield after the peak load, whereas circular specimen steel tube strains yield close to the peak load. Concrete and carbon steel tubes have a stronger bond than stainless steel specimens carry out(Qiyun, Zhaoyuan and Wanlin, 2021).

An analytical review of the design guidelines for FRP-confined concrete columns is presented in this paper. Taking into account that the majority of the research focused on applications involving carbon fiber reinforced polymers for strengthening. Concrete columns subjected to axial compressive stress can have

their strength considerably increased by external FRP confinement. The concrete confinement compressive strength predictions made by the guidelines for non-circular columns are not accurate. The predictions made by the guidelines differ significantly. In comparison to strength enhancement, there is a greater scattering of predictions for strain improvement (ductility). Compared to circular columns, square columns are more significantly affected by size in terms of nominal strength. Further experimental results from large-scale non-circular specimens are needed to improve the calibration of the models and design guidelines. Consistent with the research, the majority of the examined guidelines display a stronger ratio for circular columns compared to non-circular ones(Salesa, Esteban and Barris, 2022).

Upon comparing the ductility index of the prestressed concrete and reinforced concrete structures for the deflection ratio, the ductility index of the former was roughly twice that of the latter for the control specimens. The NSM method (P) showed a ductility index that was about twice as high as the one found in reinforced concrete structures, while the other structures showed ductility indices that were comparable. In terms of the energy area ratio concept's ductility index, all construction methods and control specimens showed higher values for the reinforced concrete structures. Furthermore, it was established that the majority of prestressed concrete structures fell into the brittleness range, while the majority of reinforced concrete structures fell into the ductility range. In this study, the NSM and EP methods of prestressed concrete and reinforced concrete structures were compared and the ductility index was analyzed using FRPs. By securing the ductile behavior of structures, it is anticipated that in the future, the best strengthening technique will be able to be determined based on the type of structure and the reinforcing material. However, more study is needed on a wider variety of FRPs, including glass fiber and aramid fiber reinforced polymers, additional strengthening techniques, and different structural shape variables in order to obtain more precise and trustworthy data(Kim and Park, 2021).

Since fiber-reinforced polymer materials have a high ultimate tensile strength to weight ratio and are resistant to corrosion in corrosive environments, they have become a competitive option to confined columns. The confining ability of fiber-reinforced polymers under concentric axial loads was the subject of numerous earlier studies. The effects of the cross-sectional shape, thickness of the steel tube, and slenderness effect of a fiber-reinforced polymer-confined concrete-filled steel tube column under eccentric load is investigated using a nonlinear finite element method in this study. By comparing the outcomes with experimental data from published studies, the FE model was verified, and good agreement was observed. The FE results showed that, in the case of the rectangular and circular cross-sections, the steel tube and carbon fiber reinforced polymer confinement enhanced the load resistance capacity by approximately 34%

to 39% and the axial shortening of the column at the peak load by 136% to 57%, respectively. The efficiencies of CFRP confinement and steel tube increase initially as the axial load eccentricity increases, but they begin to decline as the column's failure mode changes to stability(Degefa Zewdu and Wondimu Aure, 2022).

The performance of high strength concrete columns reinforced with glass fiber-reinforced polymer fabrics and subjected to uniaxial eccentricity is being experimentally investigated in this work. The purpose of the study is to determine how much the structural performance of seven 200 x 200 x 1050 mm columns strengthened by external fiber-reinforced polymer fabrics could be improved. It also looks into the best way to achieve this improvement by arranging and sizing the fiber-reinforced polymer laminates. The quantity and configuration of fabric layers as well as the load eccentricity value are taken into account as test parameters. The laminates are loaded in small eccentricity in single or double layers, with partial or complete wrapping. When specimens are subjected to large eccentricity loading, longitudinal laminates are provided along their tension side. Through an increase in flexural capacity, the study has experimentally demonstrated the effectiveness of fiber-reinforced polymer laminates in strengthening uniaxially loaded high strength concrete columns (by up to 23% and 59% for small and large eccentricity loaded specimens, respectively). however, a significant ductility enhancement was achieved in large eccentricity specimens strengthened by fiber reinforced polymers(Hassan *et al.*, 2017).

The behavior of round-cornered, rectangular carbon fiber reinforced polymer-confined concrete short columns reinforced by an inner, high-strength elliptical steel tube under axial load is examined in this article using both nonlinear finite element analysis and multiple machine learning models. By comparison with the current experimental studies, the suggested nonlinear finite element model's reliability was confirmed. This study understands the impact of variables on column behavior, including concrete grade, wall thickness of reinforcing steel tube, inner steel tube cross-sectional size, and wall thickness of carbon fiber reinforced polymer. To further predict the test specimens' ultimate axial load, ultimate axial strain, and lateral strain, a number of machine learning models were proposed. According to the results of the parametric analysis, concrete with lower compressive strength exhibited greater strength enhancement due to confinement between the inner steel tube and carbon fiber-reinforced polymer than with high-strength concrete in relation to its unconfined compressive strength. In terms of predicting the axial load and axial and lateral strains of the columns, the extreme gradient boosting and random forest machine learning models were found to yield better fit outcomes than the artificial neural network and Gaussian process regression models (Isleem *et al.*, 2024).

In a double-tube concrete column, the outer fiber-reinforced polymer tube and the surrounding concrete effectively restrain the buckling of the core concrete, while the inner high strength steel tube effectively reduces the non-uniformity of stress distribution of the concrete in a concrete-filled square fiber-reinforced polymer tube. The results of an experimental investigation on the axial compressive behavior of double-tube concrete columns featuring an outer square polymer tube reinforced with fibers are presented in this work. Axial compression tests were performed on eight square Double-tube concrete column specimens. The parameters of the fiber-reinforced polymer tube that were analyzed were its thickness, width, and type. The experimental findings demonstrate that in square Double-tube concrete columns, the fiber-reinforced polymer tube and the higher strength steel tube effectively confine the concrete. Additionally, the buckling of the steel tube exhibits effective restraint, allowing its high material strength to be utilized to the maximum, resulting in excellent column performance. The outcomes of the experiment also show that square Double-tube concrete columns have a significant post-peak strength, indicating good ductility(Zeng *et al.*, 2018).

Rectangular double-tube concrete columns, a novel hybrid form of rectangular fiber-reinforced polymer-concrete-high strength steel columns, are presented in this work. These columns are made up of an elliptical high strength steel tube for internal reinforcement and a rectangular fiber-reinforced polymer tube filled with concrete. The majority of the concrete in the rectangular section is effectively confined because it is enclosed by the inner elliptical steel tube. It is expected that the confined concrete will reduce the high susceptibility of the high strength steel elliptical tube to local buckling, allowing the high strength steel to be fully utilized. Twelve rectangular double-tube concrete columns with varying fiber-reinforced polymer tube thicknesses and aspect ratios were tested under axial compression as part of the experimental study. In the end, the confinement effect from the inner elliptical high strength steel tube is taken into account in an existing stress-strain model for fiber-reinforced polymer-confined concrete in rectangular columns so that it can be applied to the concrete in the new column(Ye *et al.*, 2020).

2.6 Review of Design code

Composite column sections used in high-rise construction can be classified into three types, (a) Fully encased composite column (FEC); (b) Partially encased composite column (PEC); and (c) Concrete filled tube (CFST). Typical cross-sections of these three types of composite columns are shown in Figure 2.3 and Figure 2.4. As shown in (Figure 2.3(a)), in FEC columns the structural steel section is fully encased by surrounding concrete whereas in PEC columns (Figure 2. 1(b) and (c)) the steel section is partially encased by concrete. On the other hand, in concrete filled tubular composite columns (Figure 2.4(d, e, and f)) the

concrete is fully confined by the surrounding steel section. These composite sections have evolved to take the best out of the two materials i.e., concrete and steel. In these composite sections concrete provides compressive strength, stability, stiffness, improved fire proofing and better corrosion protection whereas steel provides tensile strength, ductility and high speed of construction. Among these three sections FEC column renders better fire proofing and corrosion protection since the steel section is fully encased by concrete. The cost for fire proofing and corrosion resistance is not required for FEC columns as compared to PEC and CFST columns

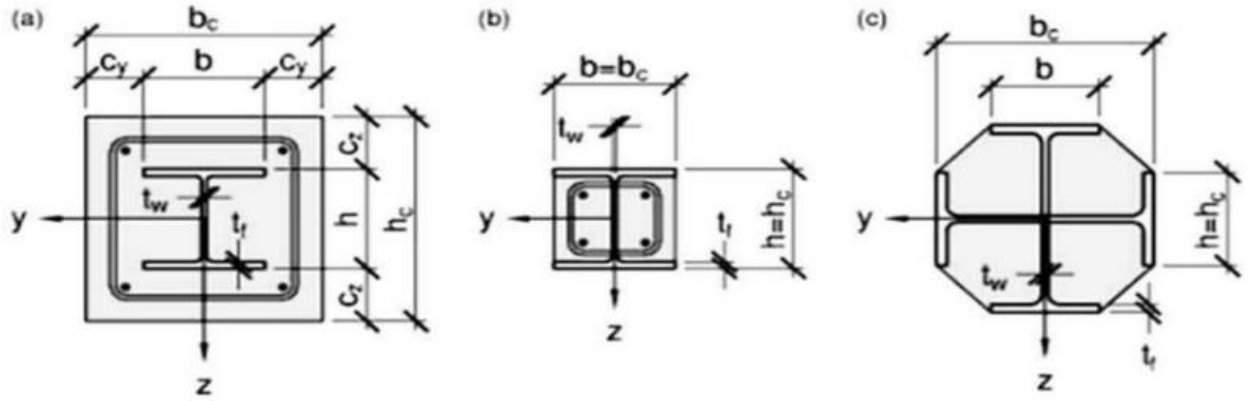

Figure 2.3: Typical Cross-Section of Composite Columns with Fully or Partially Concrete Encased H-Section(ES EN 1994, 2015)

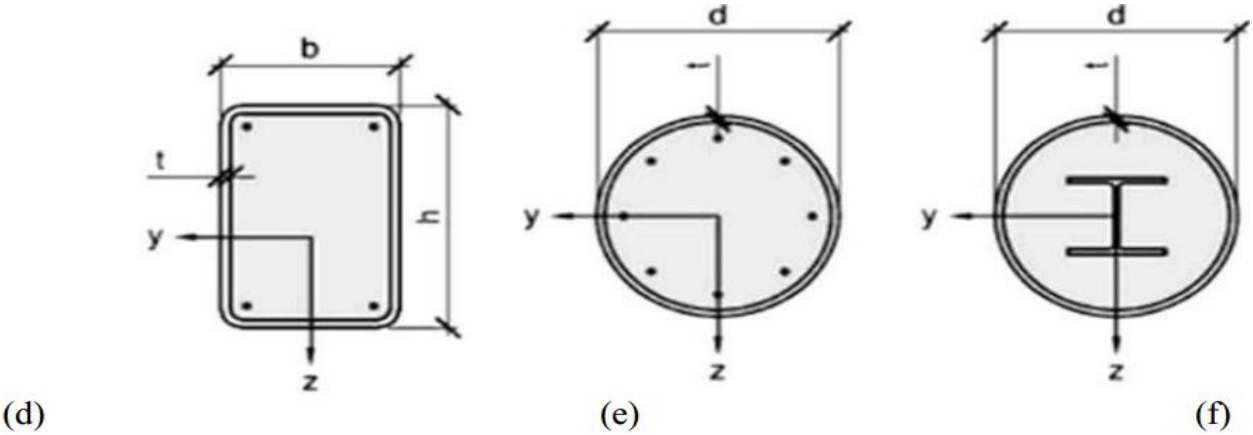

Figure 2.4: Typical Cross-Section of Composite Columns with Concrete-Filled Hollow Section(ES EN 1994, 2015)

For satisfaction of the main aim of this study; investigate the cumulative damage of composite columns subjected to axial loading by comparing the effects of different parameter on the axial capacity of composite columns, it is first necessary to review the design procedures that will be used for composite

concrete columns to be able to used them in this investigation. In fact, Eurocode presents the most recent rules and comprehensive review among other design codes and specifications. As a result, Eurocode 2, 3, and 4 were chosen for design of reinforce concrete, steel, and composite columns, respectively. For the composite columns design, Eurocode has mentioned some limitations which shall satisfy; the longitudinal reinforcement which can be used should be no more than 6% and not less than 0.3% of the concrete area, concrete grade used was normal concrete from C20/25 to C60/75, the steel contribution ratio must between 0.2 and 0.9 and 0.2 and 5 are given as limits for the depth to width ratio of the composite cross-section. In order to calculate the plastic resistance of composite columns, the plastic resistance of its components; the structural steel, the concrete and the reinforcement, should be adding. The plastic resistance equation for encased-composite column is:

$$N_{pl\ rd} = Aa\ f_{yd} + 0.85Ac\ f_{cd} + A_s\ f_{sd} \quad (2.1)$$

Where:

- ✓ Aa - the cross-sectional area of the structural steel
- ✓ Ac - the cross-sectional area of the concrete
- ✓ A_s - the cross-sectional area of the reinforcement
- ✓ f_{cd} - Design value of the cylinder compressive strength of concrete
- ✓ f_{sd} - Design value of the yield strength of reinforcing steel
- ✓ f_{yd} - Design value of the yield strength of structural steel

A new high-strength anisotropic structural material with standardized sections and less inherent variability than natural bamboo is called engineered bamboo composite. The characteristic values of mechanical behaviors are required in structural applications for safety reasons in order to construct the design values used in actual use. There has been little research on the sampling of the manufacturers in recent studies on engineered bamboo composite, instead concentrating on the mechanical properties from a single source. The current study examines the mechanical characteristics of two kinds of engineered bamboo composites that are available commercially: laminated veneer bamboo and parallel strand bamboo. This work's primary goal is to assess the mechanical properties and optimal probability distribution model (Weibull, log normal, and normal) for engineered bamboo composites in China, as well as to identify the characteristic values specified by ASTM D2915. About 4300 small, transparent specimens from seven manufacturers in five different Chinese raw bamboo origins were used to assess the mechanical properties in tensile, compression, and shear. Density and elastic modulus were the two predictors used to develop the strength grading of the

engineered bamboo composite subjected to compressive strength, based on the confidence band method. Many strength grades were constructed by utilizing the intervals of each predictor. The results of this study are crucial to the development of engineered bamboo composite standards and the continued use of these materials in structural engineering(Tang, Zhou and Li, 2021).

The primary cause of this is the lack of universally applicable standards and codes that could direct or aid in the development of the structural element design. Because of this, the use of bamboo as an engineering material was primarily reliant on long-standing customs, ancestors' instincts, and engineering expertise. This study examined current codes of practice and standards for structural element design. Based on the literary works, it was possible to draw the conclusion that in order to address various social and economic benefits as well as engineering recognition and improved status of bamboo as an engineering material, it is necessary to develop a comprehensive universally applicable bamboo design, construction standards, and code of practices(Amede *et al.*, 2021).

2.7 Summary and Research Gaps of the Literature

Based on a detailed literature survey, it is observed that we can use bamboo as construction material. Bamboo has many advantages than other construction material because good properties such as renewable material, economic benefits, low carbon content, high energy-saving and etc. bamboo is divided in to natural bamboo and engineering bamboo. Natural bamboo is anisotropic materials but Engineered bamboo aiming to mitigate the variability of the natural material can provide better material properties and structural performance, compared to original bamboo or raw bamboo. Considering the high tensile strength of bamboo fiber, bamboo slice twining tube is proposed to replace steel and fiber reinforced polymer as the confining jacket acting on concrete used for concrete-filled composite column. most studies on bamboo fiber tube concrete-filled composite column are experimental researches as described in the above literature reviews. But the existing experimental test on the replacement of steel tube by bamboo fiber tube of concrete filled composite column is insufficient, and it cannot express all behavioral aspects of this column. so, before using bamboo fiber tube use as construction material to investigate the ductility properties, the effect of eccentric loading, effect diameters of bamboo fiber tube, load application and BST-bamboo thickness by using finite element method which is not done on above literature review.

CHAPTER THREE

3. RESEARCH METHODOLOGY

3.1 General

This chapter presents and describes the approaches and techniques that I was used to collect data and investigate the research problem. This includes the research design, study population, sample size and selection, sampling techniques and procedure, data collection methods, data quality control (validity and reliability), procedure of data collection, data analysis, Ethical consideration.

3.2 Research Design

The research design was theoretical researches which were essential for the Non-Linear Finite Element Analysis of Bamboo Fiber Tube Concrete-Filled Composite Column with the ductility behavior, effects of eccentric loading, effects of bamboo fiber tube diameter, effects of load and BST-bamboo thickness on the action of uniaxial load using finite element analysis of ABAQUS©CAE. This research was a systematic investigation to fill the gap of knowledge on the Non-Linear properties of Bamboo Fiber Tube Concrete-Filled Composite Column. On the other hand, it was a process for collecting, analyzing and interpreting information to provide a recommendation to the research findings.

After comprehensively, organizing literature review of different previous published researches, designate the non-Linear Finite Element Analysis of Bamboo Fiber Tube Concrete-Filled Composite Column with the ductility behavior, effects of eccentric loading, effects of bamboo fiber tube diameter, effects of load application and BST-bamboo thickness. Validation for the finite element modeling is conducted on pre-qualified and practical tested for bamboo fiber tube concrete-filled composite column under axial loading. After that specific study parameters were introduced in this study for concrete-filled composite column to investigate the influence of these parameters on the non-Linear properties of bamboo fiber tube concrete-filled composite column in cooperative technique.

The study programs divided into four main parts of research design are: -

- ✓ Identify the property of materials (Concrete and Bamboo fiber tube) used as in put of finite element Analysis as discussed under section 3.10.2
- ✓ Modeling bamboo fiber tube concrete-filled composite column by using ABAQUS©CAE. See (section 3.10.)

- ✓ The validation of the finite element (FE) analysis result with the results from experimental test. In order to verify the simulation process is correct discussed in sec 4.2.
- ✓ Parametric study. (Discussed in section 3.12)

3.3 Study Variables

3.3.1 Independent variable

The independent variables, which will be measured and manipulated to determine its relationship to observed phenomena, are selected and listed below.

- ✓ Eccentricity.
- ✓ Bamboo fiber tube diameter.
- ✓ BST-bamboo thickness.
- ✓ Load application

3.3.2 Dependent variable

The dependent variables, which will be observed and measured to determine the effect of the independent variables is; -

- ✓ Axial load enhancement and axial load capacity of column
- ✓ Axial stress capacity enhancement of column.
- ✓ Axial strain and displacement magnitude of concrete-filled composite column.
- ✓ Ductility properties of concrete-filled composite column.
- ✓ Failure mode of concrete-filled composite column.

3.4 Population and Sampling Method

The main purpose of this study was to investigate the cumulative damage of concrete-filled composite column subjected to concentric and eccentric axial loading by comparing the effects of eccentric loading, effects of bamboo fiber tube diameter, effect of load application and BST-bamboo thickness of the column to evaluate the stiffness, strength enhancement and ductility of the column. To achieve this, a finite element analysis was conducted with all appropriate parameters considered. The finite element method is a numerical analysis technique for obtaining approximate solutions to a wide variety of engineering problems. For this study there were a total of twenty-one (21) columns which was selected as a sample with different independent variable. From twenty-one, eighteen (18) are for parametric study and three (3) columns is from experimental literature for validation of the model.

Table 3 1: Details of specimen

Table of Specifications								
S. NO	Specimen Samples	thickness of BST	Eccentric Loading	Diameter of BST-Bamboo	Load application	Diameter of core concrete	Concrete grade	Length of column
1	BCC-5	5.8mm	0mm	169.6mm	on BCC column	158mm	32.7mpa	300mm
2	BCC-51	5.8mm	5mm	169.6mm	on BCC column	158mm	32.7mpa	300mm
3	BCC-52	5.8mm	10mm	169.6mm	on BCC column	158mm	32.7mpa	300mm
4	BCC-53	5.8mm	15mm	169.6mm	on BCC column	158mm	32.7mpa	300mm
5	BCC-54	5.8mm	20mm	169.6mm	on BCC column	158mm	32.7mpa	300mm
6	BCC-8	9.5mm	0mm	177mm	on BCC column	158mm	32.7mpa	300mm
7	BCC-81	9.5mm	5mm	177mm	on BCC column	158mm	32.7mpa	300mm
8	BCC-82	9.5mm	10mm	177mm	on BCC column	158mm	32.7mpa	300mm
9	BCC-83	9.5mm	15mm	177mm	on BCC column	158mm	32.7mpa	300mm
10	BCC-84	9.5mm	20mm	177mm	on BCC column	158mm	32.7mpa	300mm
11	BCC-10	12mm	0mm	182mm	on BCC column	158mm	32.7mpa	300mm
12	BCC-101	12mm	5mm	182mm	on BCC column	158mm	32.7mpa	300mm
13	BCC-102	12mm	10mm	182mm	on BCC column	158mm	32.7mpa	300mm
14	BCC-103	12mm	15mm	182mm	on BCC column	158mm	32.7mpa	300mm
15	BCC-104	12mm	20mm	182mm	on BCC column	158mm	32.7mpa	300mm
16	BCC-55	5.8mm	0mm	211.6mm	on BCC column	200mm	32.7mpa	300mm
17	BCC-56	5.8mm	0mm	261.6mm	on BCC column	250mm	32.7mpa	300mm
18	BCC-57	5.8mm	0mm	311.6mm	on BCC column	300mm	32.7mpa	300mm
19	CBCC-5	5.8mm	0mm	169.6mm	on core concrete	158mm	32.7mpa	300mm
20	CBCC-8	9.5mm	0mm	177mm	on core concrete	158mm	32.7mpa	300mm
21	CBCC-10	12mm	0mm	182mm	on core concrete	158mm	32.7mpa	300mm

3.5 Sources of Data

The primary data from ABAQUS results and secondary data were from ES EN 2015 code and different journals including published research papers.

3.6 Data Collection Procedure

The data collection for this research used the related topic literatures from high rated journals, ongoing researches, books, and structural design journals, construction engineering journals and construction

management journals, relevant practices related to Bamboo Fiber Tube Concrete-Filled Composite Column with previous experimental results using finite elements analysis ABAQUS©CAE software and which was related to Non-Linear properties of Bamboo Fiber Tube Concrete-Filled Composite Column was accessed. An approach was going to conduct number of Finite Element Analysis to observe the behavior of non-Linear properties of Bamboo Fiber Tube Concrete-Filled Composite Column with effects of eccentric loading, effects of bamboo fiber tube diameter, load application and BST-bamboo thickness under axial loading.

3.7 Model samples and cross sections used in this study Program

The study program consisted of twenty-one (21) Bamboo Fiber Tube Concrete-Filled Composite Column. Details of these columns are given in Table 3.1. The first letter in the Specimen Samples designation refers the column and the number used in the Specimen Samples designation was simply the serial number as they appeared in the table. All columns of these groups have modeled with identical material properties, length of column but different by parametric study such as eccentric loading, bamboo fiber tube diameter, load application and BST-bamboo thickness. These columns were circle in size and constructed with normal strength concrete. The columns were tested for concentric and eccentric loads, to observe the failure behavior and non-Linear properties of Bamboo Fiber Tube Concrete-Filled Composite Column. The loads versus deformation, stress versus strain and ductility behavior of these Bamboo Fiber Tube Concrete-Filled Composite are analyzed by finite element method.

3.8 Finite Element Method

The goal of this research was to model and analyze the three-dimensional geometry of a Bamboo Fiber Tube Concrete-Filled Composite Column numerically using the commercial finite element modeling software package ABAQUS. The section that follows explains how to model and analyze a Bamboo Fiber Tube Concrete-Filled Composite Column in order to determine how it will behave under axial loading conditions.

Finite element analysis (FEA) is a process, which predicts deflection and other effects of stress on a structure. The structure is divided up into a grid of elements by FEA, creating a model of the actual structure. Every element is a straight forward shape (such as a square or a circle), for which the finite element program has the necessary data to express the governing equation as a stiffness matrix. The displacements at the node sites, or the locations where elements are joined, are the unknowns for each element. The global stiffness matrix for the entire model will be assembled by the finite element program using the stiffness

matrices for the simple elements. The unknown displacement at the nodes of this stiffness matrix is solved, and the stress at each element can be determined.

In recent years, finite element method (FEM) software like ABAQUS, DIANA, ANSYS, etc. have been used to perform the majority of numerical investigations on structural elements. A sophisticated finite element program ABAQUS was used in this study to perform nonlinear finite element analysis due to its ability to simulate one, two, and three-dimensional models and the variety of nonlinear material models it offers. The three main products in the ABAQUS program suite are ABAQUS/CAE, ABAQUS/Standard, and ABAQUS/Explicit. The primary product is the whole ABAQUS environment and uses a graphical user interface to allow users to generate, evaluate, and view model output all in one place (GUI). ABAQUS/CAE provides the option of importing CAD models that have been created by other compatible programs or drawing the model geometries using the software's drawing tools. ABAQUS/CAE supports both Standard and Explicit version for pre-processing and post-processing simulation.

In the present study, three dimensional (3-D) nonlinear finite element analyses of Bamboo Fiber Tube Concrete-Filled Composite Column are carried out using ABAQUS/Explicit. Studies employing ABAQUS to analyze the responsiveness of structural elements have usually focused on component-level responses. Additionally, some researchers simulate the full response of reinforced concrete structures under seismic loading using ABAQUS. Crack development, damage pattern and displacement ductility of a pre-stressed precast reinforced concrete frames under cyclic loading with solid 3D elements for concrete, linear-truss elements for the reinforcing and pre-stressed steel was studied.

Advantage of Finite element Method

Numerous structural and nonstructural problems have been solved using the finite element method. This approach is highly well-liked because it has several benefits. They consist of the capacity for:

- It's simple to model bodies with irregular shapes.
- Model bodies made of various materials because the element equations are evaluated separately
- Handle general load conditions without trouble
- Manage an infinite variety of boundary conditions
- Altering the finite element model is relatively simple and inexpensive.

- Vary the size of the elements to enable the usage of small elements where necessary.

- Include dynamic effects, take into account nonlinear behavior caused by significant deformations, and deal with nonlinear material.

The structural analysis finite element approach enables the designer to identify stress, vibration, and thermal problems during the design phase and to assess design changes prior to the potential prototype's construction. As a result, there is increased confidence in the prototype's acceptability. Additionally, if applied correctly, the strategy can lower the necessity for creating as many prototypes. Nowadays this is often known as the 'solver'. The output was produced as text data. The use of FEA has been the preferred method to study the behavior of Bamboo Fiber Tube Concrete-Filled Composite Column.

3.9 Data Presentation and Analysis

An analysis of Bamboo Fiber Tube Concrete-Filled Composite Column was used finite elements analysis. Finite Element Analysis (FEA) of Bamboo Fiber Tube Concrete-Filled Composite Column specimens is performed in a nonlinear static analysis format and the analysis procedure considers both material and geometric nonlinearities. In a nonlinear analysis, the total specified loads acting on a finite element body will be divided into a number of load increments. At the end of each increment the structure is in approximate equilibrium and the stiffness matrixes of structure were modified in order to reflect nonlinear changes in structure's stiffness.

The general-purpose finite element program ABAQUS©CAE used in this study is to investigate the effect of using different eccentric loading, different bamboo fiber tube diameter and load application under uniaxial load. A three-dimensional 3D finite element model will be developed to account for geometric and material nonlinear behavior of Bamboo Fiber Tube Concrete-Filled Composite Column. Every complete finite-element analysis consists of three separate stages:

- ✓ **Pre-processing or modeling:** This stage involves creating an input file, which contains an engineer's design for a finite-element analyzer. Pre-processing involves creating a geometric representation of the structure, then assigning properties, then outputting the information as a formatted data file (.dat) suitable for processing by ABAQUS©.

- ✓ **Processing or finite element analysis (solver):** This is sets of linear or nonlinear algebra equations are solved simultaneously to obtain nodal results, such as displacement values at different nodes or temperature values at different nodes in heat transfer problems.

- ✓ **Post-processing or generating:** In this process, the results can be processed to show the contour of displacements, stresses, strains, reactions and other important information. Graphs as well as the deformed shapes of a model can be plotted and report, image, animation are also prepared from this output.

ABAQUS/Standard uses the Newton-Raphson method to obtain solutions for nonlinear problems. Newton–Raphson equilibrium iterations provide convergence at the end of each load increment within tolerance limits for all degrees of freedom in the model. In addition to this commercial computer software package ABAQUS© program, the following programs will be applying: Microsoft Word and Microsoft excel were used for preparation of the report.

3.10 Finite Element Modeling of Concrete-Filled Composite Column

The modeling and analysis procedures were described one by one as shown below. This section provides a description of the finite element model developed in this study. It begins with an overview of the process that led to development of the model followed by a more in-depth look at individual aspects of the model; examining first the simplification of the physical specimen's geometry, followed by a description of the mesh elements used to discretize the geometry, an overview of boundary conditions imposed on the mesh, and a description of the various material models that define the behavior of the model. ABAQUS is a general-purpose finite element programmed and it may be used to simulate the test. The finite element method is a technique for approximating the governing different equation for a continuous system with a set of algebraic equations relating a finite number of variables. These methods are popular because they can be easily programmed the FE techniques problems The main components of the FE model included the core plain concrete and bamboo fiber tube as shown in below in detailed. All components were modelled separately and assembled together to form one test specimen. Experimental tests are needed to provide input data to the model and for the purpose of verification of simulation results. All the specimens were modeled and analyzed after the FEA software is validated for the specific case of this research. When the model has been validated it can be used for parametric studies to investigate the influence of various parameters. The validation process was described in detail in the next chapter.

3.10.1 Parts (Geometry) Modeling

3.10.1.1 Concrete Column

Concrete Column parts were modeled on a 3D modeling space as deformable type with solid shape and extrusion type base feature. The plain concrete column 150mm diameter extruded with the column lengths.

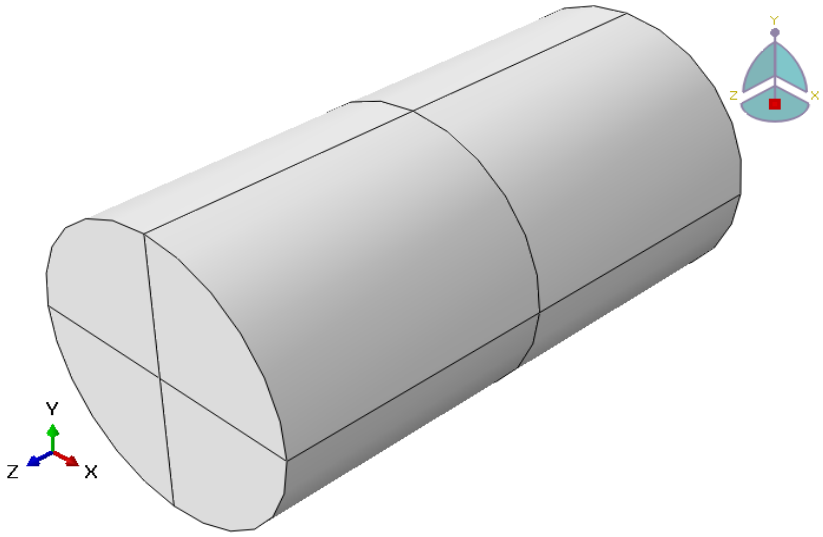

Figure 3. 1: plain Concrete Column part

3.10.1.2 Bamboo fiber tube

Bamboo fiber tube column parts were modeled on a 3D modeling space as deformable type with solid shape and extrusion type base feature. The outer bamboo fiber tube with outer diameter 169.6mm and thickness of bamboo fiber tube 5.8mm for BST-5, outer diameter 177mm and thickness of bamboo fiber tube 9.5mm for BST-8 and outer diameter 182mm and thickness of bamboo fiber tube 12mm for BST-10 extruded with column lengths.

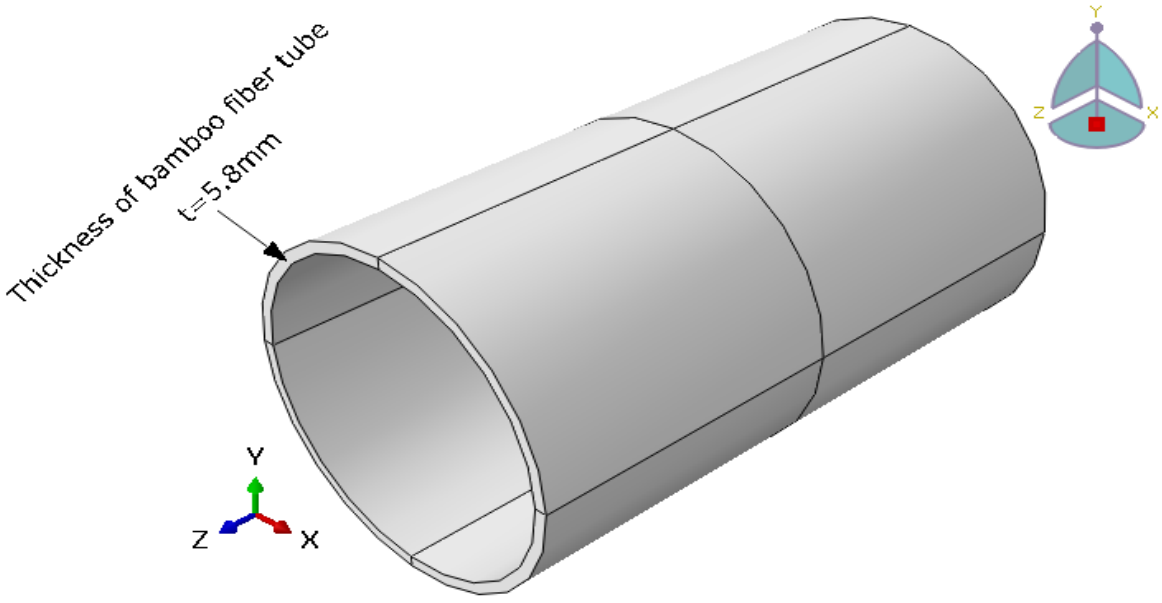

Figure 3. 2: BST-5 Column part

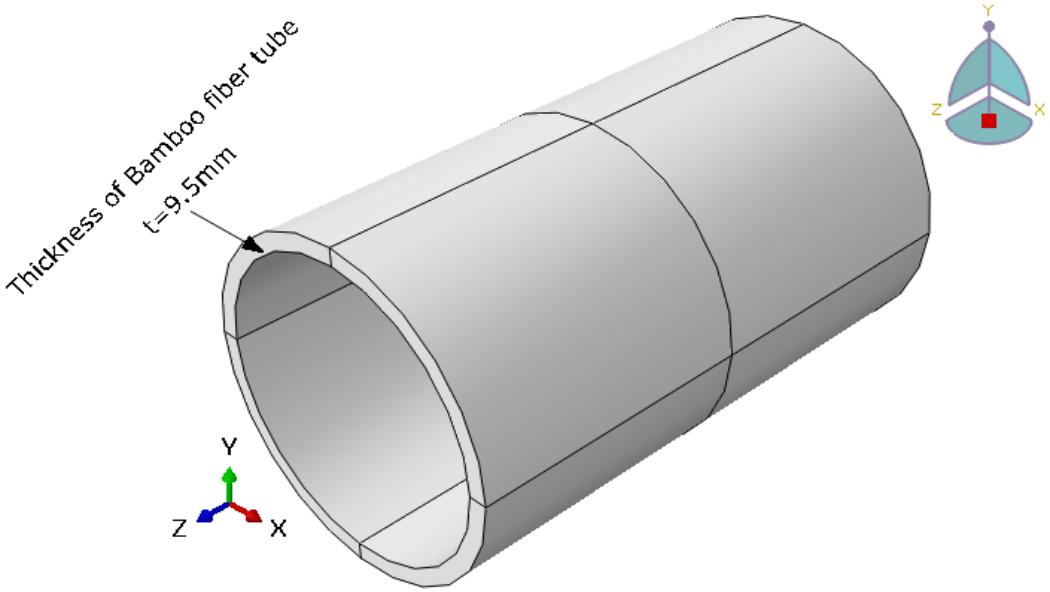

Figure 3. 3: BST-8 Column part

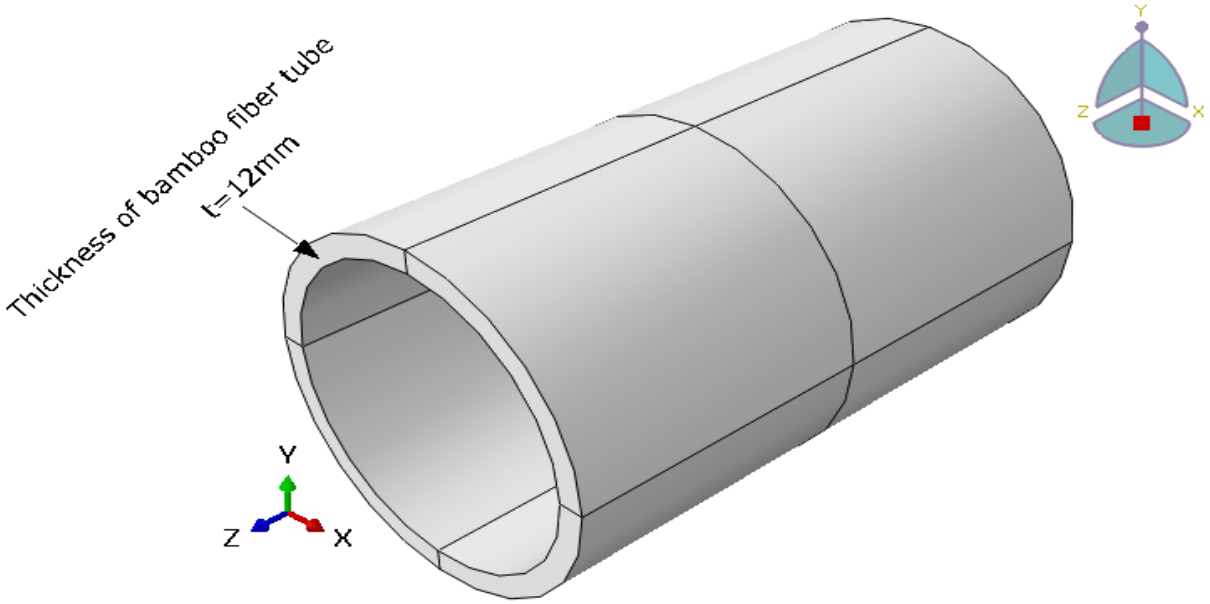

Figure 3. 4: BST-10 Column part

3.10.1.3 Support and Loading Steel Plates

Steel Plates were used at the bottom end as support and on top of the column as loading plate. They were modeled on a 3D modeling space as discrete rigid type with shell shape and planar shape base feature. The diameter of plate is 169.6mm for BCC-5, 177mm for BCC-8 and 182mm for BCC-10 column. The part is face partitioned and has reference point at the center for the purpose of support, loading and boundary conditions.

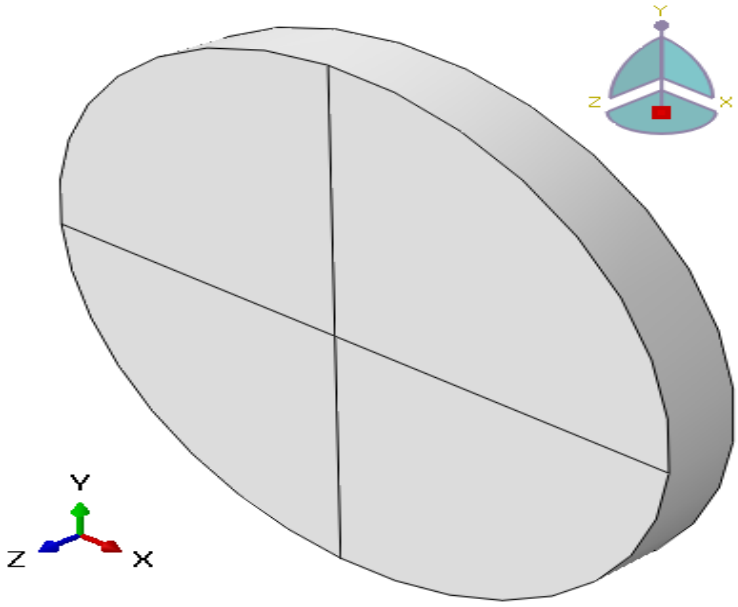

Figure 3. 5: Support and Loading Steel Plate

3.10.2 Material Modeling

The material definition is an important part of finite element analysis, and each component should be defined carefully and all parts should be defined with appropriate material parameters. Bamboo and concrete are the main materials used in construction of columns for this study. The nonlinear behavior of materials was incorporated in the FE model using the appropriate material models for concrete that available in the ABAQUS© finite element code. The nonlinear behavior of bamboo used in FE model is available in experimental (Kou, Tian and Jin, 2021) research used for validation. The description of the material models for bamboo and concrete along with their mechanical properties (stress versus strain relationship) used in the FE model is described in the following sections. After material properties were created, profile and section for each part were prepared and assign to their corresponding parts

3.10.2.1 Material model of Concrete

The concrete model is a very important part of the simulation for the push off model, the concrete is mainly subjected to compression and tensile splitting as observed in the experimental study. Therefore, a suitable concrete material model is very important for the accuracy of the FE model. In terms of the behavior of concrete, the concrete damaged plasticity model was used to define the concrete in this study. This concrete model is capable to model the concrete under arbitrary loading, including dynamic loading and assumes an isotropic damaged elasticity in tension and compression to present the inelastic behavior of concrete. The damaged plasticity model can be used for plain concrete as well as for RC structures subjected to monotonic,

cycling and dynamic loading under low confining pressure. Concrete damage plasticity model has been successfully used for the core concrete column by (Kou, Tian and Jin, 2021) in numerical modelling. The damage plasticity model may deal with two basic failure modes, compressive crushing and tensile cracking of concrete. In this study, the damage plasticity model was adopted and the maximum tensile strength of concrete was taken as 10% of its compressive strength.

a. Unconfined properties of concrete in column

(ES EN 1992, 2015) will be used in this study for the unconfined concrete, the relation between σ_c and ε_c under uniaxial loading was described in (ES EN 1992, 2015, and it proposed single equation to describe unconfined concrete stress strain behavior as follow by expression (3.1). On the basis of uniaxial compression test results one can accurately determine the way in which the material behaved. However, a problem arises when the person running such a numerical simulation has no such test results or when the analysis is performed for a new structure. Then often the only available quantity is the average compressive strength (f_{cm}) of the concrete. Another quantity which must be known in order to begin an analysis of the stress-strain curve is the longitudinal modulus of elasticity (E_{cm}) of the concrete. Its value can be calculated using the relations available in the literature(ES EN 1992, 2015).

$$\frac{\sigma_c}{f_{cm}} = \frac{k\eta - \eta^2}{1+(k-2)\eta} \quad (3.1)$$

$$where,\ \ k = 1.05E_{cm}\frac{\varepsilon_{c1}}{f_{cm}} \quad (3.2)$$

$$\eta = \frac{\varepsilon_c}{\varepsilon_{c_1}} \quad (3.3)$$

$$\varepsilon_{c_1} = 0.7(f_{cm})^{0.31} \quad (3.4)$$

$$\varepsilon_{cm} = 22(0.1f_{cm})^{0.3} \quad (3.5)$$

$$\varepsilon_{cu} = 3.5\% \quad (3.6)$$

$$f_{cm} = f_{ck} + 8 \quad (3.7)$$

Where

ε_{c_1}-is strain at average compressive strength

f_{cm}-is mean value of concrete cylindrical comparative strength (Mpa)

E_{cm}-is the longitudinal modulus of elasticity (Mpa)

f_{ck}-is characteristic cylindrical strength of concrete (Mpa) all of the above equation are from(ES EN 1992, 2015).

The above equation is valid for $0<\varepsilon_c < \varepsilon_{cu1}$ where ε_{cu1} nominal ultimate strain. Figure 3.3 describe the developed stress strain relationship as provided in(ES EN 1992, 2015).

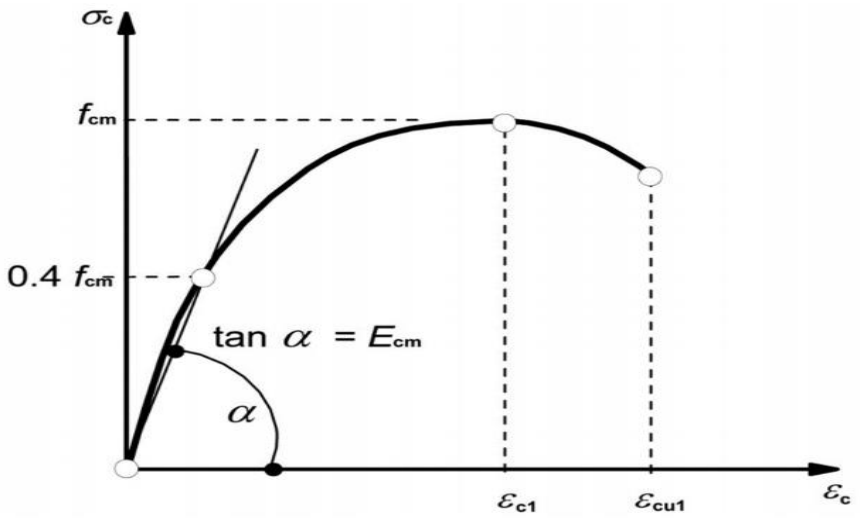

Figure 3.6: Schematic representative of the stress-strain relation of structural analysis (the use $0.4f_{cm}$for the definition of E_{cm} is approximate)(ES EN 1992, 2015).

b. Confined properties of concrete in column

Confinement of concrete results in a modification of the effective stress relationship: higher strength and higher critical strains are achieved. The other basic material characteristics may be considered as unaffected for design. In the absence of more precise data, the stress-strain relation shown in Figure 3.4 (compressive strain shown positive) may be used, with increased characteristic strength and strains according to:

$$f_{ck,c} = f_{ck}\left(1.00 + 5.0\frac{\sigma_2}{f_{ck}}\right) \qquad for\ \sigma_2 \leq\ 0.005f_{ck} \tag{3.8}$$

$$f_{ck,c} = f_{ck}\left(1.125 + 2.50\frac{\sigma_2}{f_{ck}}\right) \qquad for\ \sigma_2\ > 0.005f_{ck} \tag{3.9}$$

$$\varepsilon_{c2,c} = \varepsilon_{c2}(\frac{f_{ck,c}}{f_{ck}})^2 \tag{3.10}$$

$$\varepsilon_{cu2,c} = \varepsilon_{cu2} + 0.2\frac{\sigma_2}{f_{ck}} \quad (3.11)$$

Where: $\sigma_2=\sigma_3$ is the effective lateral compressive stress at the ULS due to confinement and ε_{c2}=2% and ε_{cu2}=3.5% follow from code provision. Confinement can be generated by adequately closed links or cross-ties, which can reach the plastic condition due to lateral extension of the concrete.

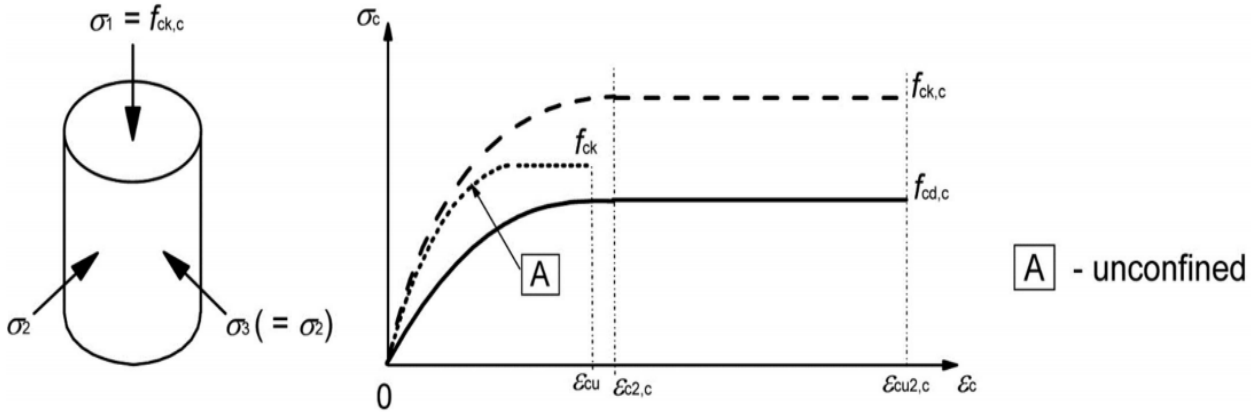

Figure 3.7: Stress-Strain relationship for Confined Concrete(ES EN 1992, 2015).

C. Tension properties of concrete

ABAQUS© provides a number of options for defining tensile behavior of concrete. The stress can be related to the strain in the direction of the cracking or displacement which refers to crack width, and fracture energy, G_f. Alternatively, the fracture energy, G_f can be specified directly as a material property; in this case, define the failure stress, as a tabular function of the associated fracture energy. This model assumes a linear loss of strength after cracking in ABAQUS© software. The cracking displacement at which complete loss of strength takes place is, therefore, $\varepsilon_{to} = 2G_f / \sigma_{to}$ Typical values of G_f range from 40 N/m for a typical construction concrete (with a compressive strength of approximately 20 MPa, to 120 N/m for a high-strength concrete (with a compressive strength of approximately 40 MPa. If tensile damage, d_t is specified, ABAQUS© automatically converts the cracking displacement values to "plastic" displacement values using the relationship:

$$\varepsilon_t^{pl} = \varepsilon_t^{ck} - \frac{d_t}{1-d_t} * \left(\frac{\sigma_t}{E_O}\right) \quad (3.12)$$

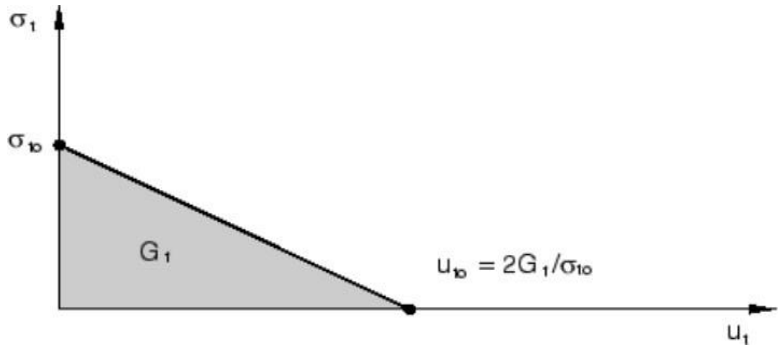

Figure 3. 8: Post failure stress-fracture energy curve. (ABAQUS user Manual)

d. Damage plasticity modeling of concrete

Damage is defined both for uniaxial tension and compression on during softening procedure in concrete damage plasticity model. Damage in compression occurs just after reaching to the maximum uniaxial compressive strength corresponding to strain level ε_o. The degradation of elastic stiffness in softening regime is characterized by two damage variables, d_t and d_c corresponding to tensile and compressive damage, respectively, which are assumed to be functions of the plastic strains. Tensile and compressive damage in concrete damage plasticity model in the presented numerical model is assumed to be according to equations above and diagrams of Figure 3.7 and Figure 3.8.

ABAQUS© software provides the capability of simulating the damage using either of the three crack models for concrete elements: (1) Smeared crack concrete model, (2) Brittle crack concrete model, and (3) Concrete damaged plasticity model. Out of the three concrete crack models, the concrete damaged plasticity model is selected in the present study as this technique has the potential to represent complete inelastic behavior of concrete both in tension and compression including damage characteristics. Further, this is the only model which can be used both in ABAQUS©/Standard and ABAQUS©/Explicit and thus enable the transfer of results between the two. Therefore, development of a proper damage simulation model using the concrete damaged plasticity model will be useful for the analysis of reinforced concrete structures under any loading combinations including both static and dynamic loading. The concrete damaged plasticity model assumes that the two main failure mechanisms in concrete are the tensile cracking and the compressive crushing. In this model, the uniaxial tensile and compressive behavior is characterized by damaged plasticity. Concrete damaged plasticity model takes into consideration the degradation of the elastic stiffness induced by plastic straining both in tension and compression. It also accounts for stiffness recovery effects under cyclic loading. The compressive behavior is elastic until initial yield and then is characterized by stress

hardening followed by strain softening after the ultimate point. ABAQUS© manual proposes an exponential function which can calculate the tensile damage variable (*dt*) and the compressive damage variable (*dc*)

$$\sigma_t = (1 - d_t)E_O(\varepsilon_t - \varepsilon_{tpl}) \quad (3.13)$$

$$\sigma_c = (1 - d_c)E_O(\varepsilon_c - \varepsilon_{cpl}) \quad (3.14)$$

e. Tension Stiffening Relationship

In order to simulate the complete tensile behavior of reinforced concrete in ABAQUS©, a post failure stress-strain relationship for concrete subjected to tension (similar to Figure 3.12) is used which accounts for tension stiffening, strain-softening, and steel concrete interaction with concrete. To develop this model, user should input young's modulus (E_o), stress (σ_t), cracking strain (ε_t^{ck}) values and the damage parameter values (dt) for the relevant grade of concrete. The cracking strain (ε_t^{ck}) should be calculated from the total strain using (equation 3.15) below:

$$\varepsilon_t{}^{ck} = \varepsilon_t - \varepsilon_{ot}{}^{el} \quad (3.15)$$

$$Where, \varepsilon_{ot}{}^{el} = \frac{\sigma_t}{E_o} \quad the\ elastic\ strain\ corresponding\ to\ the\ undamed\ mterial \quad (3.16)$$

$$\varepsilon_t = total\ strain$$

Having defined the yield stress-inelastic strain pair of variables, one needs to define now degradation variable d_c. It ranges from zero for an undamaged material to one for the total loss of load-bearing capacity. These values can also be obtained from uniaxial compression tests, by calculating the ratio of the stress for the declining part of the curve to the compressive strength of the concrete. Thanks to the above definition the CDP model allows one to calculate plastic strain from the formula:

$$\varepsilon_t{}^{pl} = \varepsilon_t{}^{ck} - \frac{d_c}{(1 - d_c)} * \left(\frac{\sigma_t}{E_o}\right) \quad (3.17)$$

Where; E_0 stands for the initial modulus of elasticity for the undamaged material. Knowing the plastic strain and having determined the flow and failure surface area one can calculate stress σ_t for uniaxial compression and its effective stress σ_t

$$\sigma_t = [1 - d_c]E_o[\varepsilon_t - \varepsilon_t{}^{pl}] \quad (3.18)$$

The damage plasticity constitutive model was based on the following stress–strain relationship:

$$\sigma_t{}^{-} = \frac{\sigma_t}{(1-d_c)} = E_o(\varepsilon_t - \varepsilon_t{}^{pl}) \tag{3.19}$$

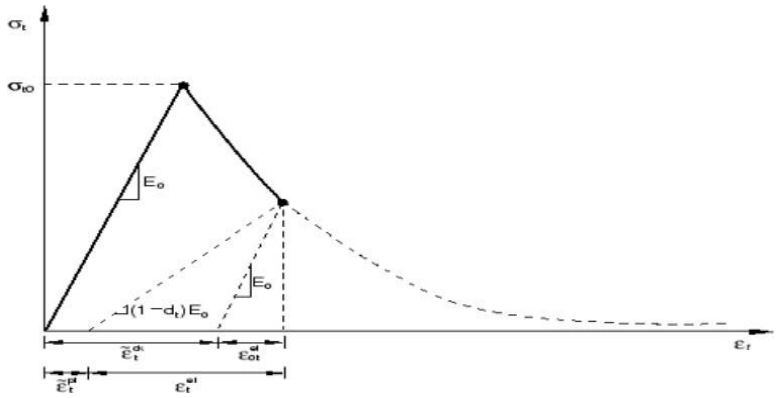

Figure 3. 9: Terms for Tension Stiffening Model (ABAQUS user Manual)

Where *dt* and *dc* were two scalar damage variables, ranging from 0 (undamaged) to 1 (fully damaged). The damage model used for concrete was based on plasticity and considered the failure process of tensile cracking and compressive crushing. The uniaxial compressive and tensile responses of concrete with respect to the concrete damage plasticity model subjected to compression and tension load were given by:

$$\varepsilon_c{}^{pl} = \varepsilon_c{}^{ck} - \frac{d_c}{(1-d_c)} * \left(\frac{\sigma_c}{E_o}\right) \tag{3.20}$$

$$\sigma_c = [1-d_c]E_o[\varepsilon_c - \varepsilon_c{}^{pl}] \tag{3.21}$$

$$\sigma_c{}^{-} = \frac{\sigma_c}{(1-d_c)} = E_o(\varepsilon_c - \varepsilon_c{}^{pl}) \tag{3.22}$$

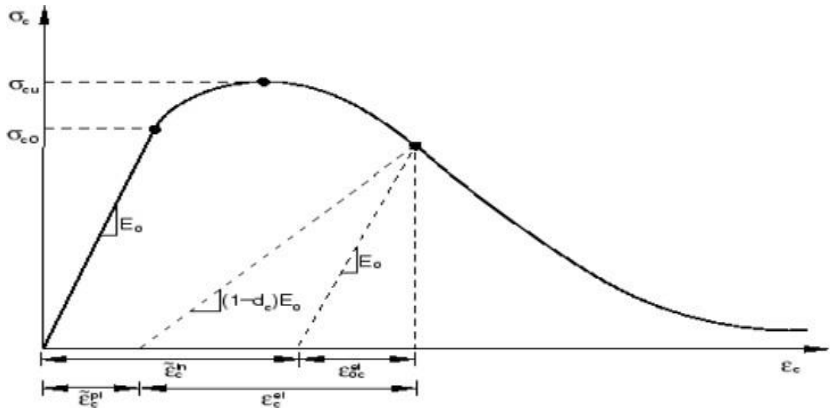

Figure 3.10: Response of concrete to a uniaxial loading in compression (Abaqus Manual)

Another parameter describing the state of the material is the point in which the concrete undergoes failure under biaxial compression. (fb0 / fc0) is a ratio of the strength in the biaxial state to the strength in the uniaxial state. The ABAQUS user's manual specifies default (fb0 / fc0) =1.16. The last parameter characterizing the performance of concrete under compound stress is dilation angle, i.e., the angle of inclination of the failure surface towards the hydrostatic axis, measured in the failure plane. Physically, dilation angle ψ is interpreted as a concrete internal friction angle. In simulations usually ψ = 33.99° were used for the corresponding concrete grades C32.7

Table 3. 2: Default parameters of CDP model under compound stress

Parameters	Dilation angle	Eccentricity	f_{b0}/f_{c0}	k	viscosity
Value	33.99	0.1	1.16	0.6667	0

3.10.2.2 Material model of Bamboo fiber tube

The tensile and compressive measured stress–strain curves are displayed in Fig. 3.1 (T–5–1) represents the first tensile coupon of the 5-layer LBL slice parallel to the fiber, and so on). LBL slices and BSTs exhibit linear stress–strain behaviors under tension parallel to fiber, and rupture at their ultimate strain. The tensile strength and elastic modulus of the BSTs increase by 120% and 50%, respectively, compared with those of the LBL slice. Through the data collected by the strain gauges, the Poisson's ratio of the BSTs under tension parallel to fiber and compression perpendicular to fiber are measured as 0.325 and 0.098 respectively. Furthermore, the mechanical properties of the BSTs are close to those of the engineered bamboo. The stress strain relationship of bamboo fiber tube for nonlinear analysis is shown in Figure 3.11(Kou, Tian and Jin, 2021).

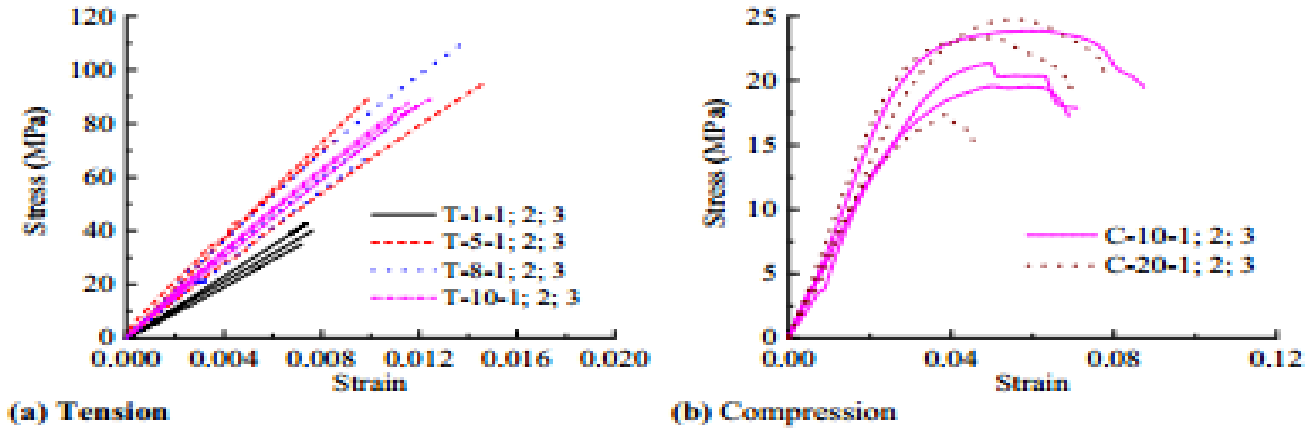

Fig. 3.11: Measured stress–strain curves of the bamboo fiber tube(Kou, Tian and Jin, 2021)

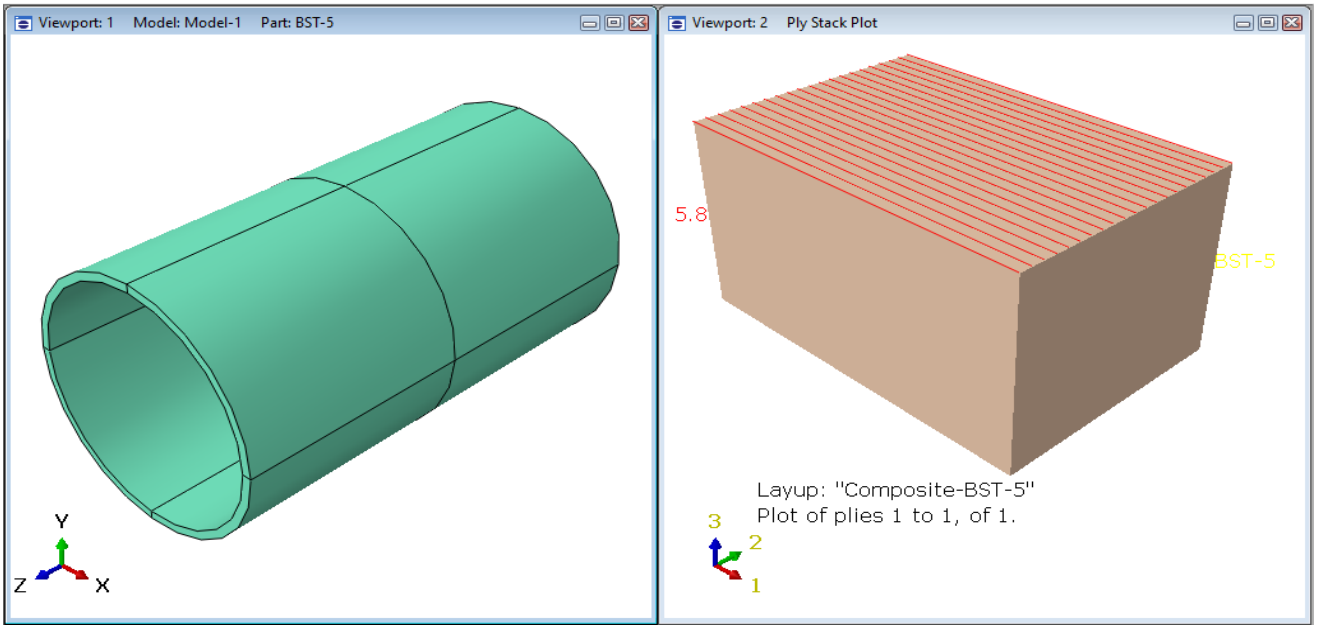

Fig. 3.12: Composite material modeling in ABAQUS 2023 for BST-5

3.10.3 Part assembly in Modeling

After material properties, profiles and sections were created and assigned for the parts; instances were created for all parts and assembled to their relative position. Dependent instance was used for all parts. In these sections all parts were arranged on theirs position according to test set up form one modeled. Here there were three types of assembled model which differentiate by the thickness of bamboo fiber tube.

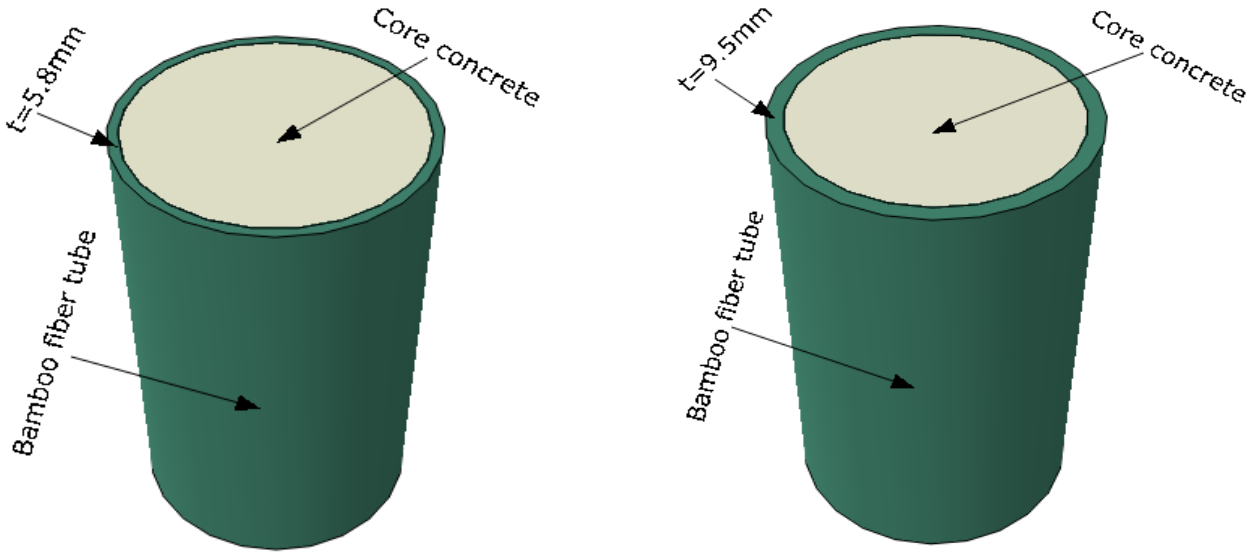

Figure 3.13: Part assembly in modeling for BCC-5 and BCC-8

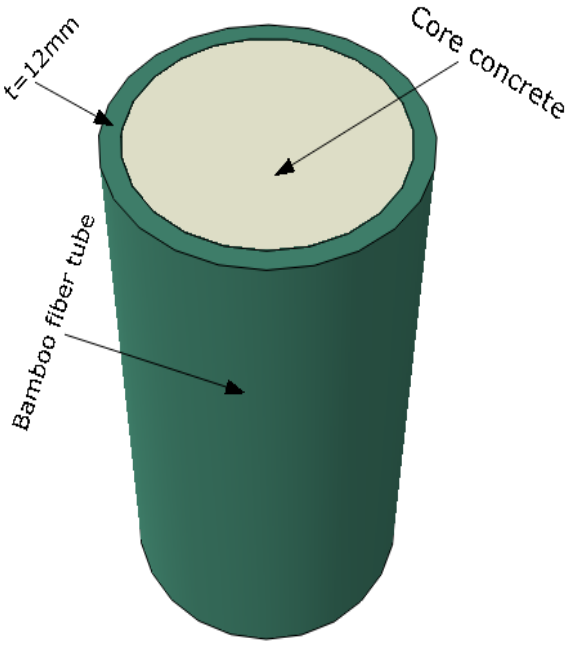

Figure 3. 15: Part assembly in Modeling for BCC-10

3.10.4 Analysis step in modeling

In addition to initial step only one step was created. In the created step dynamic explicit method was selected. Dynamic explicit method includes material nonlinearity and also geometrical nonlinearity. It is capable of analyzing post buckling analysis. In order to avoid the convergence issues of the implicit static analysis, the dynamic explicit analysis was used to analyses the Finite Element models. ABAQUS/Explicit solves each problem as a wave propagation. In more dynamic explicit was used to avoid the unresolved element error during the analysis. In this paper there were many parts assembled together to form a model, from the divergent of elements there was a formation of file product error so in this analysis dynamic explicit step was sufficient in addition to initial steps Finally, the required field output and history output was selected.

3.10.5 Interactions and Kinematic Constraints between Components in modeling

Kinematic relationships between the various components are required to be defined within the finite element model in order to ensure strain compatibility between the various components. In other words, interactions had to defined such that the equal and opposite loading applied between the bodies results in the one or more bodies deforming together. The interaction that was utilized in the construction of this model was surface to surface interaction between bamboo fiber tube and concrete.

The interactions defined in this model take the form of a surface-based constraint in which a constraint is formed between two surfaces on the geometry, a master and a slave surface. First the surfaces of different components that will be in contact must be created. After that pairs of surfaces which are going to be in contact must be identified. There are two components which define the interaction of contacting surfaces, one normal to the surfaces and one tangential. In ABAQUS© the default normal interaction between the surfaces is called the 'hard contact', meaning that the surfaces can contact each other when the clearance between them becomes zero and they can transmit between each other the unlimited magnitude of pressure but cannot penetrate each other. For interaction, surface to surface contact was created between bamboo fiber tube and concrete with tangential behavior. Penalty method (also known as stiffness method) is used for imposing frictional constraints. This stiffness method allows the relative motion between the surfaces of two materials even when they are sticking.

3.10.6 Boundary Conditions and Loading in modeling

The way in which the bodies within the finite element model interact with each other and with the imposed boundary conditions can impact both the results and stability of the analysis. The first were reactionary boundary conditions that are constant conditions externally imposed on the model. Another type of external boundary condition is those intended to load the structure and change during the course of an analysis. The boundary conditions applied in the FEA model to simulate the conditions for concentrically and eccentrically loaded specimens are shown in Figure 3.17. In concentrically and eccentrically loaded column tests, the bottom end of the column was fixed and the axial load was applied through rigid body reference node at the top end of the column. The rotations at the top surface were fixed. Since the load is applied at the top the vertical restraint was released. For the purpose of this research, the top columns are subjected to a constant concentrated load which is applied at a specific node depending on the varying eccentricities. At the other end of the bottom columns boundary condition which constrains them from translation and rotation in all direction is applied. Therefore, the support condition is fixed at the bottom columns (U1=U2=U3=UR1=UR2=UR3=0) as shown in the figure 3.16.

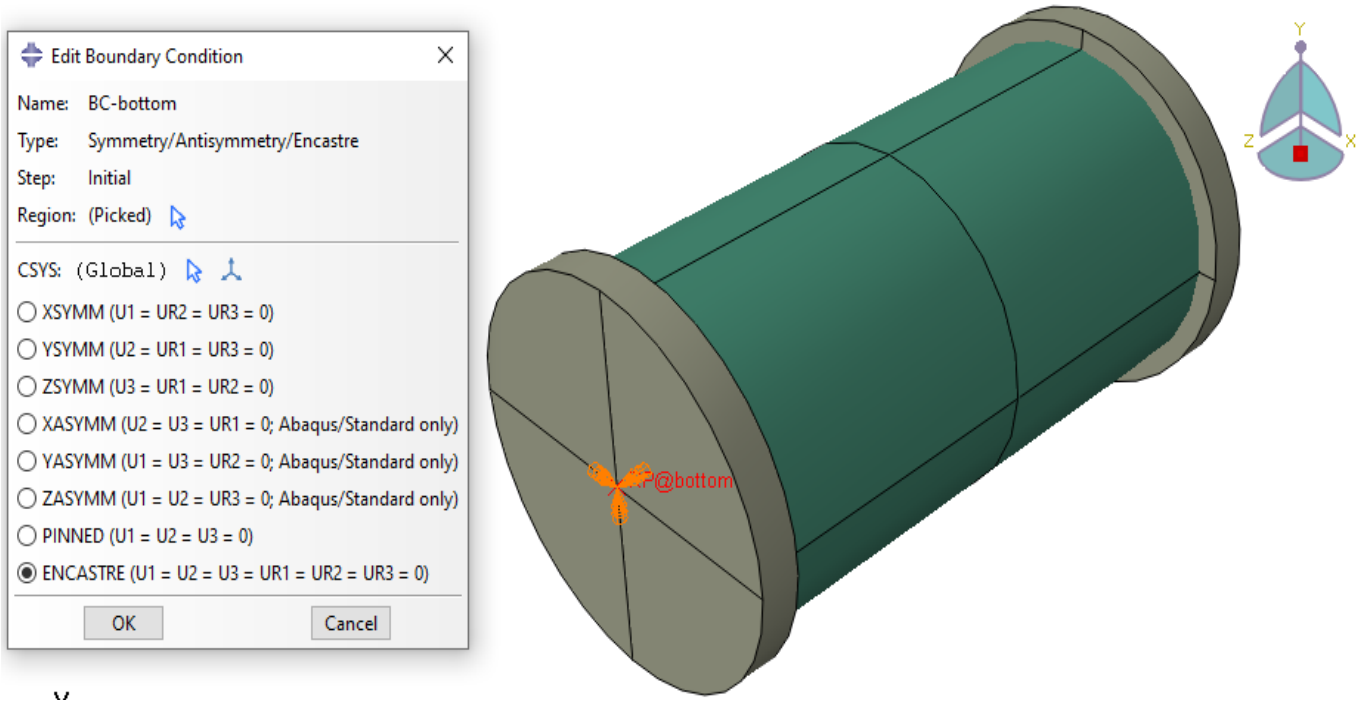

Figure 3.16: End boundary conditions (fixed support) at the bottom columns.

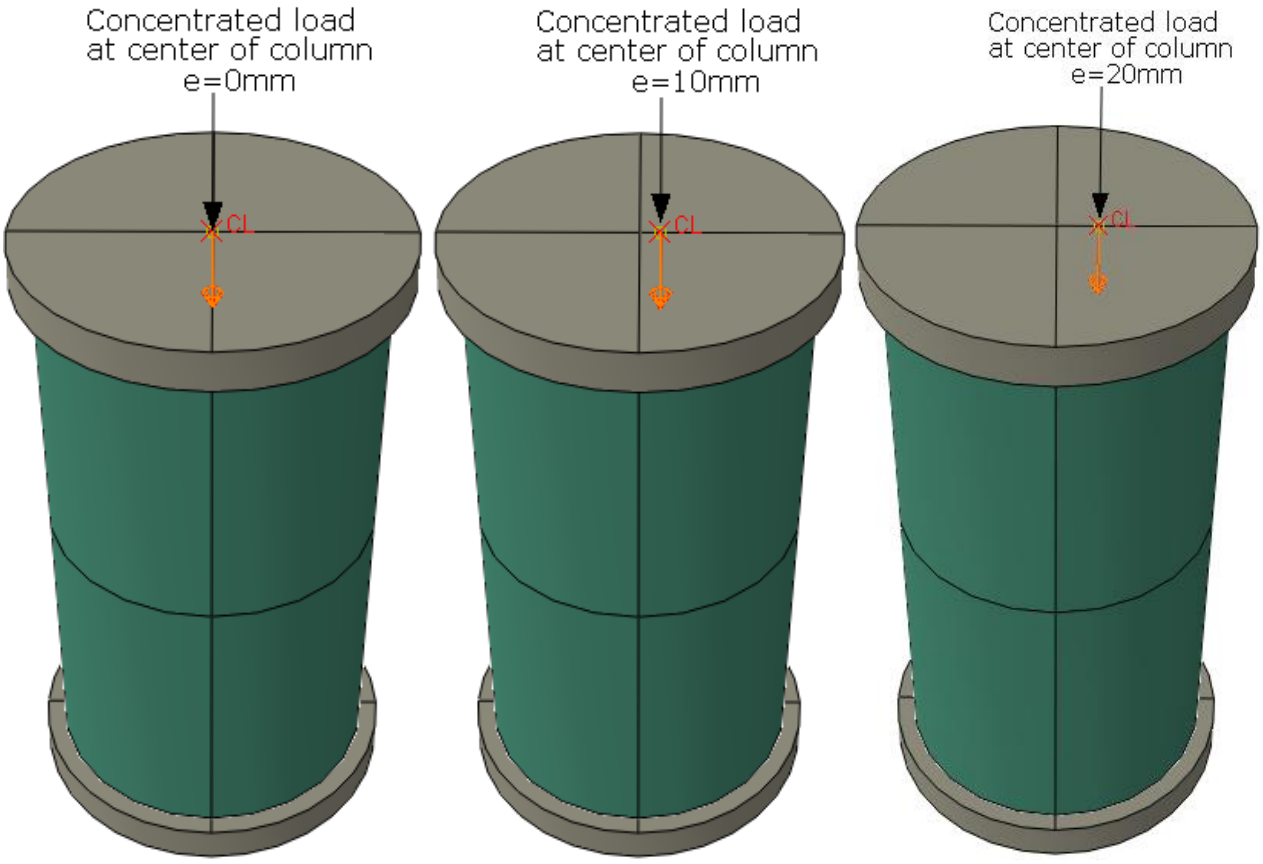

Figure 3.17: Concentric and eccentric loading at the top columns.

3.10.7 Mesh in modeling

a. Mesh size

Different analysis was done in validation work using different mesh size until the analysis result was conforming to experimental result. So, 0.02m mesh size gave the best result which conforms to experimental result and takes reasonable running time for the model. Since dependent instances were used mesh was done for parts.

b. Element type and selection

The BCC columns investigated in this study comprised of two components, such as bamboo fiber tube and concrete. The key in finite element analysis is the appropriate selection of element type. The ABAQUS©CAE standard modules consist of a comprehensive element library that provides different types of elements catering to different situations. When carrying out FEA analysis, the selection of a particular type of element is no longer necessary, as most commercially available software packages for composite column design do not offer an option. For reference, it is usual to use a „beam" element; this will provide results for flexure, shear and displacement directly. Beam and truss elements are generally triangular or quadrilateral with a node at each corner. However, elements have been developed that include an additional node on each side, this gives triangle elements with six nodes and quadrilateral elements with eight nodes. Since the only places where the forces are accurately calculated are at the nodes (they are interpolated at other positions), the accuracy of the model is directly related to the number of nodes. By introducing more nodes into an element, the accuracy of the results is increased; alternatively, the number of elements can be reduced for the same number of nodes, so reducing computational time. For this reason, 3D 8- nodded hexahedral (brick) elements having 3 degrees of freedom in each node (translations in X, Y and Z directions) are utilized for modeling concrete elements with reduced integration (C3D8R) to prevent the shear locking effect.

Table 3. 3: Various Elements Used in ABAQUS© (ABAQUS, Manual)

Element	Description	D.O.F	Element shape
C3D8	Hexagonal Element	24	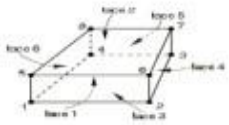
C3D4	Tetrahedral Element	12	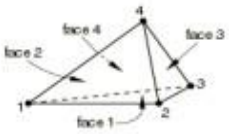
S4R	shell elements	8	
T3D2	3-dimensional 2-node truss elements	6	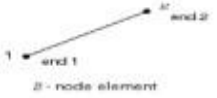
T2D3	2-dimensional 3-node truss elements	6	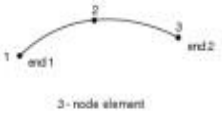

There were two of bodies needed to be discretized through meshing in this study. In this analysis parts will individually mesh and then assembled for further process. Meshes composed by tridimensional continuum solid elements with 8 nodes called C3D8R, 8 node linear brick elements with reduced integration and hourglass control are used for concrete. Meshes composed by tridimensional continuum shell elements with 8 nodes called SC8R, 8-node quadrilateral in-plane general-purpose continuum shell, reduced integration with hourglass control, finite membrane strains are used for Bamboo fiber tube.

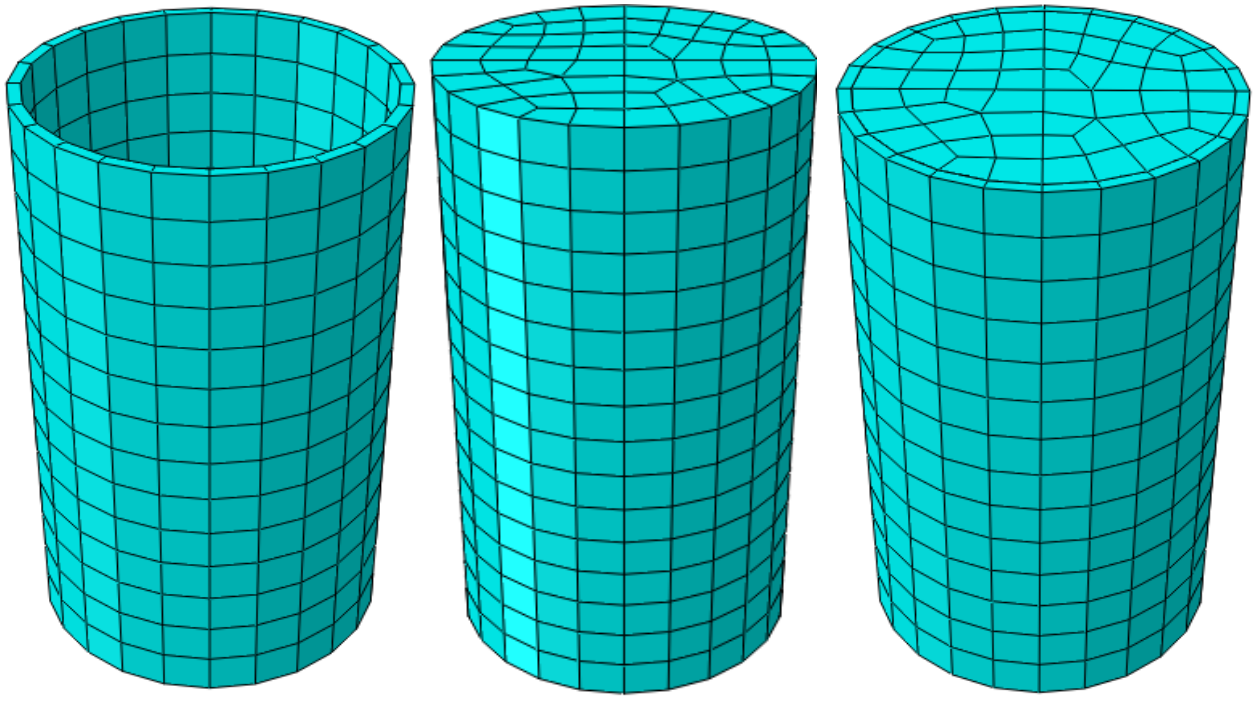

a. Bamboo fiber tube b. plain concrete c. composite column (BCC-5)

Figure 3. 18: Sample meshing in the BCC columns

3.11 Data quality assurance

In order to assure data quality, the following measure are taken:

- The ABAQUS software was checked for the known simple structural element to check whether it was working well or not.
- The loading and all structural modeling were double checked to remove errors.
- In case of any unreliable (illogical) results due to some unobserved errors, the structure was remodeled and reanalyzed.
- A due attention and care was taken when extracting results from ABAQUS and plotting them in Excel.

3.12 Parametric study

For this parametric study a circle column with outer diameter of 169.6mm for BCC-5, 177mm for BCC-8 and 182mm for BCC-10 was selected as per journal. Typical cross section and elevation of BCC column used in the parametric study are shown in figure below. This column was designed and analyzed during the parametric study to incorporate the effects of several parameters that can significantly affect the BCC column behavior. The variables are eccentric loading, bamboo fiber tube diameter, load application and BST-bamboo thickness.

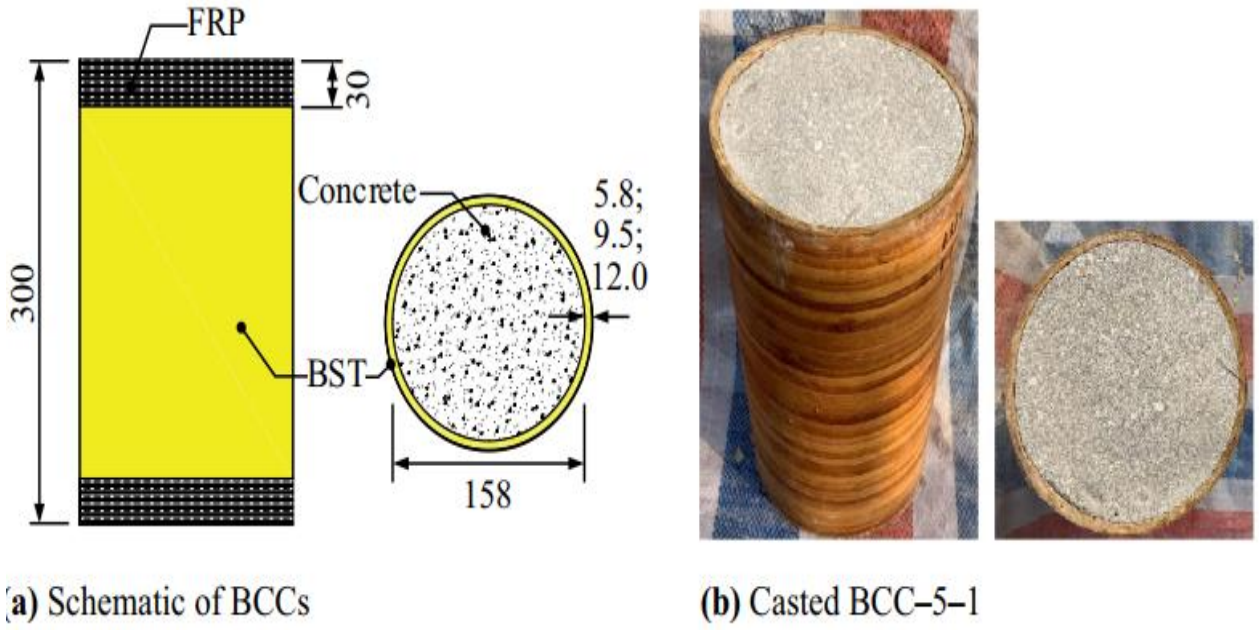

Figure :3.19: a Dimension details of specimen(Kou, Tian and Jin, 2021)

a) Eccentric loading: - The eccentricity used from the journal validation is zero (concentric loading) and the load eccentricities studied in this research include, e= (5mm, 10mm,15mm & 20mm) for control as discussed in the following tables.

b) The diameter of bamboo fiber tube: - The diameter of bamboo fiber tube used from the journal is 169.6mm for BCC-5. For the analysis three different diameter of bamboo fiber tube used are 211.6mm,261.6mm & 311.6mm of the same other parameters as the following tables.

c) Load application: -load application on BCC column is used for journal and the comparation load application on BCC column and core concrete column for analysis of composite column to know the effect of them on composite column for the same other parameters as explained in the following tables.

Table 3.4: Independent parameters sample data for column analysis

Group No.	Eccentric Loading	Diameter of BST-Bamboo	Load application	Variable Remark
	0mm	169.6mm	on BCC column	Eccentric Loading
	5mm	169.6mm	on BCC column	Eccentric Loading
	10mm	169.6mm	on BCC column	Eccentric Loading
	15mm	169.6mm	on BCC column	Eccentric Loading
Group -1	20mm	169.6mm	on BCC column	Eccentric Loading
	0mm	177mm	on BCC column	Eccentric Loading
	5mm	177mm	on BCC column	Eccentric Loading
	10mm	177mm	on BCC column	Eccentric Loading
	15mm	177mm	on BCC column	Eccentric Loading
Group -2	20mm	177mm	on BCC column	Eccentric Loading
	0mm	182mm	on BCC column	Eccentric Loading
	5mm	182mm	on BCC column	Eccentric Loading
	10mm	182mm	on BCC column	Eccentric Loading
	15mm	182mm	on BCC column	Eccentric Loading
Group -3	20mm	182mm	on BCC column	Eccentric Loading
	0mm	169.6mm	on BCC column	Diameter of BST
	0mm	211.6mm	on BCC column	Diameter of BST
	0mm	261.6mm	on BCC column	Diameter of BST
Group -4	0mm	311.6mm	on BCC column	Diameter of BST
	0mm	169.6mm	on BCC column	Load application
Group -5	0mm	169.6mm	on core concrete	Load application
	0mm	177mm	on BCC column	Load application
Group -6	0mm	177mm	on core concrete	Load application
	0mm	182mm	on BCC column	Load application
Group -7	0mm	182mm	on core concrete	Load application

CHAPTER FOUR

4. RESULTS AND DISCUSSION

4.1 General

The main purpose of this study was to determine the effect of different eccentric loading, effect of BST-bamboo diameter, load application and BST-thickness on the non-linear properties of bamboo fiber tube concrete-filled composite column. To achieve this, a finite element analysis was conducted with all appropriate parameters considered and data was collected. This data was then analyzed to provide understandings into concrete-filled composite column non-linear properties under uniaxial loading. Factors explored included axial stress capacity enhancement, axial stress capacity, axial load capacity enhancement, axial strain magnitude, axial load capacity, axial deformation magnitude and failure mode. Observations are made through the aid of plots of output data and photographs in developing relationships between parameters and behavior. Next sections provide a summary of key specimen results.

4.2 Validation of Finite Element Analysis by Experimental Result

Before starting modeling of all specimens, the validation work was done in order to decide on different parameters. Experimental research done by(Kou, Tian and Jin, 2021) With a title, Experimental study on axial compressive behavior of bamboo slices twining tube-confined concrete was used as benchmark experiment.

Table 4. 1: Details of specimen from experiment for validation

Group No.	Specimen Samples	Thickness of BST	Diameter of BST-Bamboo	Diameter of Core concrete	Concrete grade	Length of column
Group -1	BCC-5	5.8mm	169.6mm	158mm	32.7mpa	300mm
Group -2	BCC-8	9.5mm	177mm	158mm	32.7mpa	300mm
Group -3	BCC-10	12mm	182mm	158mm	32.7mpa	300mm

Three tested specimens were used for verification are shown on above table 4.1. BCC columns consisted of three groups of the specimens with different wall thicknesses. The first specimens BCC-5 is BST-confined concrete column has five number of twining layers with 5.8mm wall thickness of bamboo fiber tube. The second specimens BCC-8 is BST-confined concrete column has eight number of twining layers with 9.5mm wall thickness of bamboo fiber tube. The third specimens BCC-10 is BST-confined concrete

column has 10 number of twining layers with 12mm wall thickness of bamboo fiber tube. The nominal diameter and height of the concrete in all specimens were 158 and 300 mm, respectively.

Simulations data from finite element analysis were compared with those from the experimental testing data obtained from the journal. The axial stress capacity, axial strain magnitude and failure modes obtained by the FE models are compared with experimental observations. The results of FE modelling have very good agreement with the experimental results.

According to finite element analysis and experimental result main failure modes were observed in these tests. The failure mode of the BCC is the rupture of the BST wall in the middle of the columns. Therefore, using the method, which is described in chapter three, the above-described specimen was modeled. Bulk viscosity and mesh size different analysis was done and stress-strain curve was recorded. These of them are selected and presented here together with the experimental curve. Bulk viscosity of zero and mesh size of 20mm had given the axial stress that was closest to the experimental result. The difference Between FEA and Experimental test of axial stress capacity is less than 5% is the best result and this proves that ABAQUS program is an appropriate method to predict the non-linear finite element analysis of bamboo fiber tube concrete-filled composite column. Moreover, the stress-strain curve of the FEA result matched with the stress-strain curve of the experimental result. This indicates that FEA result well conformed to the experimental result. Therefore, it has been modeled and analyzed the specimens using this FEA software. The comparison of axial stress versus axial strain shown in Table 4.1 as below.

Table 4. 2: Axial stress-strain of experimental and FE model comparation.

Test specimen	Axial stress, f_{cc} (MPa)		Percentage of difference	Axial strain, ε_{cc} (mm/mm)		Percentage of difference
	Experimental	FEA		Experimental	FEA	
Validation- 1 (BCC-5)	41.30	42.9	3.94%	0.0089	0.0082	8.07%
Validation- 2 (BCC-8)	47.8	45.80	4.18%	0.0115	0.0106	7.88%
Validation- 3 (BCC-10)	52.7	50.2	4.78%	0.0136	0.0126	7.18%
Difference in average (%)			4.30%			7.71%

The axial stress capacity enhancement ratio (f_{cc} /f_{co}) and axial strain magnitude enhancement ratio ($\varepsilon_{cc}/\varepsilon_{co}$) of bamboo fiber slices twining tube confined concrete, which were obtained from FEA, were compared against the available experimental test results. The axial stress capacity enhancement ratio (f_{cc} /f_{co}) shows that the lateral confinement from bamboo fiber slices twining tube contributed for an improvement in the axial stress capacity of the concrete. The effectiveness of confinement provided by bamboo fiber slices twining tube is shown by the higher stress capacity enhancement ratio. Table 4.3 shows the comparisons between the axial stress capacity enhancement ratio (f_{cc} /f_{co}) and axial strain magnitude enhancement ratio (ε_{cc} /ε_{co}) obtained from FEA and the existing experimental tests(Kou, Tian and Jin, 2021). Table 4.3 shows that, with only minor deviations, the axial stress capacity enhancement ratio and strain enhancement ratio calculated by FEA show a strong agreement with the results of the experimental tests. In order to investigate the axial compressive behavior of bamboo slices twining tube-confined concrete, the proposed FEM in this study can effectively replicate the experimental test results.

Table 4. 3: Axial stress capacity and strain magnitude enhancement ratios

Test specimen	Axial stress f_{cc} (Mpa)		Stress enhancement ratio f_{cc}/f_{co}		Axial strain ε_{cc}, (mm/mm)		Strain enhancement ratio $\varepsilon_{cc}/\varepsilon_{co}$	
	Exp	FEA	Exp	FEA	Exp	FEA	Exp	FEA
Validation-1 (BCC-5)	41.30	42.9	1.26	1.31	0.0089	0.0082	4	3.72
Validation-2 (BCC-8)	47.8	45.8	1.46	1.40	0.012	0.0106	5.23	4.82
Validation-3 (BCC-10)	52.7	50.2	1.61	1.53	0.0136	0.0126	6.19	5.75

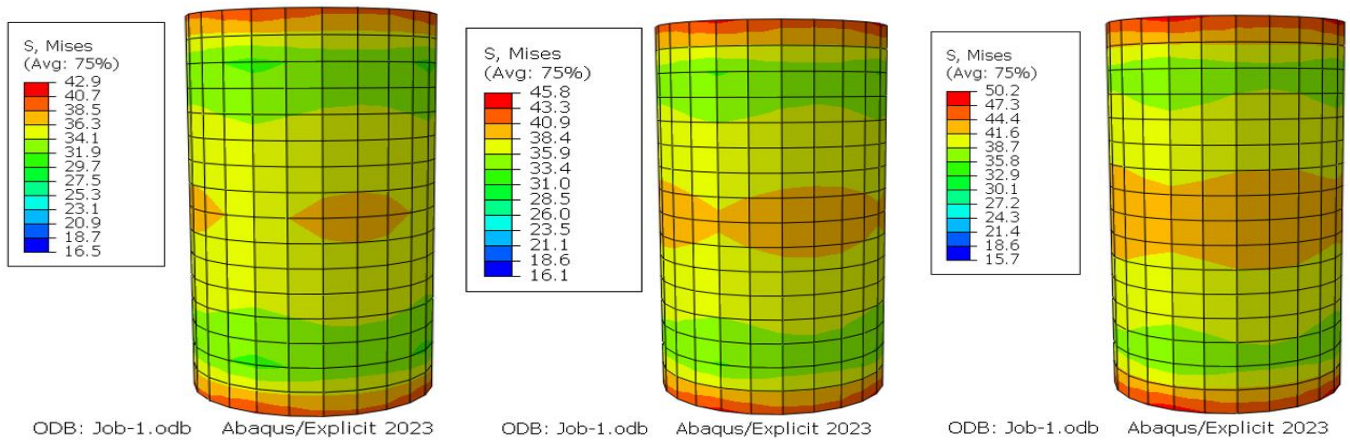

Core concrete of BCC-5 Core concrete of BCC-8 Core concrete of BCC-10

Figure 4.1: Axial stress contour compression failure of core concrete for BCC-5, BCC-8, BCC-10

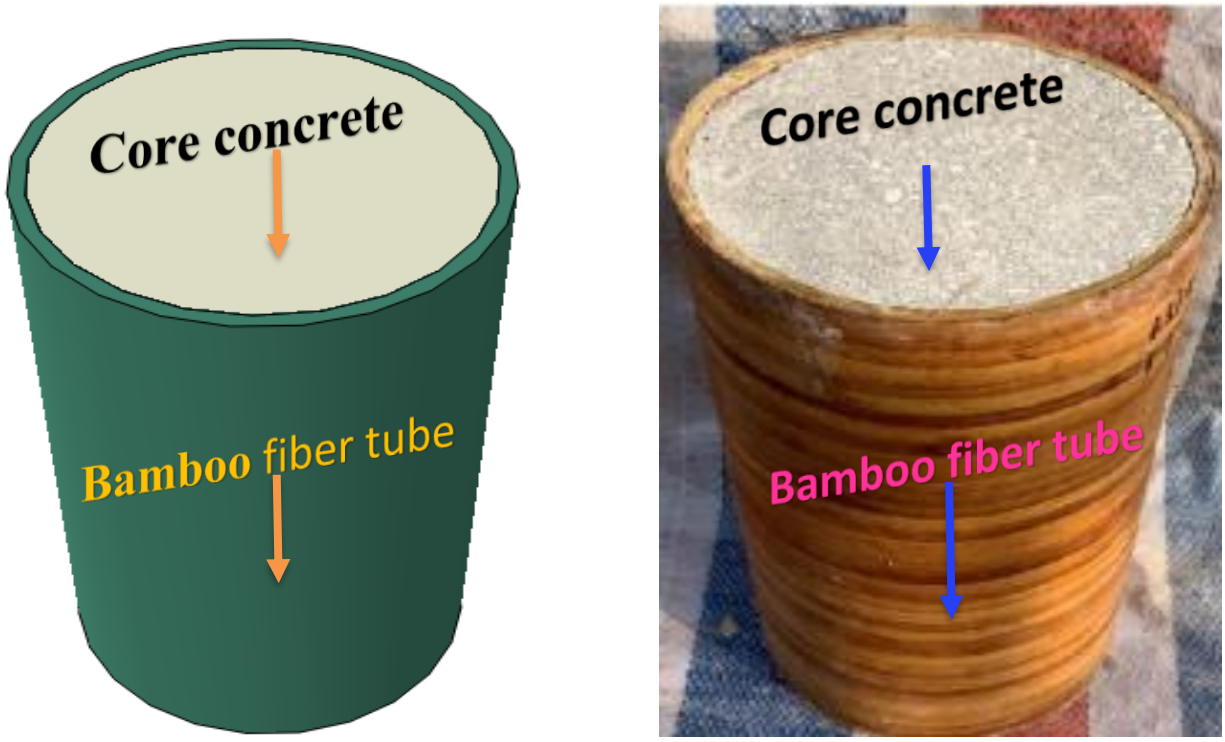

Model of BCC- sections in ABAQUS 2023 BCC section in Experiment(Kou, Tian and Jin, 2021)

Figure 4. 2: Experiment and FEA Model for BST-confined concrete column.

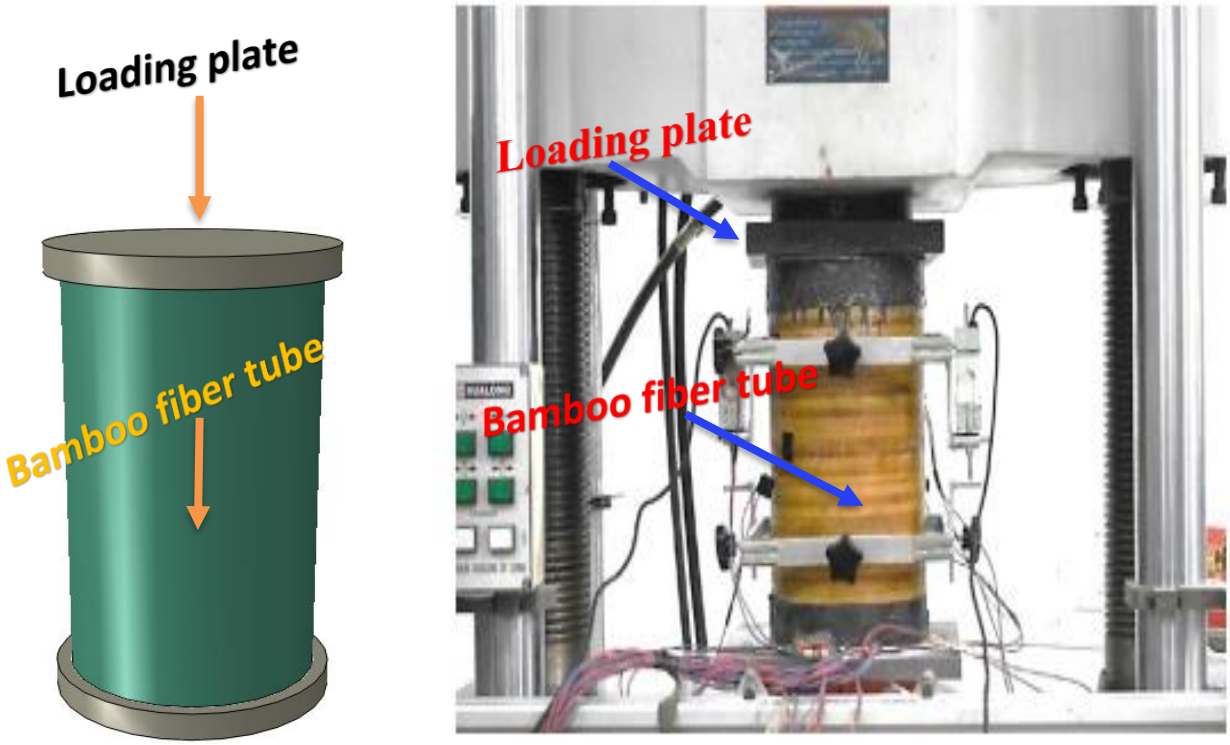

Test setup and loading in Abaqus 2023 Test setup and loading in Experiment (Kou, Tian and Jin, 2021)

Figure 4. 3: Experiment and FEA Test set up and loading for BST-confined concrete column

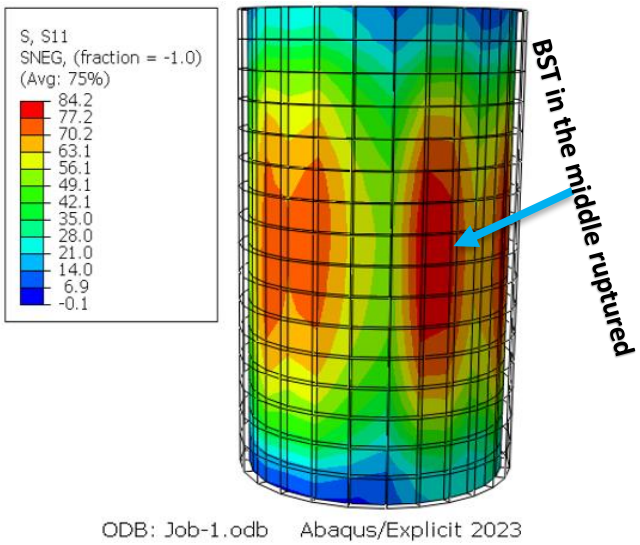

Failure mode of BCC in Abaqus 2023

failure mode of BCC in Experiment(Kou, Tian and Jin, 2021)

Figure 4. 4: FEA and Experimental Failure mode for BST-confined concrete column for validation

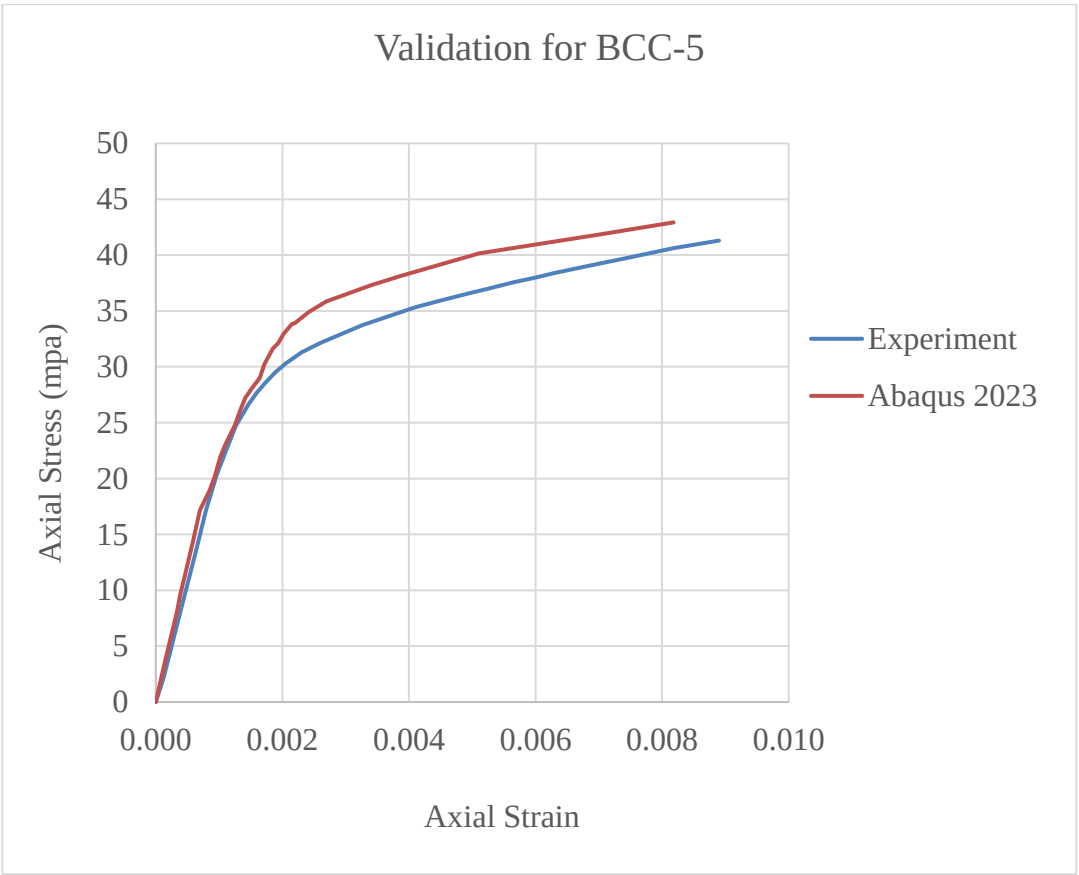

Figure 4. 5: FEA Axial Stress-Strain Vs Experimental Axial Stress-Strain curve for BCC-5

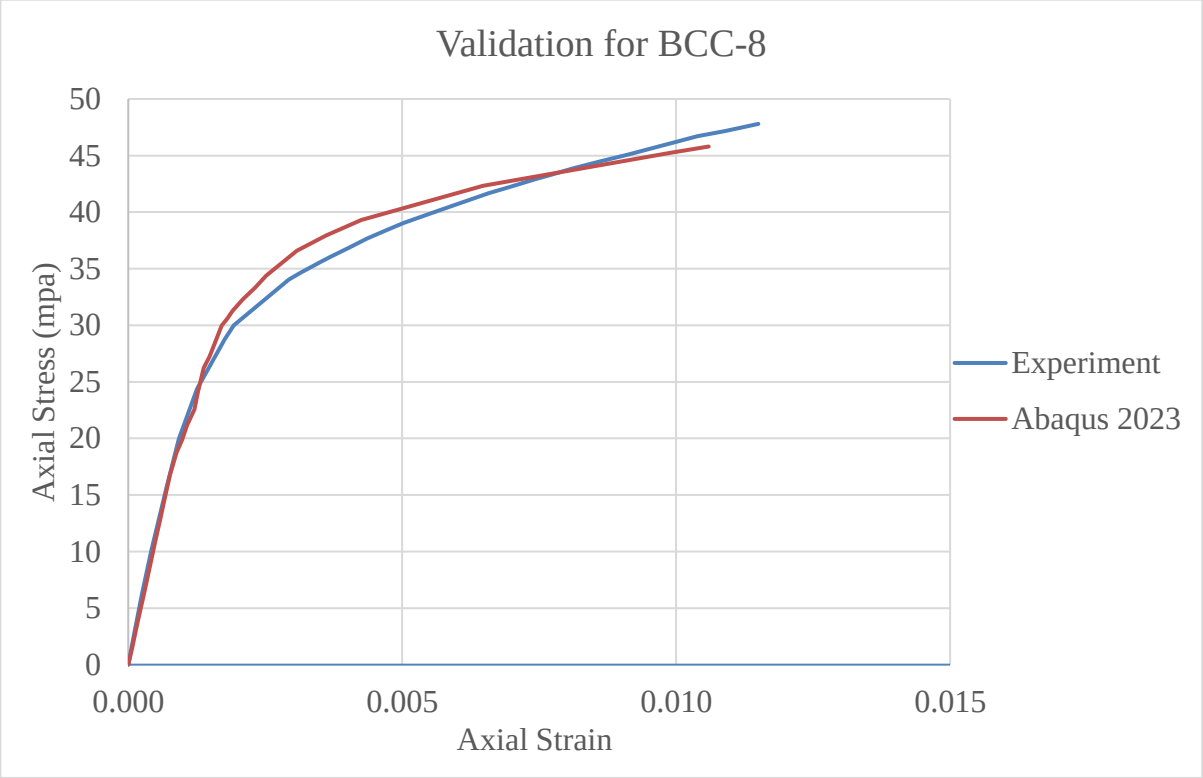

Figure 4. 6: FEA Axial Stress-Strain Vs Experimental Axial Stress-Strain curve for BCC-8

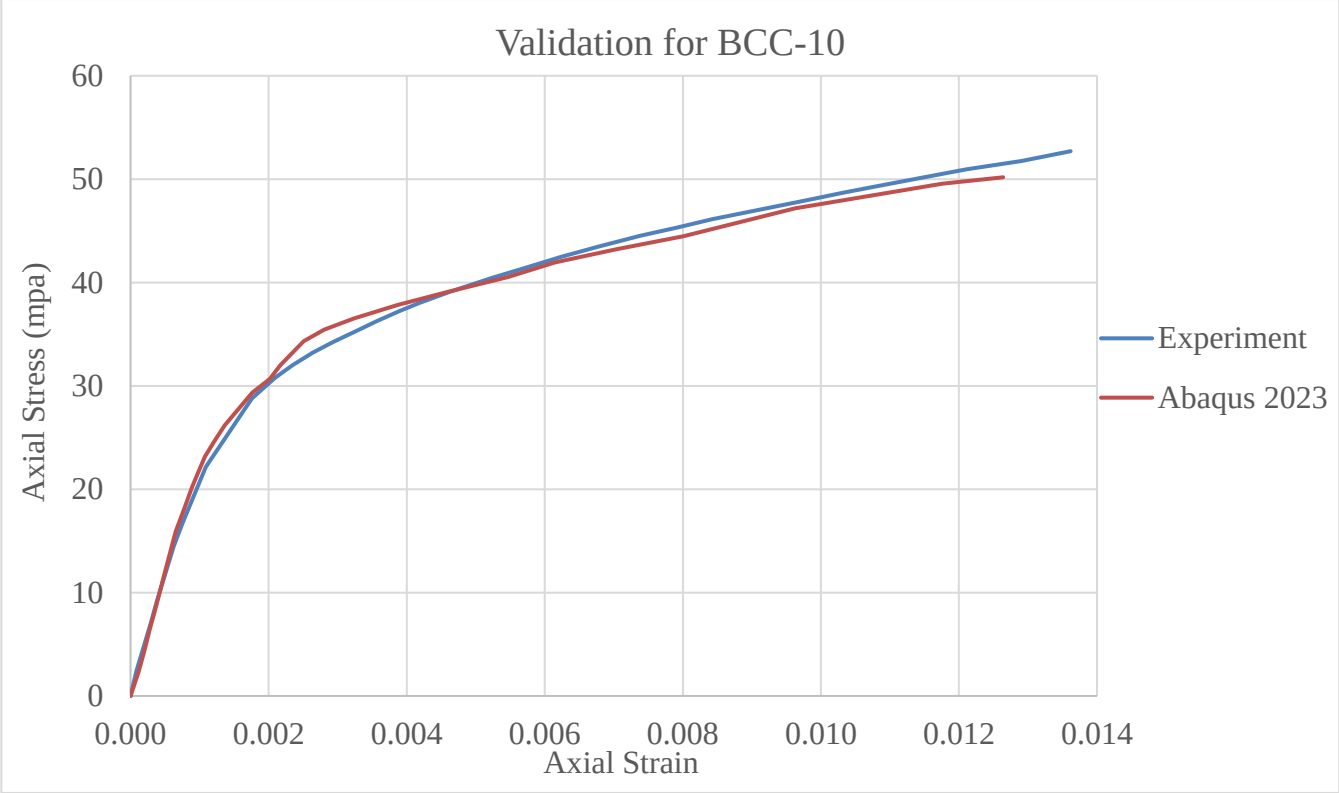

Figure 4. 7: FEA Axial Stress-Strain Vs. Experimental Axial Stress-Strain curve for BCC-10

Table 4.4: Axial stress – axial strain of experimental and FEA for BCC-5, BCC-8, BCC-10

BCC-5				BCC-8				BCC-10			
Experiment		Abaqus 2023		Experiment		Abaqus 2023		Experiment		Abaqus 2023	
Axial strain	Axial stress	Axial strain	Axial stress	Axial strain	Axial stress	Axial strain	Axial stress	Axial strain	Axial stress	Axial strain	Axial stress
ε_c	f_c mpa	ε_c	f_c mpa	ε_c	f_c mpa	ε_c	f_c mpa	ε_c	f_c mpa	ε_c	f_c mpa
0	0	0	0	0	0	0	0	0	0	0	0
0.0001	2.2	0.0001	3.3	0.0001	3.2	0.0001	1.4	0.0001	2.4	0.0001	2.2
0.0004	7.9	0.0002	5.2	0.0003	6.2	0.0002	3.8	0.0003	7.0	0.0002	4.1
0.0006	13.3	0.0003	8.1	0.0004	10.1	0.0003	6.2	0.0004	9.1	0.0003	6.7
0.0008	17.2	0.0004	9.6	0.0007	15.9	0.0004	9.2	0.0006	14.5	0.0004	8.2
0.0010	20.4	0.0005	11.4	0.0009	19.9	0.0005	11.0	0.0008	16.7	0.0005	11.8
0.0013	24.6	0.0006	14.4	0.0013	24.4	0.0006	12.8	0.0011	22.1	0.0006	13.8
0.0015	26.7	0.0007	17.2	0.0018	28.8	0.0007	14.8	0.0018	28.8	0.0007	15.9
0.0016	27.7	0.0008	18.9	0.0019	30.0	0.0008	16.8	0.0021	30.8	0.0008	18.1
0.0017	28.5	0.0009	20.1	0.0029	34.0	0.0009	18.7	0.0023	32.0	0.0009	20.2
0.0019	29.5	0.0010	22.0	0.0031	34.6	0.0010	19.8	0.0026	33.2	0.0010	21.7
0.0021	30.3	0.0011	23.1	0.0035	35.6	0.0011	21.2	0.0029	34.2	0.0011	23.2
0.0023	31.3	0.0012	24.8	0.0037	36.0	0.0012	22.6	0.0033	35.4	0.0012	24.7
0.0026	32.1	0.0013	26.3	0.0040	36.8	0.0013	24.1	0.0036	36.2	0.0014	26.2
0.0029	32.9	0.0014	27.2	0.0044	37.7	0.0014	26.2	0.0039	37.2	0.0016	27.8
0.0033	33.7	0.0015	28.1	0.0047	38.5	0.0015	27.2	0.0042	38.1	0.0018	29.4
0.0037	34.5	0.0016	29.0	0.0050	39.1	0.0016	28.4	0.0046	39.1	0.0020	30.7
0.0041	35.4	0.0017	30.2	0.0057	40.3	0.0017	30.0	0.0052	40.5	0.0022	32.0
0.0045	36.0	0.0018	31.6	0.0066	41.7	0.0018	30.6	0.0057	41.3	0.0025	34.3
0.0049	36.6	0.0019	32.1	0.0070	42.3	0.0019	31.3	0.0062	42.5	0.0028	35.4
0.0052	37.0	0.0020	32.9	0.0074	42.9	0.0021	32.3	0.0068	43.5	0.0032	36.5
0.0057	37.6	0.0021	33.8	0.0077	43.3	0.0023	33.3	0.0074	44.5	0.0039	37.8
0.0060	38.0	0.0022	34.0	0.0081	43.9	0.0025	34.4	0.0079	45.3	0.0046	39.1
0.0063	38.4	0.0024	34.9	0.0086	44.5	0.0028	35.5	0.0084	46.1	0.0055	40.5
0.0066	38.8	0.0027	35.9	0.0091	45.1	0.0031	36.6	0.0098	47.9	0.0061	41.9
0.0070	39.2	0.0034	37.3	0.0096	45.7	0.0036	37.9	0.0103	48.7	0.0070	43.2
0.0073	39.6	0.0039	38.2	0.0099	46.1	0.0042	39.3	0.0110	49.5	0.0080	44.5
0.0078	40.2	0.0051	40.1	0.0104	46.7	0.0065	42.3	0.0121	50.9	0.0096	47.2
0.0082	40.6	0.0070	41.8	0.0109	47.2	0.0099	45.3	0.0129	51.7	0.0118	49.5
0.0089	41.3	0.0082	42.9	0.0115	47.8	0.0106	45.8	0.0136	52.7	0.0126	50.2

4.3 Results from FE Analysis

After the verification of the finite element model, the effects of eccentric Loading, diameter of bamboo fiber tube, load application and ductility behavior analysis have taken and finally the results are presented in this section. Load-displacement and Stress-strain data were taken from the software and the load vs displacement and Stress vs strain curves are drawn. axial load enhancement and axial stress enhancement also calculated. From these curves, the load-displacement and stress - strain were taken for all of the specimens and presented below.

4.3.1 Effect of eccentric loading on axial load enhancement ratio and axial load for BCC column.

The effect of eccentric loading was assessed on axial load enhancement ratio and axial load capacity for the BCC model. While eccentric loading value increases, axial load enhancement ratio increases and the axial load capacity of BCC column decreases as compared with the same model**.**

4.3.1.1 Effect of eccentric loading on axial load enhancement ratio and axial load for BCC-5.

The axial load enhancement ratio increases with increasing eccentric loading, from eccentric loading value e=0 to e= 20mm the axial load enhancement ratio increases from 1.46 to 1.71 as shown in table 4.5. The Percentage of axial load capacity enhancement ratio for concentric loading(e=0) due to confining concrete by BST-5 is 46% and the percentage of axial load capacity enhancement ratio for eccentric loading value(e=20mm) due to confining concrete by BST-5 is 71% as shown in table 4.5 and figure 4.8. The difference percentage of axial stress enhancement ratio between e=0 and e=20mm is about 26%. The enhancement axial load capacity ratio (P_{cc}/P_{co}) of the BCC column with e=20 eccentric loading value had a better axial load capacity enhancement ratio than the test specimens with e=0 concentric loading value. BST confinement is more effective in BCC columns with larger eccentric loading value than with smaller eccentric loading value. The ratio of the axial load capacity enhancement (P_{cc} /P_{co}) shows the concrete capacity gained from confinement proportion to its eccentric loading value. The BST tube's confinement effectiveness is demonstrated by the higher enhancement ratio.

The axial load capacity of the composite columns decrease with increasing eccentric loading, from eccentric loading value e=0 to e= 5mm the load capacity decreased by 14% between 933KN to 800KN, e=5 to e= 10mm the load capacity decreased by 13% between 800KN to 693KN, e=10 to e= 15mm the load capacity decreased by 12% between 693KN to 609KN, e=15 to e= 20mm the load capacity decreased by 11% between 609KN to 545KN, and the difference axial load capacity between e=0 and e=20mm is about 42% between 933KN to 545KN as shown in table 4.5 and Figure 4.9. From this finite element analysis of

composite columns with varying eccentric loading values, the higher eccentric loading value has a low load-bearing capacity in bamboo fiber tube concrete-filled composite columns.

In general, from this finite element analysis of composite columns with varying eccentric loading value, we can conclude that the higher eccentric loading value have low axial load capacity and high axial load capacity enhancement ratio in Bamboo Fiber Tube Concrete-Filled Composite Columns. For this reason, under eccentric loading as compared to concentric loading, the BST confinement is more significant under eccentric loading, and similar previous research supports this conclusion as well (Degefa Zewdu and Wondimu Aure, 2022), (Hassan *et al.*, 2017).

Table 4.5: Effect of eccentric loading on axial load and axial load enhancement ratio.

Type of Specimen	Eccentric loading	P_{co} (KN)	P_{cc} (KN)	Axial load enhancement ratio P_{cc}/P_{co}	Percentage of enhancement ratio
BCC-5	0	641	933	1.46	46%
BCC-51	5	511	800	1.57	57%
BCC-52	10	425	693	1.63	63%
BCC-53	15	364	609	1.67	67%
BCC-54	20	318	545	1.71	71%

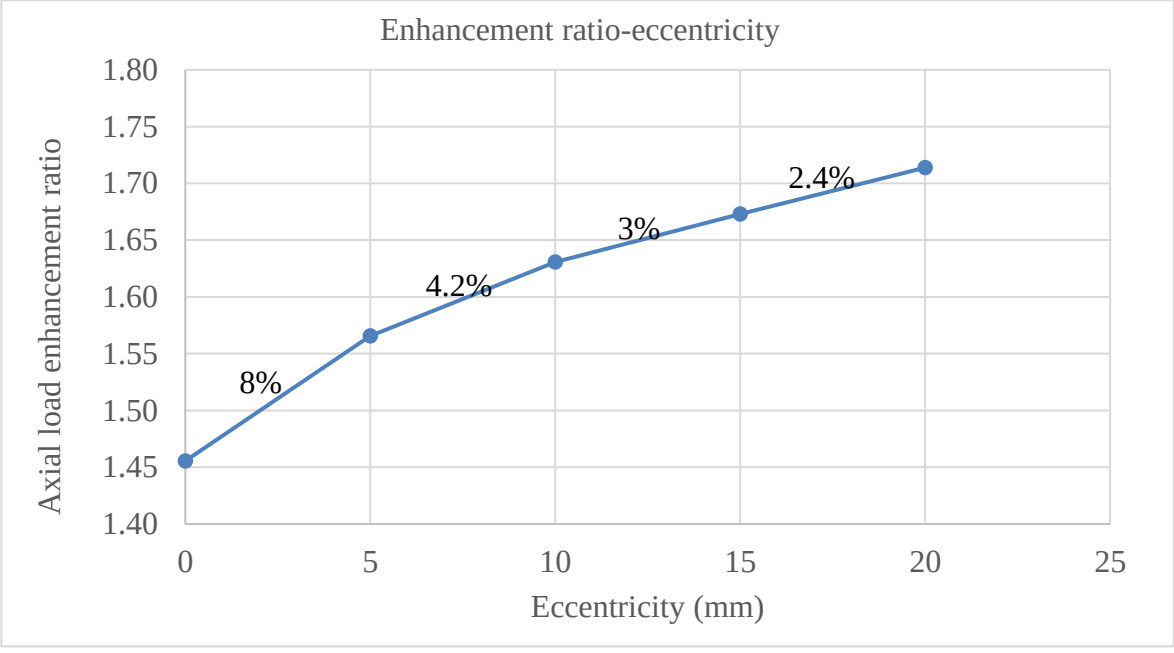

Figure 4.8: Comparison between eccentric loading and load enhancement ratio for BCC-5.

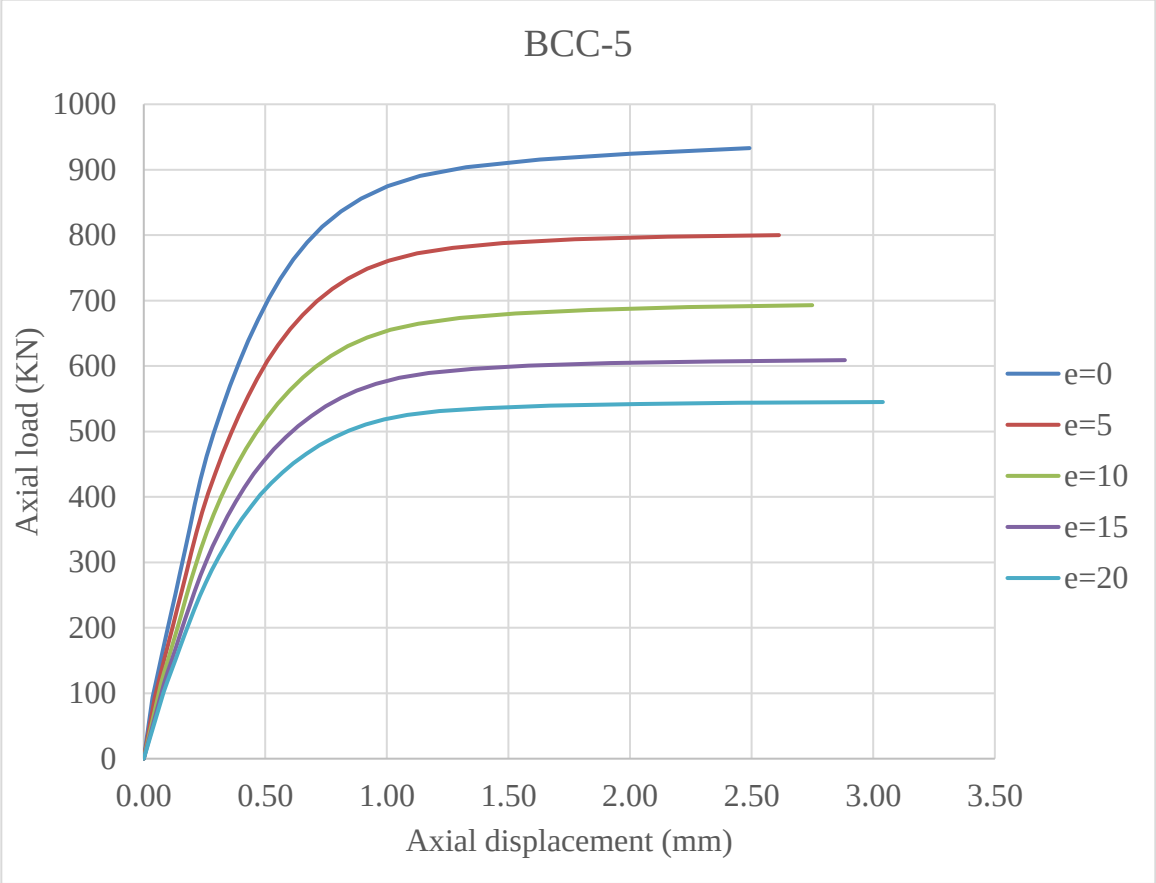

Figure: 4.9 Effects of eccentric loading on axial loading and axial displacement for BCC-5

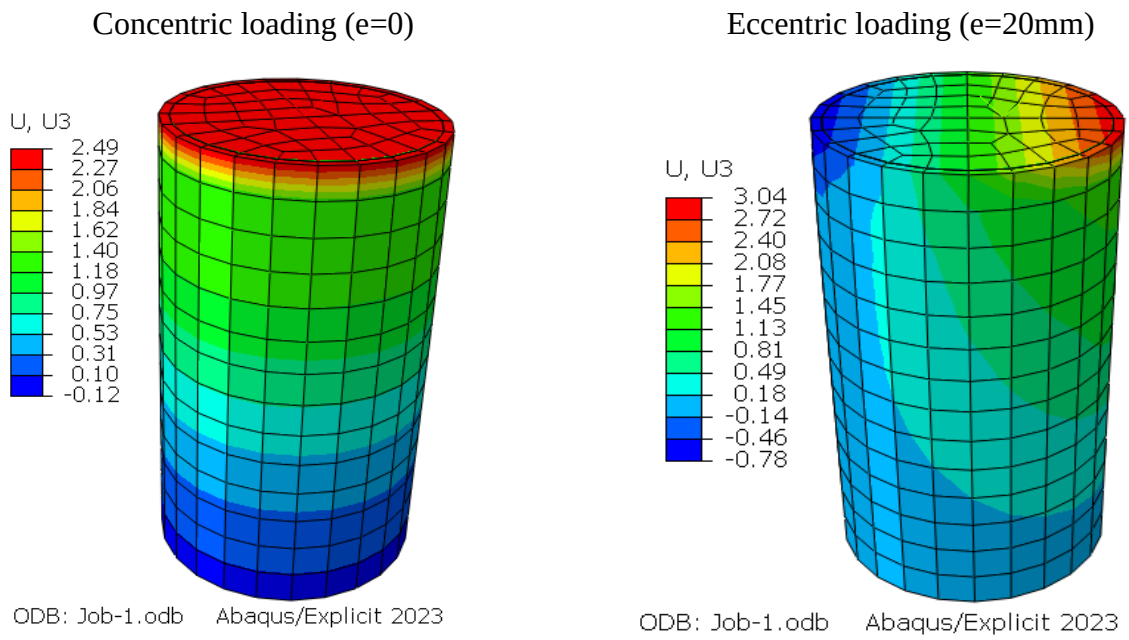

Figure 4.10: Axial displacement contour with varying eccentricity at ultimate for BCC-5

Table 4.6: Axial Load – axial displacement of eccentric loading for BCC-5

BCC-5									
Eccentricity (e=0)		Eccentricity (e=5)		Eccentricity (e=10)		Eccentricity (e=15)		Eccentricity (e=20)	
U_a(mm)	P_{cc} (KN)	U_a(mm)	P_{cc} (KN)	U_a(mm)	P_{cc} (KN)	U_a(mm)	P_{cc} (KN)	U_a(mm)	P_{cc} (KN)
0.00	0	0.00	0	0.00	0	0.00	0	0.00	0
0.04	94	0.05	94	0.07	114	0.08	115	0.08	102
0.05	115	0.07	133	0.08	132	0.10	132	0.10	117
0.06	138	0.09	155	0.10	152	0.12	152	0.13	152
0.08	163	0.12	204	0.12	174	0.13	171	0.15	169
0.09	192	0.14	231	0.14	197	0.15	191	0.17	188
0.11	220	0.16	257	0.15	221	0.17	214	0.19	208
0.13	252	0.18	287	0.17	245	0.19	235	0.21	227
0.15	284	0.20	315	0.19	271	0.21	256	0.23	249
0.17	318	0.22	346	0.21	294	0.23	280	0.25	268
0.19	354	0.24	377	0.23	321	0.26	302	0.28	288
0.21	389	0.27	406	0.26	347	0.28	325	0.31	309
0.23	427	0.29	437	0.29	373	0.31	348	0.34	328
0.26	462	0.32	466	0.32	400	0.34	370	0.37	348
0.29	498	0.36	497	0.35	425	0.38	393	0.40	366
0.32	535	0.39	525	0.39	451	0.41	414	0.44	386
0.36	570	0.43	554	0.42	473	0.45	435	0.48	403
0.39	606	0.47	581	0.46	497	0.49	454	0.52	421
0.43	639	0.51	608	0.50	520	0.53	473	0.57	437
0.47	671	0.55	632	0.55	542	0.58	491	0.62	451
0.52	704	0.60	657	0.60	563	0.63	508	0.67	466
0.56	733	0.65	678	0.65	582	0.69	524	0.72	479
0.62	763	0.71	699	0.71	599	0.75	539	0.78	491
0.67	789	0.78	718	0.77	615	0.81	552	0.84	501
0.73	813	0.84	734	0.84	630	0.88	562	0.91	511
0.81	836	0.92	749	0.92	644	0.96	573	0.99	519
0.89	856	1.01	761	1.01	655	1.05	582	1.08	525
1.00	875	1.12	772	1.13	665	1.17	589	1.21	531
1.14	890	1.27	781	1.30	674	1.36	596	1.40	536
1.33	904	1.48	788	1.53	680	1.58	600	1.67	539
1.63	916	1.77	794	1.84	686	1.92	604	2.03	542
2.00	925	2.16	798	2.24	690	2.34	607	2.45	544
2.49	933	2.61	800	2.75	693	2.88	609	3.04	545

4.3.1.2 Effect of eccentric loading on axial load enhancement ratio and axial load for BCC-8.

The axial load enhancement ratio increases with increasing eccentric loading, from eccentric loading value e=0 to e= 20mm the axial load enhancement ratio increases from 1.83 to 2.29 as shown in table 4.7. The Percentage of axial load capacity enhancement ratio for concentric loading(e=0) due to confining concrete by BST-5 is 83% and the percentage of axial load capacity enhancement ratio for eccentric loading value(e=20mm) due to confining concrete by BST-5 is 129% as shown in table 4.7 and figure 4.11. The difference percentage of axial stress enhancement ratio between e=0 and e=20mm is about 46%. The enhancement axial load capacity ratio (P_{cc}/P_{co}) of the BCC column with e=20 eccentric loading value had a better axial load capacity enhancement ratio than the test specimens with e=0 concentric loading value. BST confinement is more effective in BCC columns with larger eccentric loading value than with smaller eccentric loading value. The ratio of the axial load capacity enhancement (P_{cc} /P_{co}) shows the concrete capacity gained from confinement proportion to its eccentric loading value. The BST tube's confinement effectiveness is demonstrated by the higher enhancement ratio.

The axial load capacity of the composite columns decreases with increasing eccentric loading, from eccentric loading value e=0 to e= 20mm the load capacity decreased by 38% between 1176KN to 729KN as shown in table 4.7 and Figure 4.12. From this finite element analysis of composite columns with varying eccentric loading values, the higher eccentric loading value has a low load-bearing capacity in bamboo fiber tube concrete-filled composite columns.

In general, from this finite element analysis of composite columns with varying eccentric loading value, we can conclude that the higher eccentric loading value have low axial load capacity and high axial load capacity enhancement ratio in Bamboo Fiber Tube Concrete-Filled Composite Columns. For this reason, under eccentric loading as compared to concentric loading, the BST confinement is more significant under eccentric loading, and similar previous research supports this conclusion as well(Degefa Zewdu and Wondimu Aure, 2022),(Hassan *et al.*, 2017).

Table 4.7: Effect of eccentric loading on axial load and axial load enhancement ratio.

Type of Specimen	Eccentric loading	P_{co} (KN)	P_{cc} (KN)	Axial load enhancement ratio P_{cc}/P_{co}	Percentage of enhancement ratio
BCC-5	0	641	1176	1.83	83%
BCC-51	5	511	1028	2.01	101%
BCC-52	10	425	910	2.14	114%
BCC-53	15	364	807	2.22	122%
BCC-54	20	318	729	2.29	129%

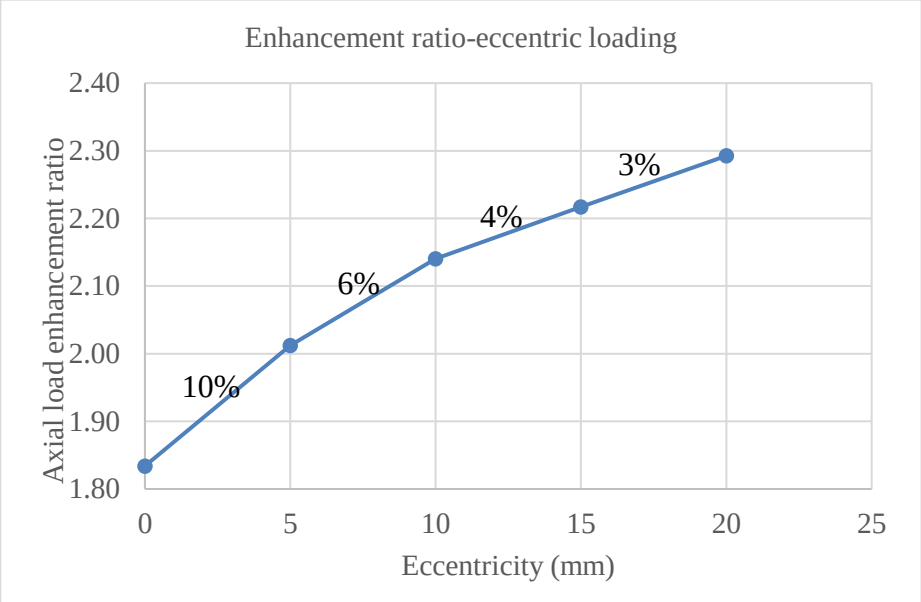

Figure 4.11: Comparison between eccentric loading and load enhancement ratio for BCC-8.

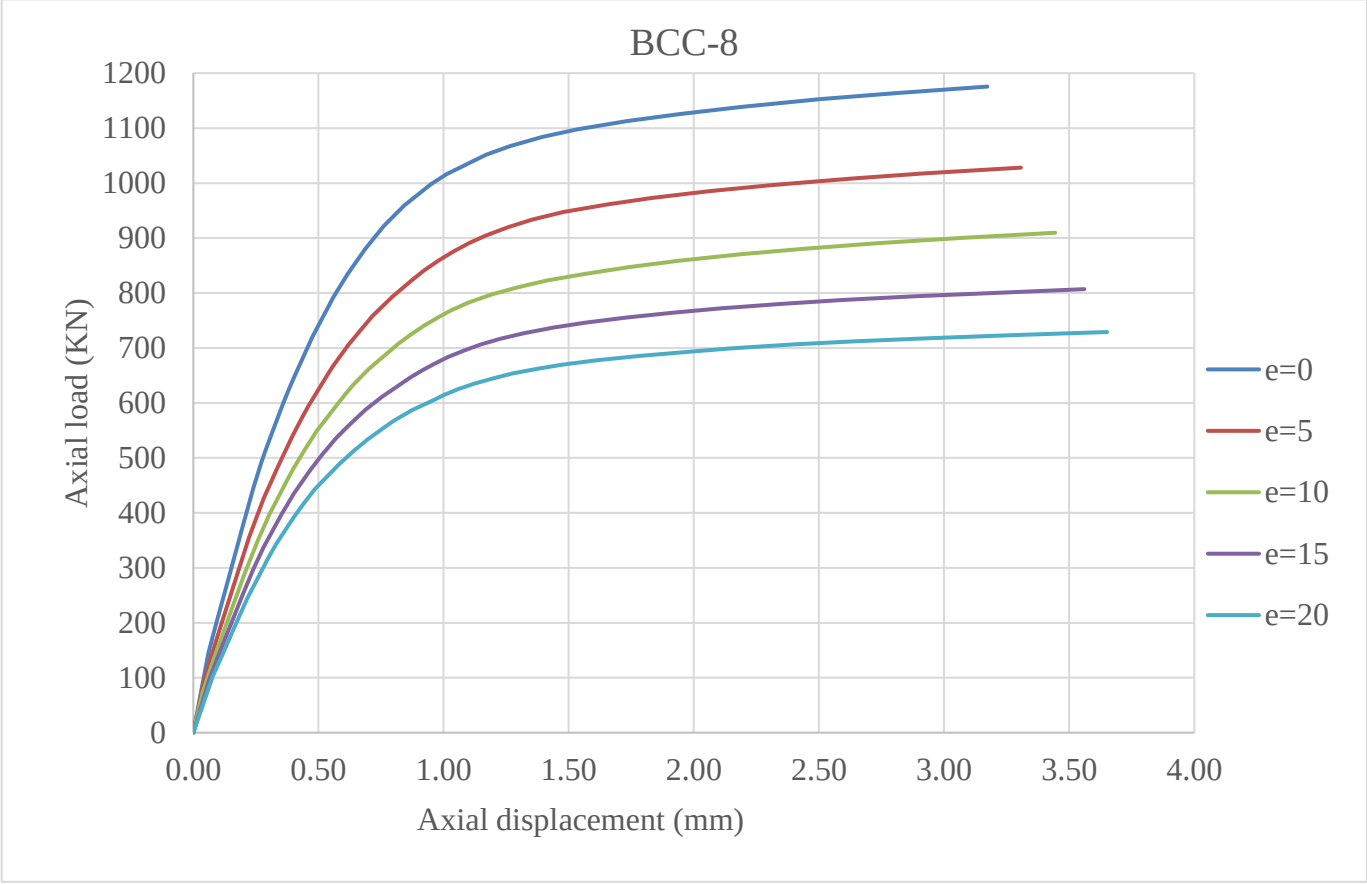

Figure: 4.12: Effects of eccentric loading on axial loading and axial displacement for BCC-8

Table 4.8: Axial Load – axial displacement of eccentric loading for BCC-8

BCC-8									
Eccentricity (e=0)		Eccentricity (e=5)		Eccentricity (e=10)		Eccentricity (e=15)		Eccentricity (e=20)	
U_a(mm)	P_{cc} (KN)	U_a(mm)	P_{cc} (KN)	U_a(mm)	P_{cc} (KN)	U_a(mm)	P_{cc} (KN)	U_a(mm)	P_{cc} (KN)
0	0	0.00	0	0	0	0	0	0	0
0.06	144	0.04	95	0.04	72	0.06	99	0.08	102
0.08	175	0.06	126	0.08	129	0.12	160	0.12	147
0.10	206	0.10	178	0.16	227	0.20	255	0.16	190
0.14	278	0.16	267	0.20	287	0.24	296	0.22	246
0.20	378	0.22	356	0.26	350	0.28	336	0.30	318
0.24	445	0.28	426	0.30	397	0.35	395	0.33	344
0.27	489	0.34	483	0.38	462	0.40	435	0.40	392
0.29	511	0.40	541	0.40	482	0.47	478	0.44	418
0.30	533	0.44	577	0.45	515	0.51	506	0.49	443
0.34	582	0.46	594	0.49	549	0.57	536	0.58	489
0.36	605	0.53	650	0.58	599	0.62	560	0.64	513
0.38	627	0.56	667	0.60	614	0.69	587	0.70	535
0.41	650	0.62	706	0.64	633	0.75	611	0.76	555
0.45	700	0.68	740	0.70	662	0.83	636	0.80	568
0.48	722	0.72	758	0.78	692	0.87	647	0.88	587
0.56	792	0.80	794	0.82	709	0.92	660	0.96	605
0.62	835	0.88	825	0.87	724	0.97	672	1.00	615
0.69	880	0.92	841	0.92	740	1.02	683	1.06	625
0.76	922	0.98	860	0.98	755	1.08	695	1.12	635
0.84	959	1.04	875	1.03	768	1.15	706	1.19	644
0.95	998	1.10	891	1.10	782	1.23	717	1.27	653
1.01	1016	1.17	904	1.19	797	1.32	727	1.37	661
1.17	1052	1.26	920	1.30	811	1.44	737	1.47	669
1.27	1068	1.35	933	1.41	822	1.56	746	1.62	678
1.40	1084	1.48	947	1.57	835	1.73	755	1.78	685
1.53	1097	1.66	961	1.74	847	1.91	764	1.96	693
1.73	1112	1.83	973	1.94	859	2.11	772	2.15	699
1.95	1126	2.06	985	2.19	870	2.35	780	2.39	706
2.20	1139	2.31	996	2.44	881	2.59	787	2.64	712
2.51	1153	2.62	1008	2.74	891	2.89	794	2.95	718
2.80	1163	2.92	1018	3.09	901	3.23	801	3.30	724
3.17	1176	3.31	1028	3.44	910	3.56	807	3.65	729

4.3.1.3 Effect of eccentric loading on axial load enhancement ratio and axial load for BCC-10.

The axial load enhancement ratio increases with increasing eccentric loading, from eccentric loading value e=0 to e= 20mm the axial load enhancement ratio increases from 2.14 to 2.89 as shown in table 4.9. The Percentage of axial load capacity enhancement ratio for concentric loading(e=0) due to confining concrete by BST-5 is 114% and the percentage of axial load capacity enhancement ratio for eccentric loading value(e=20mm) due to confining concrete by BST-5 is 189% as shown in table 4.9 and figure 4.13. The difference percentage of axial stress enhancement ratio between e=0 and e=20mm is about 75%. The enhancement axial load capacity ratio (P_{cc}/P_{co}) of the BCC column with e=20 eccentric loading value had a better axial load capacity enhancement ratio than the test specimens with e=0 concentric loading value. BST confinement is more effective in BCC columns with larger eccentric loading value than with smaller eccentric loading value. The ratio of the axial load capacity enhancement (P_{cc} /P_{co}) shows the concrete capacity gained from confinement proportion to its eccentric loading value. The BST tube's confinement effectiveness is demonstrated by the higher enhancement ratio.

The axial load capacity of the composite columns decreases with increasing eccentric loading, from eccentric loading value e=0 to e= 20mm the load capacity decreased by 33% between 1370KN to 919KN as shown in table 4.9 and Figure 4.14. From this finite element analysis of composite columns with varying eccentric loading values, the higher eccentric loading value has a low load-bearing capacity in bamboo fiber tube concrete-filled composite columns.

In general, from this finite element analysis of composite columns with varying eccentric loading value, we can conclude that the higher eccentric loading value have low axial load capacity and high axial load capacity enhancement ratio in Bamboo Fiber Tube Concrete-Filled Composite Columns. For this reason, under eccentric loading as compared to concentric loading, the BST confinement is more significant under eccentric loading, and similar previous research supports this conclusion as well (Degefa Zewdu and Wondimu Aure, 2022), (Hassan *et al.*, 2017).

Table 4.9: Effect of Eccentric loading on axial load and axial load enhancement ratio.

Type of Specimen	Eccentric loading	P_{co} (KN)	P_{cc} (KN)	Axial load enhancement ratio P_{cc}/P_{co}	Percentage of enhancement ratio
BCC-5	0	641	1370	2.14	114%
BCC-51	5	511	1226	2.40	140%
BCC-52	10	425	1109	2.61	161%
BCC-53	15	364	1004	2.76	176%
BCC-54	20	318	919	2.89	189%

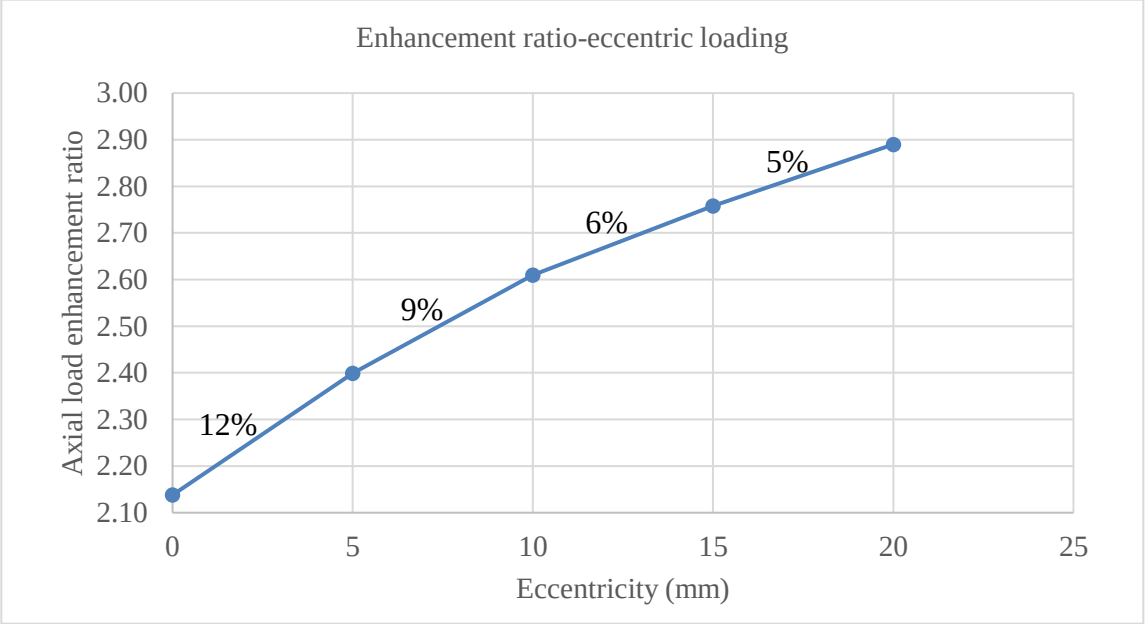

Figure 4.13: Comparison between eccentric loading and load enhancement ratio for BCC-10.

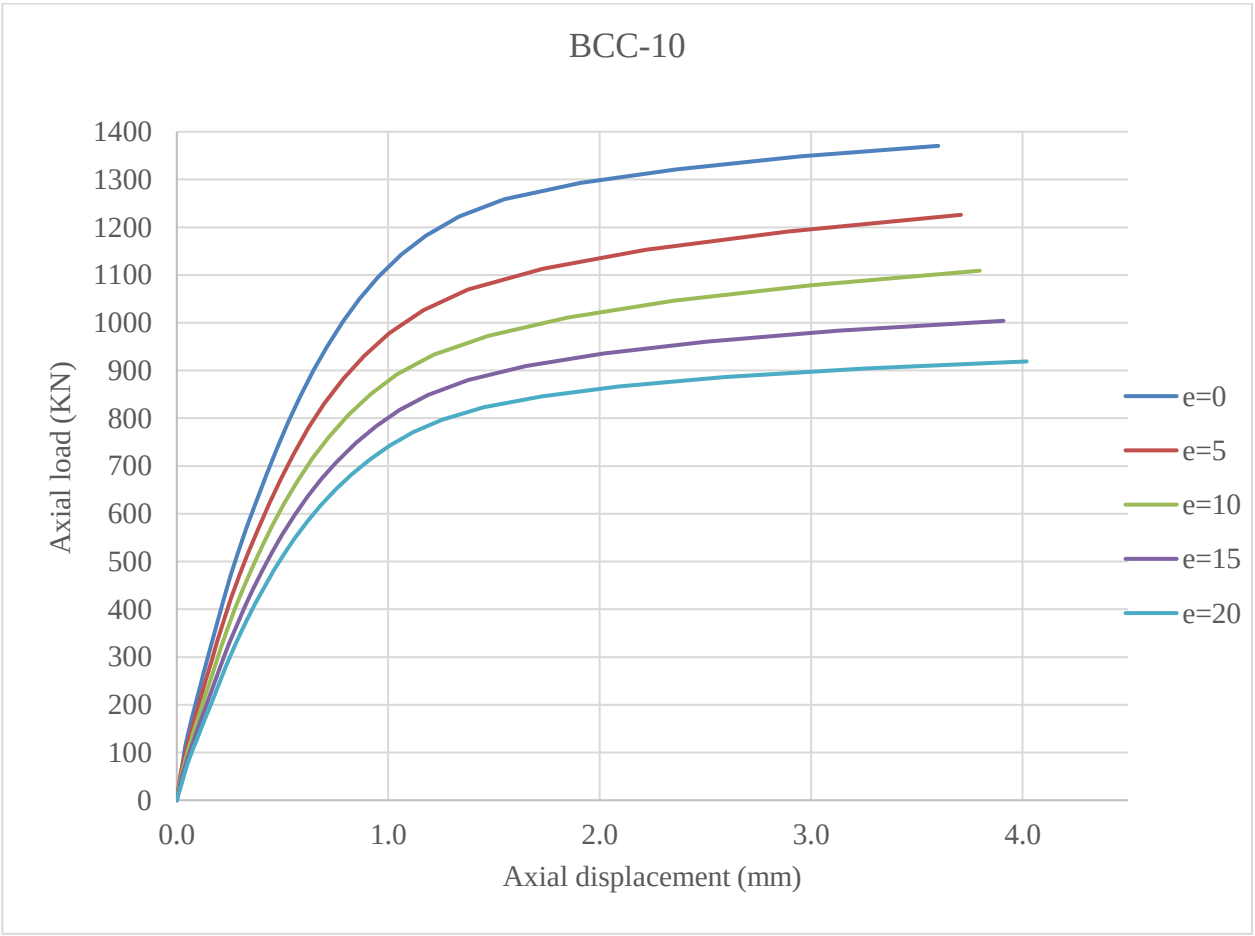

Figure: 4.14: Effects of eccentric loading on axial loading and axial displacement for BCC-10

Table 4.10: Axial Load – axial displacement of eccentric loading for BCC-10

BCC-10									
Eccentricity (e=0)		Eccentricity (e=5)		Eccentricity (e=10)		Eccentricity (e=15)		Eccentricity (e=20)	
u_a(mm)	P_{cc} (KN)	u_a(mm)	P_{cc} (KN)	u_a(mm)	P_{cc} (KN)	u_a(mm)	P_{cc} (KN)	u_a(mm)	P_{cc} (KN)
0	0	0	0	0	0	0	0	0.00	0
0.04	113	0.01	42	0.01	34	0.03	51	0.05	70
0.05	140	0.02	56	0.02	47	0.04	66	0.06	86
0.07	170	0.03	76	0.03	63	0.05	83	0.08	105
0.09	204	0.04	97	0.04	81	0.06	102	0.09	124
0.10	224	0.05	123	0.05	101	0.08	124	0.11	146
0.11	244	0.07	150	0.06	114	0.10	148	0.13	171
0.13	263	0.08	166	0.07	127	0.12	173	0.16	195
0.14	283	0.09	183	0.09	152	0.14	201	0.18	224
0.16	325	0.10	200	0.11	180	0.17	231	0.21	252
0.19	369	0.11	216	0.13	214	0.19	262	0.24	283
0.22	421	0.14	251	0.15	246	0.22	295	0.26	313
0.25	469	0.16	293	0.18	281	0.25	329	0.30	344
0.29	519	0.19	333	0.21	319	0.28	368	0.33	379
0.33	576	0.22	380	0.24	357	0.32	404	0.37	411
0.38	627	0.26	423	0.27	401	0.36	439	0.41	447
0.43	684	0.30	473	0.31	442	0.40	479	0.46	480
0.47	734	0.34	519	0.36	488	0.45	519	0.51	517
0.53	791	0.39	570	0.41	534	0.50	556	0.56	550
0.58	843	0.44	623	0.45	576	0.56	597	0.62	586
0.65	899	0.49	674	0.51	622	0.62	637	0.68	618
0.71	949	0.55	725	0.57	669	0.69	675	0.75	652
0.79	1003	0.62	780	0.64	716	0.76	709	0.83	683
0.86	1049	0.70	830	0.72	760	0.85	748	0.92	715
0.95	1095	0.79	883	0.81	808	0.94	784	1.01	743
1.06	1143	0.89	930	0.92	851	1.05	817	1.12	771
1.18	1182	1.00	978	1.04	892	1.19	849	1.26	797
1.34	1223	1.17	1026	1.21	933	1.38	880	1.45	823
1.55	1259	1.38	1070	1.47	972	1.65	909	1.73	846
1.91	1293	1.73	1113	1.85	1011	2.02	936	2.09	867
2.36	1321	2.22	1153	2.35	1046	2.51	961	2.59	886
2.95	1348	2.89	1191	3.00	1078	3.12	983	3.25	904
3.60	1370	3.71	1226	3.80	1109	3.91	1004	4.02	919

4.3.2 Effect of BST diameter on enhancement of axial Stress and strain for BCC column.

The BST diameters studied in this research include D_b = (169.6mm, 211.6mm, 261.6mm, and 311.6mm). While BST diameter increases, the axial stress enhancement ratio of the BCC column decreases as compared to the same model. The axial stress enhancement ratio of the composite columns decreases with increasing the diameter of the Bamboo Fiber Tube. From BST diameter value Db=169.6mm to Db=211.6mm, the axial stress enhancement ratio decreased by 7.8%, from Db=211.6mm to Db=261.6mm, the axial stress enhancement ratio decreased by 7.6%; and from Db=261.6mm to Db=311.6mm, the axial stress enhancement ratio decreased by 5.1%. The difference in axial stress enhancement ratio between Db = 211.6 mm and Db = 311.6 mm is about 22%, as shown in table 4.11 and figure 4.15. The axial stress capacity of the BCC columns decreased as the diameter of the BST increased, as shown in figure 4.16. The enhancement axial stress capacity ratio (f_{cc}/f_{co}) of the BCC column with 169.6mm diameter of BST had a better axial stress capacity and axial strain magnitude enhancement ratio than the test specimens with 311.6mm diameter of BST. BST confinement is more effective in BCC columns with small diameter of BST than with larger diameter of BST. The ratio of the axial stress capacity and axial strain magnitude enhancement (f_{cc}/f_{co} and $\varepsilon_{cc}/\varepsilon_{co}$) shows the concrete capacity gained from confinement in proportion to its BST diameter. The larger enhancement ratio points out the effectiveness of confinement from BST tube. In general, from this finite element analysis of composite columns with varying diameters of Bamboo Fiber Tube, we can conclude that the higher diameters of Bamboo Fiber Tube have a low axial stress and axial strain enhancement ratio in Bamboo Fiber Tube Concrete-Filled Composite Columns, and similar previous research supports this conclusion as well(Wang *et al.*, 2021a).

Table 4.11: Effect of BST diameter on axial stress and strain enhancement ratio

Specimen	BST diameter	P_a KN	f_{cc} Mpa	ε_{cc} mm/mm	Stress enhancement ratio f_{cc}/f_{co}	Strain enhancement ratio $\varepsilon_{cc}/\varepsilon_{co}$
BCC-5	169.6	978	42.9	0.0082	1.31	3.7
BCC-55	211.6	890	39.8	0.0075	1.22	3.4
BCC-56	261.6	835	37	0.007	1.13	3.2
BCC-57	311.6	795	35.2	0.0064	1.08	2.9

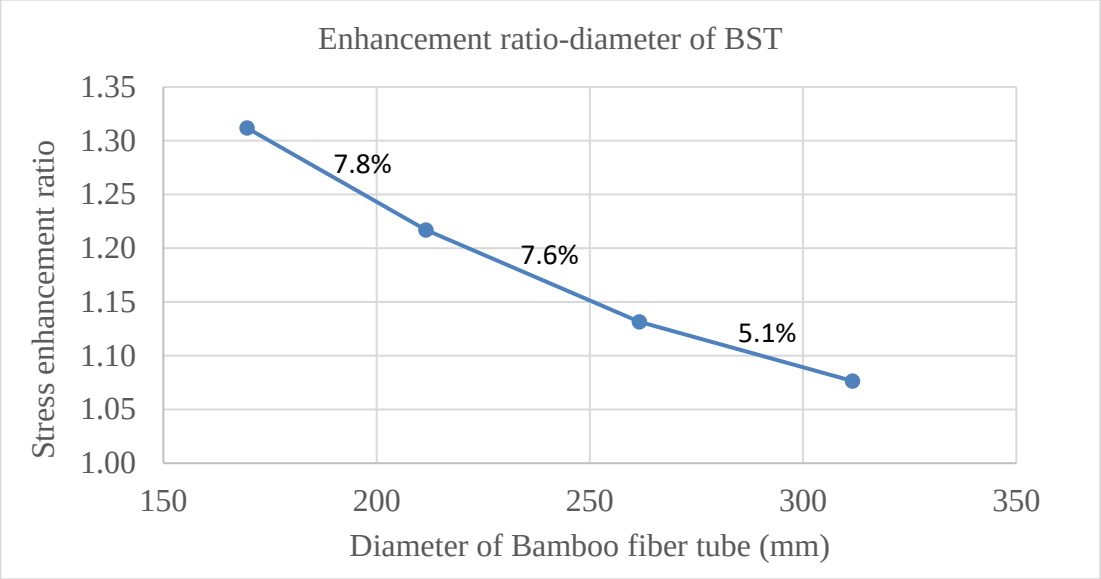

Figure 4.15: Comparisons between diameter of BST and stress enhancement ratio for column.

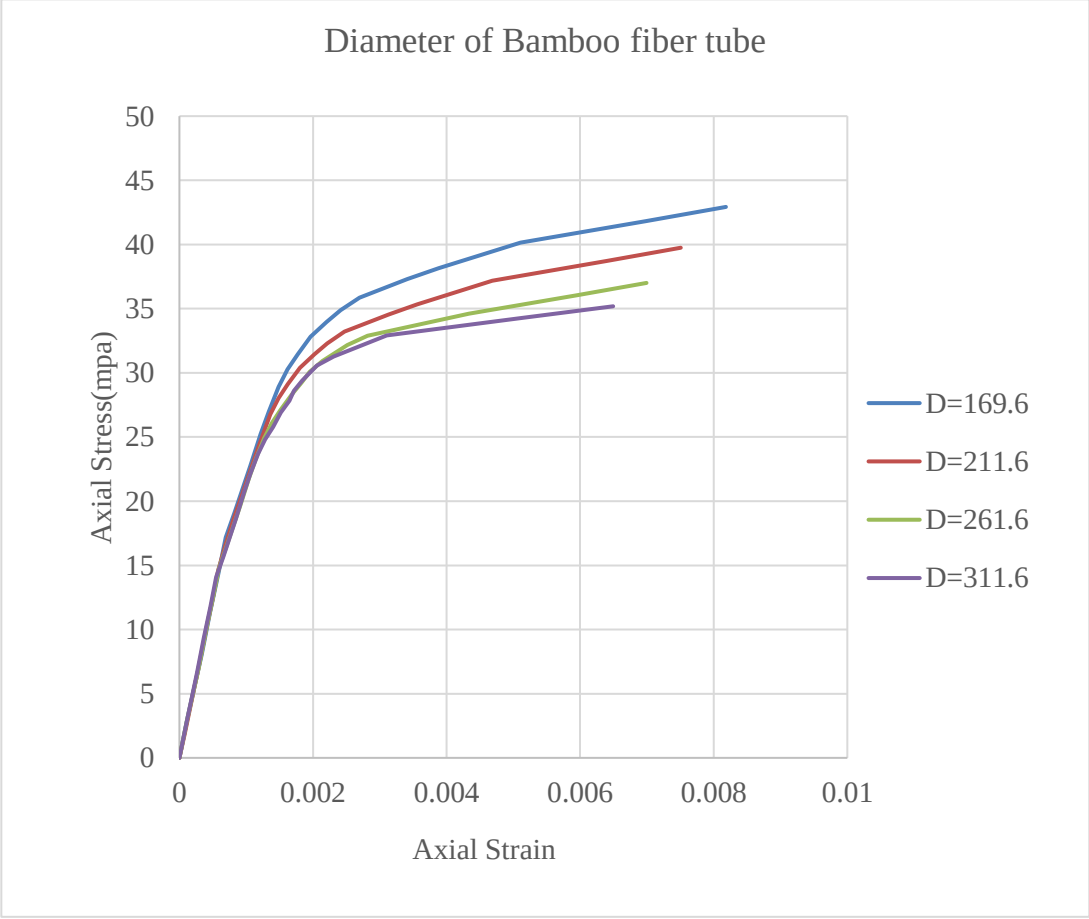

Figure 4. 16: Effect of BST diameter on BCC column.

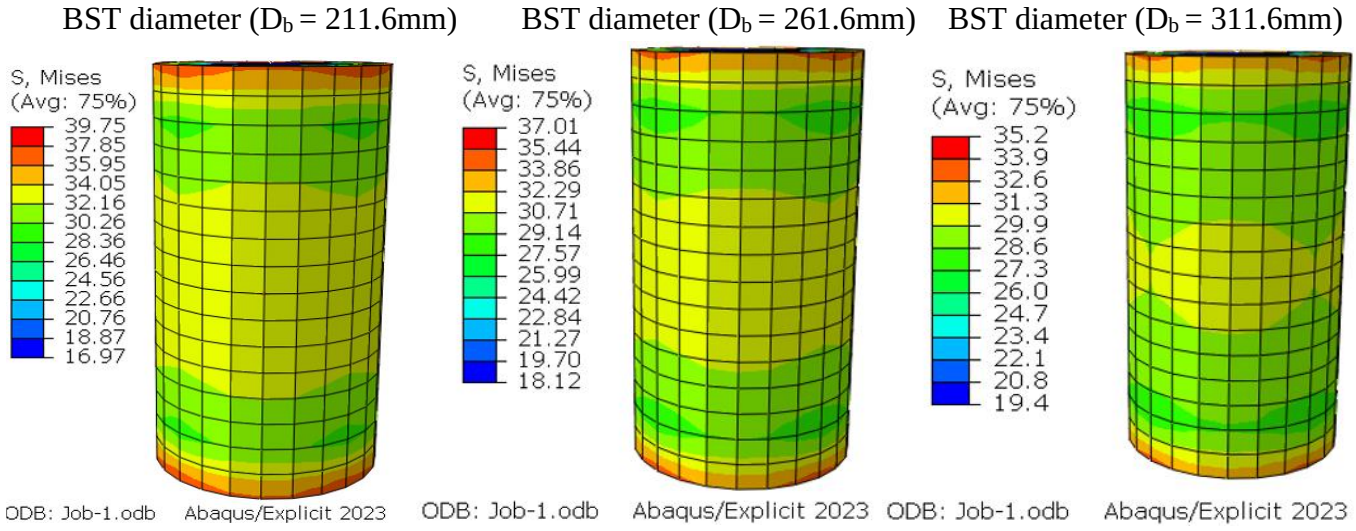

Figure 4.17: Axial stress contour with varying BST diameter at ultimate for BCC-5

Table 4.12: Effect of BST diameter on Axial stress – axial strain for BCC column

D=169.6mm		D=211.6mm		D=261.6mm		D=311.6mm	
Axial strain	Axial Stress	Axial strain	Axial Stress	Axial strain	Axial Stress	Axial strain	Axial Stress
ε_c	f_c (mpa)	ε_c	f_c (mpa)	ε_c	f_c (mpa)	ε_c	f_c (mpa)
0	0	0	0	0	0	0	0
0.0001	3.29	0.0001	1.77	0.0001	2.83	0.0001	2.69
0.0003	8.06	0.0002	5.75	0.0003	6.95	0.0003	6.61
0.0005	11.35	0.0003	6.53	0.0004	9.79	0.0004	9.31
0.0006	14.35	0.0004	10.51	0.0005	12.37	0.0005	11.76
0.0007	17.19	0.0005	12.36	0.0006	14.82	0.0006	14.09
0.0008	19.09	0.0006	14.60	0.0007	16.46	0.0007	15.65
0.0011	22.76	0.0007	16.59	0.0009	19.62	0.0008	18.66
0.0012	25.23	0.0008	18.48	0.0010	21.75	0.0010	20.68
0.0013	27.01	0.0012	24.20	0.0011	23.28	0.0011	22.14
0.0015	28.90	0.0014	26.76	0.0013	24.91	0.0012	23.69
0.0016	30.26	0.0015	28.02	0.0014	26.09	0.0013	24.80
0.0018	31.44	0.0016	29.11	0.0015	27.11	0.0014	25.77
0.0020	32.82	0.0018	30.39	0.0017	28.29	0.0015	26.90
0.0022	33.95	0.0020	31.44	0.0018	29.27	0.0016	27.83
0.0024	34.88	0.0022	32.30	0.0020	30.07	0.0017	28.59
0.0027	35.87	0.0025	33.21	0.0021	30.92	0.0018	29.40
0.0034	37.30	0.0031	34.54	0.0025	32.16	0.0021	30.58
0.0039	38.16	0.0036	35.33	0.0028	32.89	0.0023	31.28
0.0051	40.14	0.0047	37.17	0.0043	34.61	0.0031	32.90
0.0070	41.83	0.0064	38.73	0.0060	36.06	0.0051	34.28
0.0082	42.93	0.0075	39.75	0.0070	37.01	0.0065	35.19

4.3.3 Load application effect on Axial load capacity of Bamboo Fiber Tube Concrete-Filled Composite Column

The Load application effect was assessed for the BCC model having D_{PC}=150mm & L=300mm for t_b= (5.8mm, 9.5mm & 12mm). The following graphs from the ABACUS results which used to compare the effect of Load application on axial load capacity of Bamboo Fiber Tube Concrete-Filled Composite Column.

i. Effect of Load application for thickness of bamboo is 5.8mm.

As introduced in the following graph and table the load application on BCC column with the ultimate load 978KN has the greater axial load carrying capacity than the load application on core concrete column with the ultimate load 907KN about 7.3%.

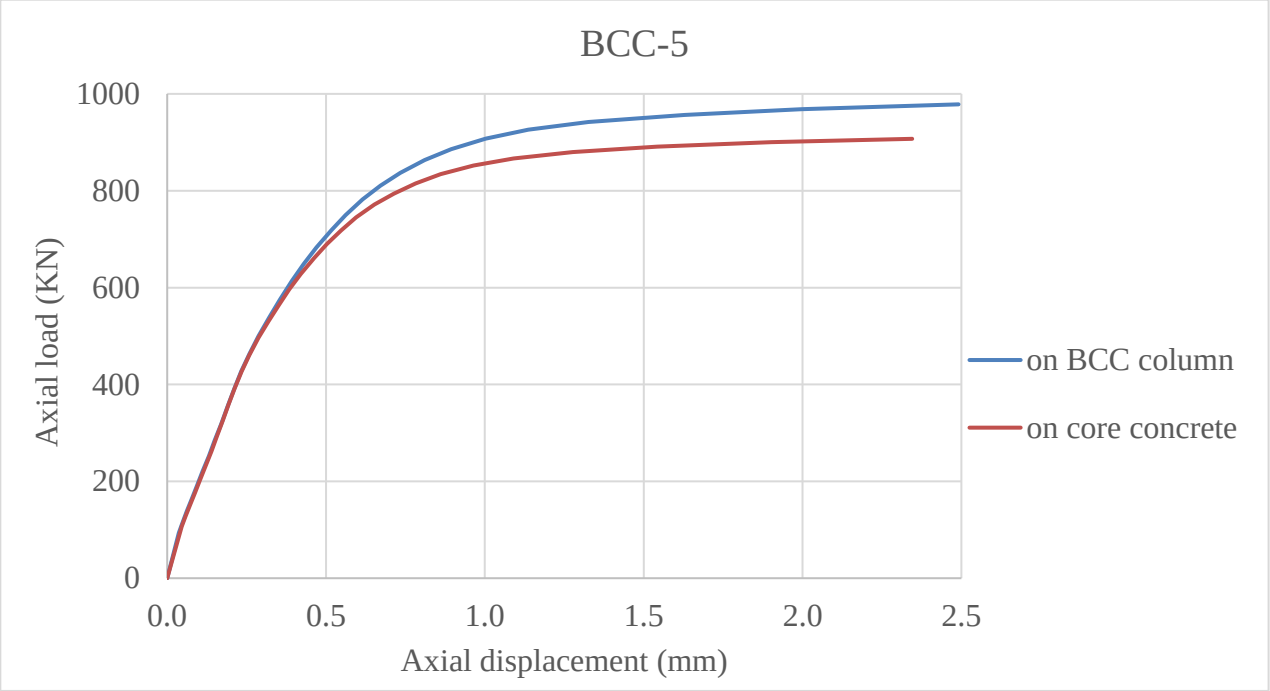

Figure 4. 18: Effect of load application on BCC-5 column.

ii. Effect of load application for thickness of bamboo is 9.5mm

As introduced in the following graph and table the load application on BCC column with the ultimate load 1170KN has the greater load carrying capacity than the load application on core concrete column with the ultimate load 1065KN about 8.94%.

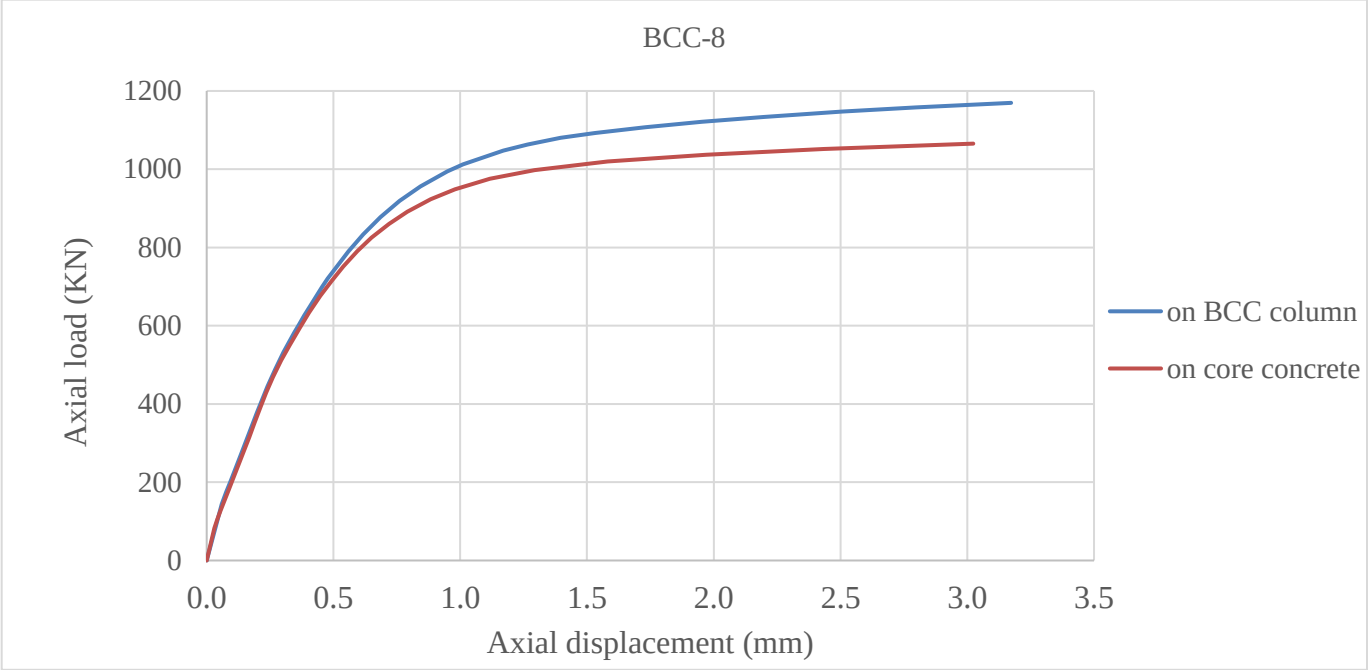

Figure 4. 19: Effect of load application on BCC-8 column.

iii. Effect of load application for thickness of bamboo is 12mm

As introduced in the following graph and table the load application on BCC column with the ultimate load 1394KN has the greater load carrying capacity than the load application on core concrete column with the ultimate load 1260KN about 9.64%.

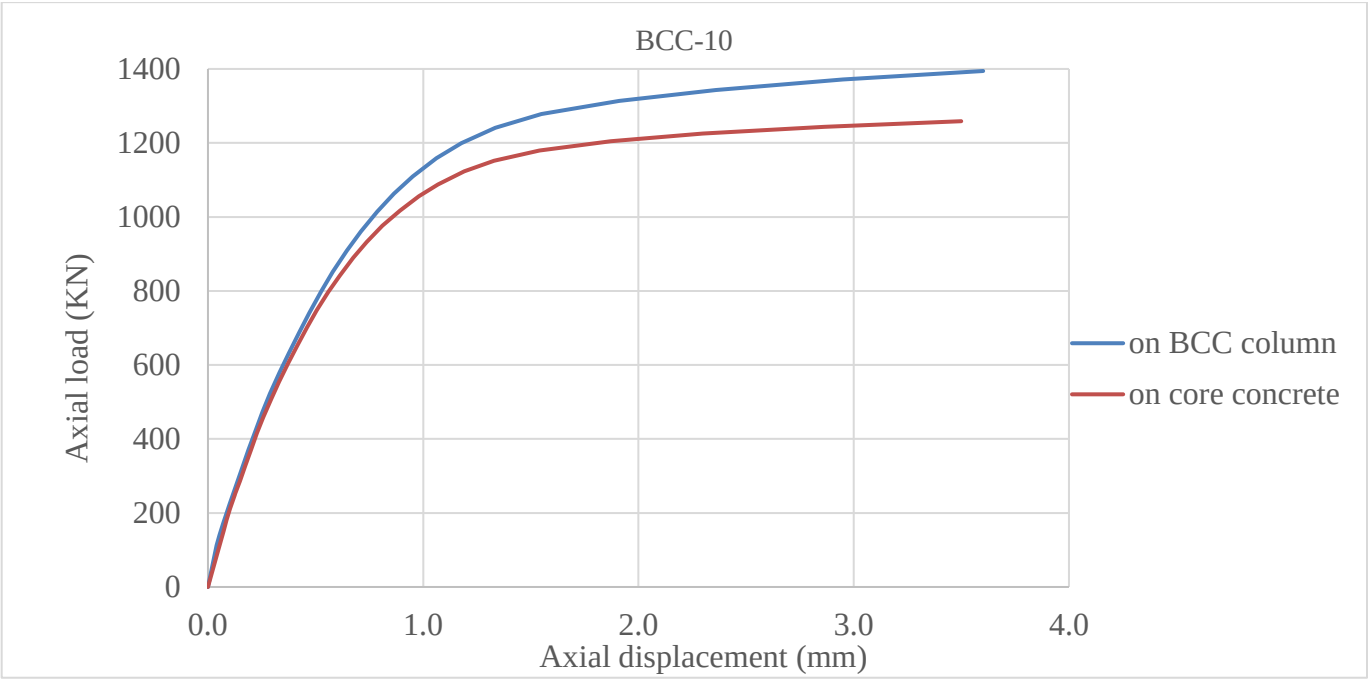

Figure 4. 20: Effect of load application on BCC-10 column.

Table 4.13: Effect of BST-Bamboo and FRP-Bamboo thickness on BCC column

BCC-5				BCC-8				BCC-10			
on BCC column		on core concrete		on BCC column		on core concrete		on BCC column		on core concrete	
U_a (mm)	P_c (KN)	U_a (mm)	P_c (KN)	U_a (mm)	P_c (KN)	U_a (mm)	P_c (KN)	U_a (mm)	P_c (KN)	U_a (mm)	P_c (KN)
0.00	0	0.00	0	0	0	0.00	0	0	0	0.00	0
0.04	94	0.05	107	0.06	144	0.03	82	0.04	113	0.04	90
0.05	115	0.06	128	0.08	175	0.04	104	0.05	140	0.07	151
0.06	138	0.07	151	0.10	206	0.05	127	0.07	171	0.09	180
0.08	163	0.09	176	0.14	277	0.07	154	0.09	204	0.10	212
0.09	192	0.10	202	0.20	378	0.09	181	0.10	224	0.13	249
0.11	220	0.12	233	0.24	445	0.10	210	0.11	245	0.13	250
0.13	252	0.14	262	0.27	488	0.13	244	0.13	264	0.15	286
0.15	284	0.16	293	0.29	510	0.15	277	0.14	284	0.17	329
0.17	318	0.17	325	0.30	532	0.17	315	0.16	327	0.20	369
0.19	354	0.19	360	0.34	581	0.19	351	0.19	371	0.23	416
0.21	389	0.21	393	0.36	604	0.21	391	0.22	423	0.26	459
0.23	427	0.23	427	0.38	626	0.24	430	0.25	472	0.29	509
0.26	464	0.26	460	0.41	649	0.26	468	0.29	523	0.33	554
0.29	500	0.29	497	0.45	698	0.29	512	0.33	580	0.37	605
0.32	539	0.32	530	0.48	720	0.33	551	0.38	632	0.41	652
0.36	575	0.35	564	0.56	790	0.37	594	0.43	690	0.46	703
0.39	613	0.38	596	0.62	833	0.40	634	0.47	741	0.51	748
0.43	648	0.42	628	0.69	877	0.45	676	0.53	799	0.56	797
0.47	683	0.46	661	0.76	919	0.49	714	0.58	851	0.61	842
0.52	718	0.50	690	0.84	956	0.54	751	0.65	909	0.68	890
0.56	750	0.55	718	0.95	995	0.59	790	0.71	960	0.74	932
0.62	782	0.60	745	1.01	1013	0.65	825	0.79	1015	0.81	976
0.67	810	0.65	771	1.17	1048	0.72	861	0.86	1063	0.89	1017
0.73	837	0.71	794	1.27	1063	0.79	892	0.95	1109	0.98	1056
0.81	863	0.78	815	1.40	1080	0.88	923	1.06	1158	1.07	1088
0.89	886	0.86	834	1.53	1093	0.98	949	1.18	1199	1.19	1123
1.00	908	0.96	852	1.73	1108	1.12	975	1.34	1241	1.33	1152
1.14	926	1.09	867	1.95	1121	1.29	998	1.55	1278	1.54	1180
1.33	942	1.28	880	2.20	1134	1.58	1019	1.91	1313	1.87	1204
1.63	957	1.54	891	2.51	1147	1.97	1037	2.36	1343	2.30	1225
2.00	968	1.90	900	2.80	1158	2.43	1052	2.95	1371	2.86	1244
2.49	978	2.35	907	3.17	1170	3.02	1065	3.60	1394	3.50	1259

4.3.4 The effect of BST- Bamboo thickness on the ductility behavior of bamboo fiber tube concrete-filled composite column.

The BST- Bamboo thickness effect on the ductility behavior was assessed for the BCC model having d_{pc}=150mm, L=300mm and t_b= (5.8mm, 9.5mm & 12mm) for load eccentricities studied in this research include, e= (5mm, 10mm,15mm & 20mm). while BST- Bamboo thickness increases, the ductility behavior of BCC column increases as compared with the same model**.**

i. Effect of BST- Bamboo thickness on ductility behavior for concentric loading (e=0)

The BST- Bamboo thickness effect on the ductility behavior was assessed for the BCC model having d_{pc}=150mm, L=300mm and varying BST- Bamboo thickness from t_b=5.8mm to t_b=12mm) for concentric loading (e=0). The ductility behavior of the composite columns increases with increasing BST- Bamboo thickness, from BST- Bamboo thickness value t_b=5.8mm to tb=9.5mm the ductility index ($\varepsilon_{cu}/\varepsilon_{cy}$) increased by 21.5% between 14.4 to 18.3, tb=9.5mm to tb=12mm the ductility index increased by 12% between 18.3 to 20.8 and the difference ductility index between tb=5.8mm and tb=12mm is about 31% as shown in Table 4.14 and Figure 4.20. In general, from this finite element analysis of composite columns by varying BST-Bamboo thickness, we can conclude as the higher BST- Bamboo thickness have high ductility behavior in Bamboo Fiber Tube Concrete-Filled Composite Column.

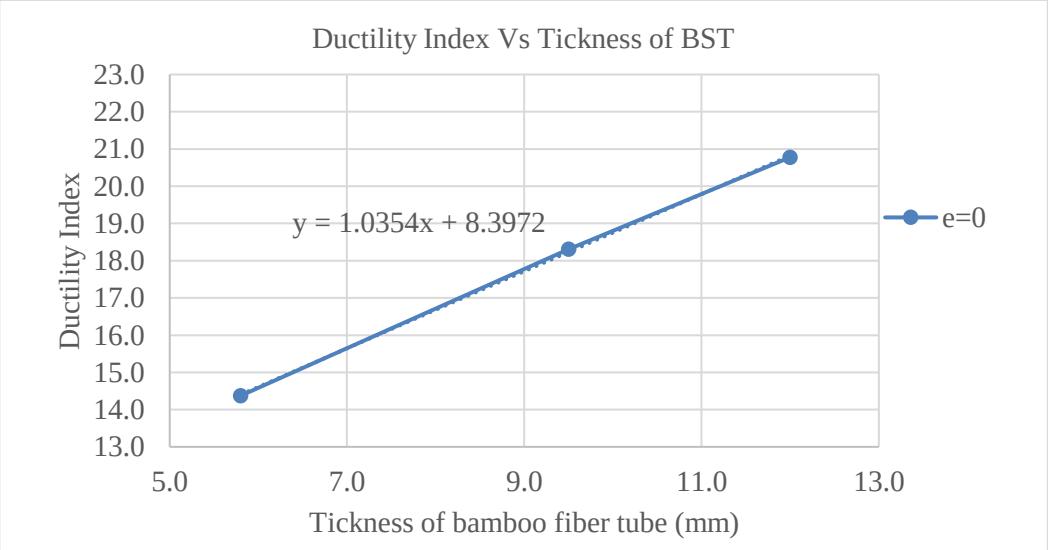

Figure 4.21: Effect of BST- Bamboo thickness on ductility behavior.

ii. Effect of BST- Bamboo thickness on ductility behavior for eccentric loading (e=5mm)

The BST- Bamboo thickness effect on the ductility behavior was assessed for the BCC model having d_{pc}=150mm, L=300mm and varying BST- Bamboo thickness from tb=5.8mm to tb=12mm) for eccentric

loading (e=5mm). The ductility behavior of the composite columns increases with increasing BST- Bamboo thickness, from BST- Bamboo thickness value tb=5.8mm to tb=9.5mm the ductility index ($\varepsilon_{cu}/\varepsilon_{cy}$) increased by 21% between 15.1 to 19.1, tb=9.5mm to tb=12mm the ductility index increased by 11% between 19.1 to 21.4. and the difference ductility index between tb=5.8mm and tb=12mm is about 30% as shown in Table 4.14 and Figure 4.21. In general, from this finite element analysis of composite columns by varying BST- Bamboo thickness, we can conclude as the higher BST- Bamboo thickness have high ductility behavior in Bamboo Fiber Tube Concrete-Filled Composite Column.

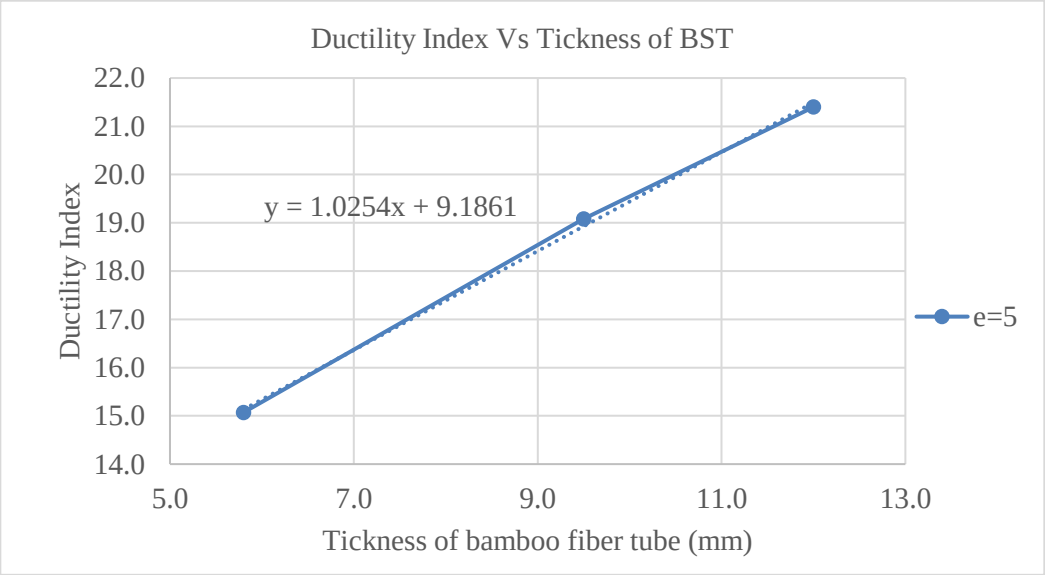

Figure 4.22: Effect of BST- Bamboo thickness on ductility behavior.

iii. Effect of BST- Bamboo thickness on ductility behavior for eccentric loading (e=10mm)

The BST- Bamboo thickness effect on the ductility behavior was assessed for the BCC model having d_{pc}=150mm, L=300mm and varying BST- Bamboo thickness from tb=5.8mm to tb=12mm) for eccentric loading (e=10mm). The ductility behavior of the composite columns increases with increasing BST- Bamboo thickness, from BST- Bamboo thickness value tb=5.8mm to tb=9.5mm the ductility index ($\varepsilon_{cu}/\varepsilon_{cy}$) increased by 20% between 15.9 to 19.9, tb=9.5mm to tb=12mm the ductility index increased by 9% between 19.9 to 21.9. and the difference ductility index between tb=5.8mm and tb=12mm is about 28% as shown in Table 4.14 and Figure 4.22. In general, from this finite element analysis of composite columns by varying BST- Bamboo thickness, we can conclude as the higher BST- Bamboo thickness have high ductility behavior in Bamboo Fiber Tube Concrete-Filled Composite Column.

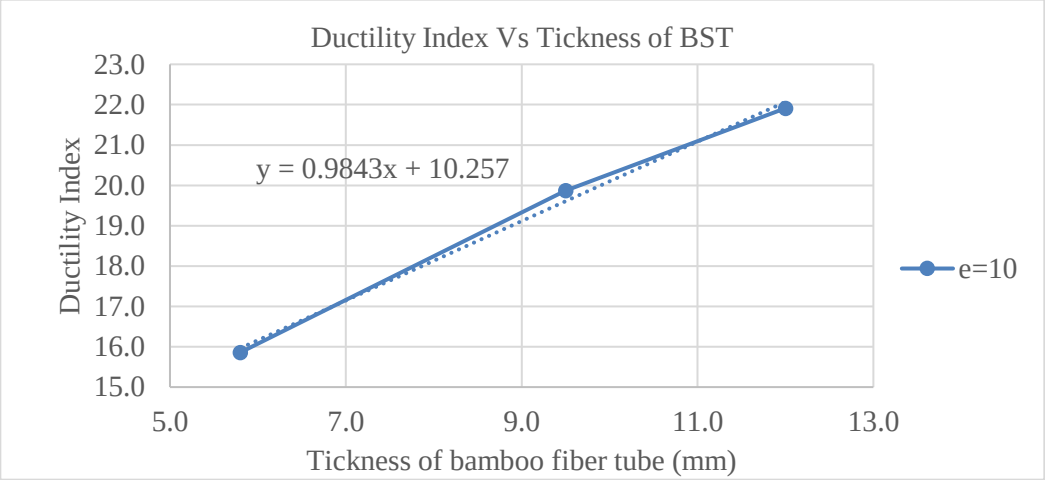

Figure 4.23: Effect of BST- Bamboo thickness on ductility behavior.

iv. Effect of BST- Bamboo thickness on ductility behavior for eccentric loading (e=15mm)

The BST- Bamboo thickness effect on the ductility behavior was assessed for the BCC model having d_{pc}=150mm, L=300mm and varying BST- Bamboo thickness from tb=5.8mm to tb=12mm) for eccentric loading (e=15mm). The ductility behavior of the composite columns increases with increasing BST- Bamboo thickness, from BST- Bamboo thickness value tb=5.8mm to tb=9.5mm the ductility index ($\varepsilon_{cu}/\varepsilon_{cy}$) increased by 19% between 16.6 to 20.5, tb=9.5mm to tb=12mm the ductility index increased by 9% between 20.5 to 22.6. and the difference ductility index between tb=5.8mm and tb=12mm is about 26% as shown in Table 4.14 and Figure 4.23. In general, from this finite element analysis of composite columns by varying BST- Bamboo thickness, we can conclude as the higher BST- Bamboo thickness have high ductility behavior in Bamboo Fiber Tube Concrete-Filled Composite Column.

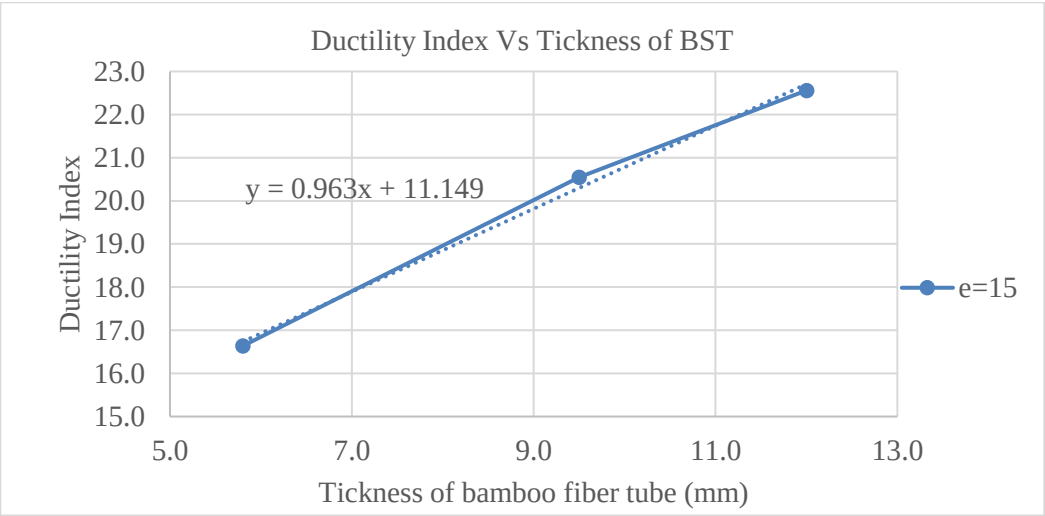

Figure 4.24: Effect of BST- Bamboo thickness on ductility behavior.

v. Effect of BST- Bamboo thickness on ductility behavior for eccentric loading (e=20mm)

The BST- Bamboo thickness effect on the ductility behavior was assessed for the BCC model having d_{pc}=150mm, L=300mm and varying BST- Bamboo thickness from tb=5.8mm to tb=12mm) for eccentric loading (e=20mm). The ductility behavior of the composite columns increases with increasing BST- Bamboo thickness, from BST- Bamboo thickness value tb=5.8mm to tb=9.5mm the ductility index ($\varepsilon_{cu}/\varepsilon_{cy}$) increased by 17% between 17.5 to 21.1, tb=9.5mm to tb=12mm the ductility index increased by 9% between 21.1 to 23.2. and the difference ductility index between tb=5.8mm and tb=12mm is about 24% as shown in Table 4.14 and Figure 4.24. In general, from this finite element analysis of composite columns by varying BST- Bamboo thickness, we can conclude as the higher BST- Bamboo thickness have high ductility behavior in Bamboo Fiber Tube Concrete-Filled Composite Column.

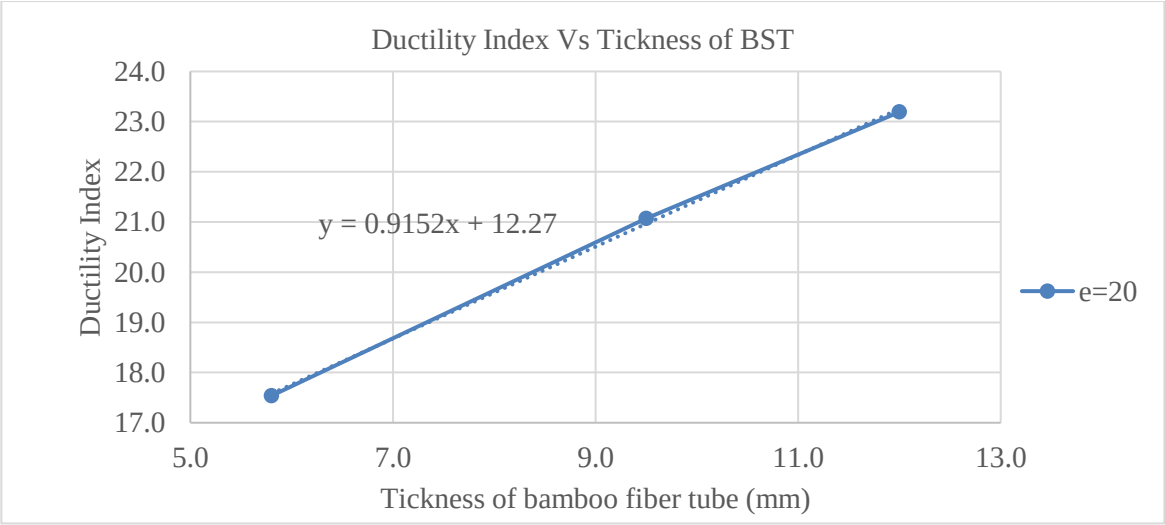

Figure 4. 25: Effect of BST- Bamboo thickness on ductility behavior

Table 4.14: Ductility index value of BCC- column for different BST thickness.

Eccentricity (e=0)		Eccentricity (e=5)		Eccentricity (e=10)		Eccentricity (e=15)		Eccentricity (e=20)	
t_b (mm)	DI ($\varepsilon_{cu}/\varepsilon_{cy}$)	t_b (mm)	DI ($\varepsilon_{cu}/\varepsilon_{cy}$)	t_b (mm)	DI ($\varepsilon_{cu}/\varepsilon_{cy}$)	t_b (mm)	DI ($\varepsilon_{cu}/\varepsilon_{cy}$)	t_b (mm)	DI ($\varepsilon_{cu}/\varepsilon_{cy}$)
5.8	14.4	5.8	15.1	5.8	15.9	5.8	16.6	5.8	17.5
9.50	18.3	9.50	19.1	9.50	19.9	9.50	20.5	9.50	21.1
12.00	20.8	12.00	21.4	12.00	21.9	12.00	22.6	12.00	23.2

CHAPTER FIVE

5. CONCLUSIONS AND RECOMMENDATIONS

5.1 Conclusions

The aim of this study was to assess the Non-Linear Finite Element Analysis of Bamboo Fiber Tube Concrete-Filled Composite Column under axial loading and uniaxial eccentricity using non-linear analysis by ABAQUS/CAE 2023. The effect of eccentric loading, diameters of Bamboo Fiber Tube, load application and BST-Bamboo thickness on Composite Columns was assessed. A non-linear 3-D finite element models were developed to model different Composite Columns. Based on the findings of this study and within the present scope of work, the investigation carryout. In some cases, the load carrying capacity enhancement ratio, stress carrying capacity enhancement ratio, axial load, and ductility behavior of the columns is observed to increase as the value of the parameter under the study increases. The reverse is observed for other parameters. After the careful check of the analysis results, the following conclusions are drawn.

- The axial load capacity enhancement ratio increases with increasing eccentric loading values of the Bamboo Fiber Tube Concrete-Filled Composite Column for BCC-5. As the eccentric loading increased from 0 to 20mm, the axial load capacity enhancement ratio of BCC-5 columns increased by 26%.
- The axial load capacity of the Bamboo Fiber Tube Concrete-Filled Composite Column for BCC-5 decreases with increasing eccentric loading values. As the eccentric loading increased from 0 to 20mm, the axial load capacity of BCC-5 columns decreased by 42%.
- The axial load capacity enhancement ratio increases with increasing eccentric loading values of the Bamboo Fiber Tube Concrete-Filled Composite Column for BCC-8. As the eccentric loading increased from 0 to 20mm, the axial load capacity enhancement ratio of BCC-8 columns increased by 46%.
- As the eccentric loading increased from 0 to 20mm, the axial load capacity of BCC-8 columns decreased by 38%.
- The axial load capacity enhancement ratio increases with increasing eccentric loading values of the Bamboo Fiber Tube Concrete-Filled Composite Column for BCC-10. As the eccentric loading increased from 0 to 20mm, the axial load capacity enhancement ratio of BCC-10 columns increased by 75%.
- As the eccentric loading increased from 0 to 20mm, the axial load capacity of BCC-10 columns reduced by 33%.

- The axial stress enhancement ratio decreases with increasing the diameter of the bamboo fiber tube. As the diameter of bamboo fiber tubes increased from 169.6mm to 311.6mm, the axial stress capacity enhancement ratio of BCC columns decreased by 22%.
- The load application on the top BCC column has a greater load-carrying capacity than the load application on the top core concrete column for columns BCC-5, BCC-8, and BCC-10 by 7.3%. 8.94% and 9.64%, respectively.
- As the BST-Bamboo thickness increases from 5.8mm to 12mm, the ductility index ($\varepsilon_{cu}/\varepsilon_{cy}$) for the composite columns with eccentric loadings e=0, e=5, e=10, e=15, and e=20 increases by 31%, 30%, 28%, 26%, and 24%, respectively.
- As concluded from the analysis results of this study, BST confinement is more effective under eccentric loading than concentric loading.
- The axial stress capacity enhancement ratio of the Bamboo Fiber Tube Concrete-Filled Composite Column decreases with increasing the diameter of Bamboo Fiber Tube.
- The axial load capacity of the Bamboo Fiber Tube Concrete-Filled Composite Column increases when the load is applied to the BCC column compared to the core concrete column.
- The ductility behavior of the BCC column increases when BST-Bamboo thickness increases for the Bamboo Fiber Tube Concrete-Filled Composite Column under uniaxial eccentricity.

5.2 Recommendations

The following recommendations are made for future researches, which are not covered in the present study: -

- The ductility behavior of Bamboo Fiber Tube Concrete-Filled Composite Column under biaxial loading.
- This research has to be checked by laboratory works before implementation.
- Axial load capacity of Bamboo Fiber Tube Concrete-Filled Composite Column under biaxial loading.

REFERENCES

Ahmed, M. *et al.* (2020a) 'Computational simulation of eccentrically loaded circular thin-walled concrete-filled double steel tubular slender columns', *Engineering Structures*, 213(December 2019), p. 110571. doi:10.1016/j.engstruct.2020.110571.

Ahmed, M. *et al.* (2020b) 'Experimental and numerical investigations of eccentrically loaded rectangular concrete-filled double steel tubular columns', *Journal of Constructional Steel Research*, 167, p. 105949. doi:10.1016/j.jcsr.2020.105949.

Al-Fasih, M.Y. *et al.* (2022) 'Tensile properties of bamboo strips and flexural behaviour of the bamboo reinforced concrete beams', *European Journal of Environmental and Civil Engineering*, 26(13), pp. 6444–6460. doi:10.1080/19648189.2021.1945954.

Albero, V. *et al.* (2021) 'Behaviour of slender concrete-filled dual steel tubular columns subjected to eccentric loads', *Journal of Constructional Steel Research*, 176, p. 106365. doi:10.1016/j.jcsr.2020.106365.

Albero, V. *et al.* (2022) 'Experimental analysis on circular concrete-filled steel tubular beam-columns under unequal load eccentricities', *Engineering Structures*, 259(March). doi:10.1016/j.engstruct.2022.114206.

Amede, E.A. *et al.* (2021) 'A Review of Codes and Standards for Bamboo Structural Design', *Advances in Materials Science and Engineering*, 2021. doi:10.1155/2021/4788381.

Ampangallo, B.A. and Ambali, D.P.P. (2021) 'Comparison bending strength of simple reinforced concrete beams with bamboo reinforcement in the form of circle and square sections', *INVOTEK: Jurnal Inovasi Vokasional dan Teknologi*, 21(2), pp. 87–94. doi:10.24036/invotek.v21i2.840.

Chen, G.M. *et al.* (2020) 'Compressive behavior of FRP-confined steel-reinforced high strength concrete columns', *Engineering Structures*, 220(June). doi:10.1016/j.engstruct.2020.110990.

Chen, M. *et al.* (2020) 'Flexural strength and ductility of moso bamboo', *Construction and Building Materials*, 246, p. 118418. doi:10.1016/j.conbuildmat.2020.118418.

Chen, S. *et al.* (2021) 'Experimental investigation of timber beams strengthened by bamboo scrimber with anchorage structure', *Structures*, 33(April), pp. 1–11. doi:10.1016/j.istruc.2021.04.038.

Cui, J. *et al.* (2020) 'Multiscale structural insights of load bearing bamboo: A computational modeling approach', *Journal of the Mechanical Behavior of Biomedical Materials*, 107(April 2018), p. 103743. doi:10.1016/j.jmbbm.2020.103743.

Degefa Zewdu, B. and Wondimu Aure, T. (2022) 'Numerical Investigation of Carbon Fiber Reinforced Polymer Confined Concrete-Filled Steel Tube Columns under Eccentric Load', *Advances in Civil Engineering*, 2022. doi:10.1155/2022/4807436.

ES EN 1992 (2015) 'Compulsory Ethiopian Standard Design of Concrete Structures-Part 1-1 : General rules and rules for buildings', *Ces En 1994-1-1*, PART 1-1.

ES EN 1994 (2015) 'Design of Composite Steel and Concrete Structures. 1-1: General Rules and Rules for Buildings Control', *European Committee for Standardization, British Standards Institution* [Preprint].

Gan, D. *et al.* (2020) 'Axial compressive behaviour of circular concrete-filled steel tubular stub columns with an inner bamboo culm', *Structures*, 26(November 2019), pp. 156–168. doi:10.1016/j.istruc.2020.04.016.

Hassan, W.M. *et al.* (2017) 'Behavior of eccentrically loaded high strength concrete columns jacketed with FRP laminates', *Construction and Building Materials*, 138, pp. 508–527. doi:10.1016/j.conbuildmat.2017.02.016.

Hu, H.S. *et al.* (2020) 'Behavior of eccentrically loaded square spiral-confined high-strength concrete-filled steel tube columns', *Engineering Structures*, 216(May). doi:10.1016/j.engstruct.2020.110743.

Huang, L., Yu, T. and Zhang, S.S. (2021) 'FRP-Confined concrete-encased cross-shaped steel columns: Effects of key parameters', *Composite Structures*, 272(December 2020), p. 114252. doi:10.1016/j.compstruct.2021.114252.

Hussain, Q. *et al.* (2020) 'Behavior of concrete confined with epoxy bonded fiber ropes under axial load', *Construction and Building Materials*, 263, p. 120093. doi:10.1016/j.conbuildmat.2020.120093.

Isleem, H.F. *et al.* (2024) 'Parametric investigation of rectangular CFRP-confined concrete columns reinforced by inner elliptical steel tubes using finite element and machine learning models', *Heliyon*, 10(2). doi:10.1016/j.heliyon.2023.e23666.

Kim, T.K. and Park, J.S. (2021) 'Evaluation of the performance and ductility index of concrete structures using advanced composite material strengthening methods', *Polymers*, 13(23). doi:10.3390/polym13234239.

Kou, Y. feng, Tian, L. min and Jin, B. bei (2021) 'Axial compressive behavior of bamboo slices twining tube-confined concrete', *European Journal of Wood and Wood Products*, 80(1), pp. 115–129. doi:10.1007/s00107-021-01737-8.

Ma, Y.X., Zhao, O. and Tan, K.H. (2021) 'Experimental and numerical studies of concrete-encased concrete-filled steel tube stub columns under uniaxial and biaxial eccentric compression', *Engineering Structures*, 232(July 2020), p. 111796. doi:10.1016/j.engstruct.2020.111796.

Naeimi, N. and Moustafa, M.A. (2021) 'Compressive behavior and stress–strain relationships of confined and unconfined UHPC', *Construction and Building Materials*, 272, p. 121844. doi:10.1016/j.conbuildmat.2020.121844.

Qiyun, Q., Zhaoyuan, Y. and Wanlin, C. (2021) 'Axial compressive behavior of stainless steel tube confined concrete column piers', *Marine Structures*, 78(October 2020), p. 103021. doi:10.1016/j.marstruc.2021.103021.

Rong, C. and Shi, Q. (2021) 'Analysis constitutive models for actively and passively confined concrete', *Composite Structures*, 256(June 2020), p. 113009. doi:10.1016/j.compstruct.2020.113009.

Salesa, A., Esteban, L.M. and Barris, C. (2022) 'Confinement of FRP concrete columns: Review of design guidelines and comparison with experimental results', *Materiales de Construccion*, 72(345). doi:10.3989/mc.2022.03821.

Shu, B. *et al.* (2020) 'Review on the application of bamboo-based materials in construction engineering', *Journal of Renewable Materials*, 8(10), pp. 1215–1242. doi:10.32604/jrm.2020.011263.

Siddiqui, N. *et al.* (2020) 'Compression behavior of FRP-strengthened RC square columns of varying slenderness ratios under eccentric loading', *Journal of Building Engineering*, 32(May), p. 101512. doi:10.1016/j.jobe.2020.101512.

Sun, X., He, M. and Li, Z. (2020) 'Novel engineered wood and bamboo composites for structural applications: State-of-art of manufacturing technology and mechanical performance evaluation', *Construction and Building Materials*, 249(1239), p. 118751. doi:10.1016/j.conbuildmat.2020.118751.

Tahmasebinia, F. *et al.* (2021) 'Sustainable architecture creating arches using a bamboo grid shell structure: Numerical analysis and design', *Sustainability (Switzerland)*, 13(5), pp. 1–25. doi:10.3390/su13052598.

Tang, S., Zhou, A. and Li, J. (2021) 'Mechanical Properties and Strength Grading of Engineered Bamboo Composites in China', *Advances in Civil Engineering*, 2021. doi:10.1155/2021/6666059.

Tokuda, E.N. *et al.* (2020) 'Design Procedure for Reinforced Concrete Beams and Reinforcement Replacement by Bamboo', *Computational Water, Energy, and Environmental Engineering*, 09(03), pp. 37–47. doi:10.4236/cweee.2020.93004.

Vijayabanu K and Sivakumar M (2021) 'Experimental Study on Bamboo as Reinforced Concrete and Compare the Strength, Durability of Conventional Clay Bricks with Light Weight Interlocking Bricks', *Irish Interdisciplinary Journal of Science & Research (IIJSR)*, 5(3), pp. 33–37. Available at: www.iijsr.comelectroniccopyavailableat:https://ssrn.com/abstract=3898743.

Wang, Y. *et al.* (2021a) 'Axial compressive behavior and con fi nement mechanism of circular FRP-steel tubed concrete stub columns', *Composite Structures*, 256(May 2020), p. 113082. doi:10.1016/j.compstruct.2020.113082.

Wang, Y. *et al.* (2021b) 'Axial compressive behavior and confinement mechanism of circular FRP-steel tubed concrete stub columns', *Composite Structures*, 256(May 2020), p. 113082. doi:10.1016/j.compstruct.2020.113082.

Wei, J. *et al.* (2021) 'Experimental study on circular steel tube-confined reinforced UHPC columns under axial loading', *Engineering Structures*, 230(June 2020), p. 111599. doi:10.1016/j.engstruct.2020.111599.

Ye, Y.Y. *et al.* (2020) 'Rectangular double-tube concrete columns with an internal elliptical high-strength steel tube: Concept and behavior', *Engineering Structures*, 216(March). doi:10.1016/j.engstruct.2020.110742.

Zeng, J.J. *et al.* (2018) 'Compressive behavior of double-tube concrete columns with an outer square FRP tube and an inner circular high-strength steel tube', *Construction and Building Materials*, 184, pp. 668–680. doi:10.1016/j.conbuildmat.2018.07.034.

Zhang, R. *et al.* (2020) 'Structural behavior of UHPC filled steel tubular columns under eccentric loading', *Thin-Walled Structures*, 156(July), p. 106959. doi:10.1016/j.tws.2020.106959.

APPENDICES

A. MATERIAL INPUT DATA SHEET FOR ANALYSIS OF CONTROL AS A SAMPLE

In chapters 4 in Finite Element Analysis, detailed material models were used. The input data for the ABAQUS material models were obtained from equation and formulas thus discussed in chapter 3 of all sections. The consistent unit used for Finite element modeling is SI (mm) as shown on table A.1.

Table A.1: Consistent unit used is SI (mm)

Table → Consistent units.

Quantity	SI	SI (mm)	US Unit (ft)	US Unit (inch)
Length	m	mm	ft	in
Force	N	N	lbf	lbf
Mass	kg	tonne (10^3 kg)	slug	lbf s^2/in
Time	s	s	s	s
Stress	Pa (N/m^2)	MPa (N/mm^2)	lbf/ft^2	psi (lbf/in^2)
Energy	J	mJ (10^{-3} J)	ft lbf	in lbf
Density	kg/m^3	$tonne/mm^3$	$slug/ft^3$	lbf s^2/in^4

A.1 Concrete for C-32.7

Table A. 2: Density and Elastic for Concrete

Density(tonne/mm^3)	2.40E-09
Elasticity (Isotropic)	
young's Modulus (Mpa=N/mm^2), E_c	poison's Ratio, V
28300	0.2

Table A. 3: Concrete Damaged Plasticity for Concrete

Concrete Damage plasticity				
Dilation angle	Eccentricity	f_{bo}/f_{co}	K	Viscocity Parameter
33.99	0.1	1.16	0.667	0

Table A. 4: Unconfined compression concrete input stress-strain

Total strain (ε_c)	Yield stress (MPa)
0	0
0.000644365	16.35
0.000742613	18.35
0.000847983	20.35
0.00096229	22.35
0.001088289	24.35
0.001230527	26.35
0.001397595	28.35
0.00161023	30.35
0.0022	32.7
0.00278977	30.35
0.003002405	28.35
0.003169473	26.35

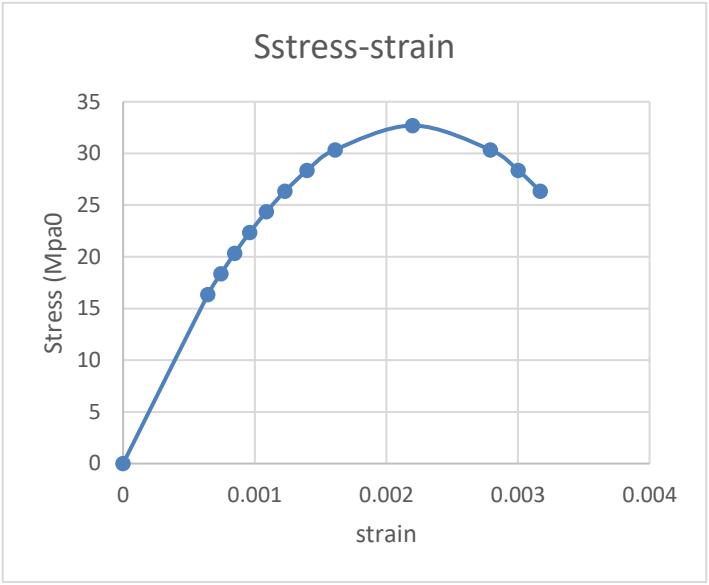

Figure A. 1: Unconfined Compression concrete input stress-strain curve

Table A. 5: Concrete compressive behavior Concrete Hardening

Concrete compressive behavior	
Yield stress (MPa)	Inelastic strain (ε_{inc})
16.35	0
18.35	0.000094204
20.35	0.000128901
22.35	0.000172537
24.35	0.000227865
26.35	0.000299432
28.35	0.000395829
30.35	0.000537792
32.7	0.001044523
30.35	0.001717332
28.35	0.002000638
26.35	0.002238377
24.35	0.002451287
22.35	0.002647958
20.35	0.002832936
18.35	0.003008977
16.35	0.003177896
14.35	0.003340969
12.35	0.00349913
10.35	0.003653087
8.35	0.003803393

Table A. 6: Concrete compressive behavior Concrete Damage

Concrete compression damage	
Compression damage(d_c)	Inelastic strain (ε_{cin})
0	0
0	9.42036E-05
0	0.000128901
0	0.000172537
0	0.000227865
0	0.000299432
0	0.000395829
0	0.000537792
0	0.001044523
0.071865443	0.001717332
0.133027523	0.002000638
0.194189602	0.002238377
0.255351682	0.002451287
0.316513761	0.002647958
0.377675841	0.002832936
0.43883792	0.003008977
0.5	0.003177896
0.56116208	0.003340969
0.622324159	0.00349913
0.683486239	0.003653087
0.744648318	0.003803393

Table A. 7: Unconfined tension concrete input stress-strain

Total strain (ε_t)	Yield stress (MPa)
0	0
0.000115176	3.259483088
0.000345528	2.172988725
0.000676659	1.222306158
0.001209349	0.543247181
0.001526083	0.271623591
0.00168445	0.135811795
0.001763634	0.067905898

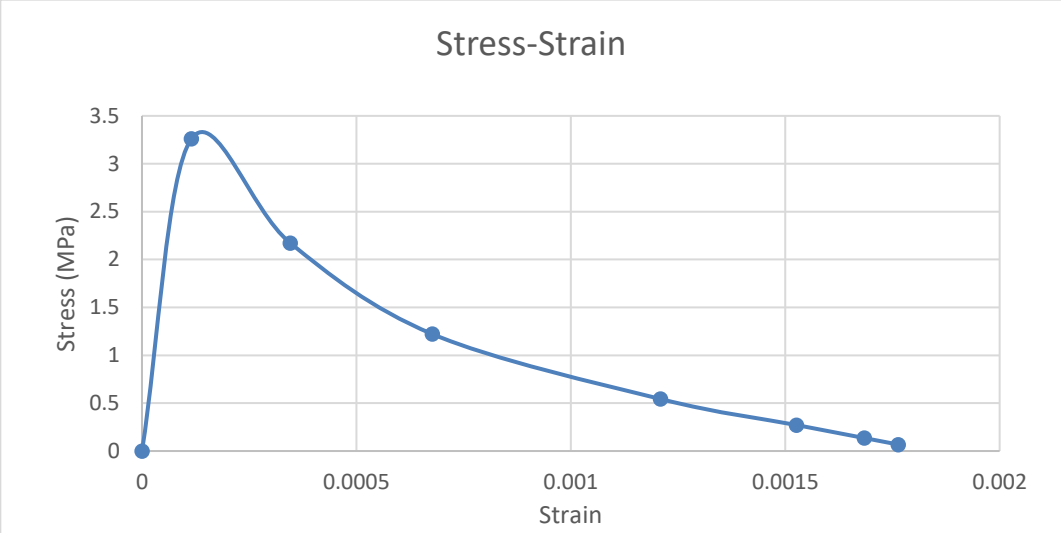

Figure A. 2: Unconfined tension concrete input stress-strain curve

Table A. 8: Concrete tension behavior Concrete Hardening

Concrete Tension behavior	
Yield stress (MPa)	Cracking strain
3.259483088	0
2.172988725	0.000268744
1.222306158	0.000633468
0.543247181	0.001190153
0.271623591	0.001516485
0.135811795	0.001679651
0.067905898	0.001761234

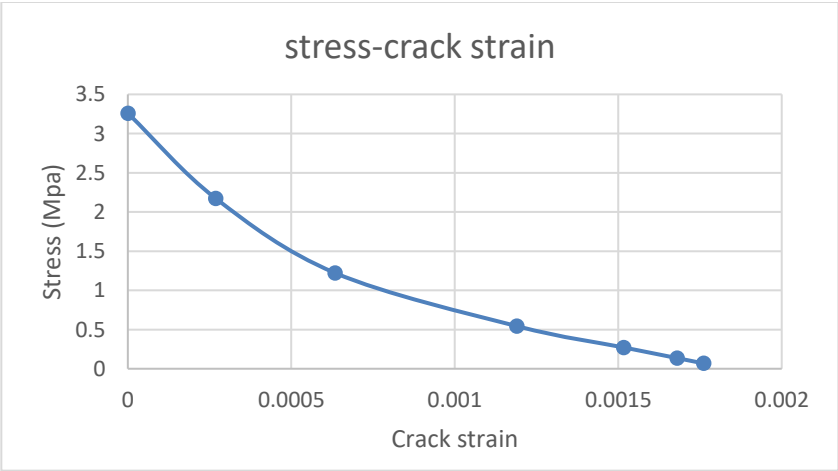

Figure A. 3: Concrete tension behavior Concrete Hardening

Table A. 9: Concrete tension behavior Concrete Damage

Concrete Tension damage	
Tension damage(d_t)	Cracking strain
0	0
0.333333333	0.000268744
0.625	0.000633468
0.833333333	0.001190153
0.916666667	0.001516485
0.958333333	0.001679651
0.979166667	0.001761234

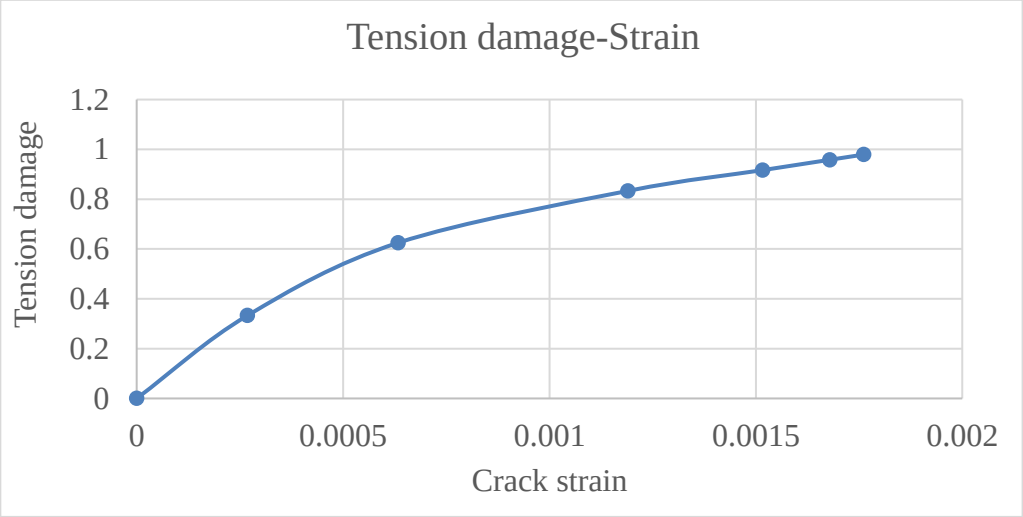

Figure A. 4: Concrete tension damage

A.2 Bamboo fiber tube

Table A. 10: Density and Elastic for bamboo fiber tube

Density(N/mm^3)			7.00E-10					
Elasticity (Orthotropic)								
young's Modulus (Mpa=N/mm^2)			poison's Ratio, V			Shear Modulus (Mpa=N/mm^2)		
E_1	E_2	E_3	V_{12}	V_{13}	V_{13}	G_{12}	G_{13}	G_{23}
8040	2010	2010	0.325	0.325	0.098	2580	2580	2540

Table A. 11: Hashin Damage for bamboo fiber tube

Longitudinal Tensile strength (N/mm^2)	Longitudinal Compressive strength (N/mm^2)	Transverse Tensile strength (N/mm^2)	Transverse Compressive strength (N/mm^2)	Longitudinal Shear strength (N/mm^2)	Transverse Shear strength (N/mm^2)
86.1	61.54	4.46	16.37	8.16	8.24

B. MODEL OF COLUMN UNDER STUDY

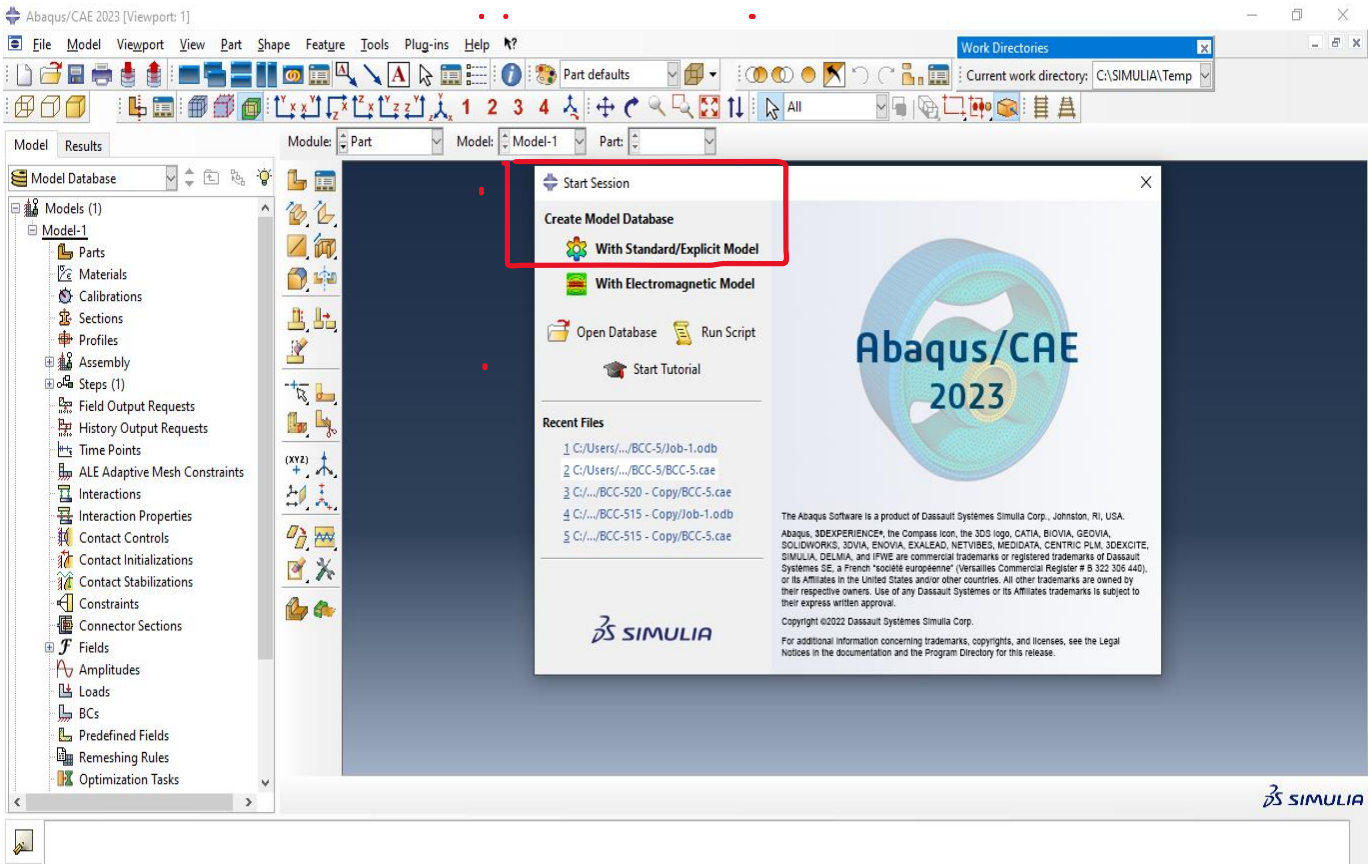

Figure B. 1: Start session and main window for AQUS /CAE 2023

Plain concrete

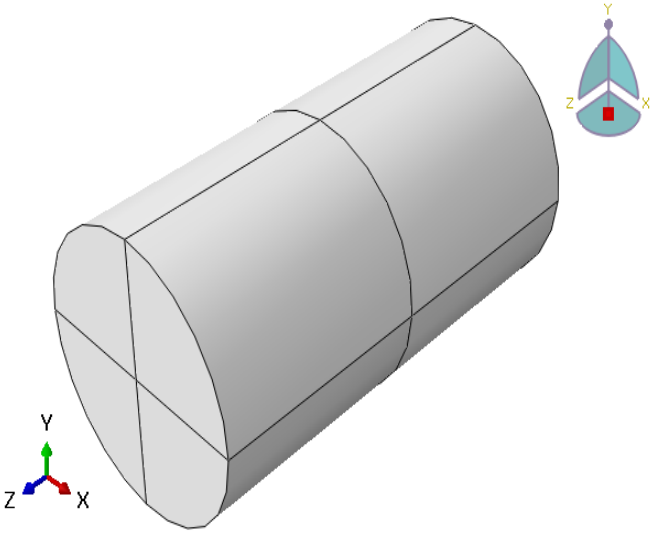

Bamboo fiber tube (t=5.8mm)

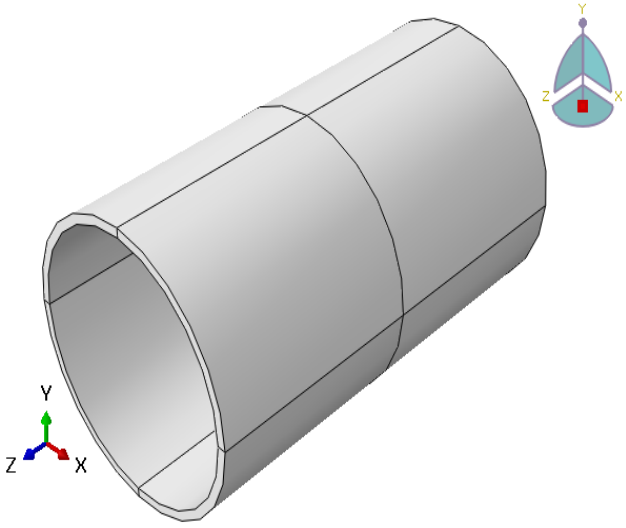

Bamboo fiber tube (t=9.5mm)

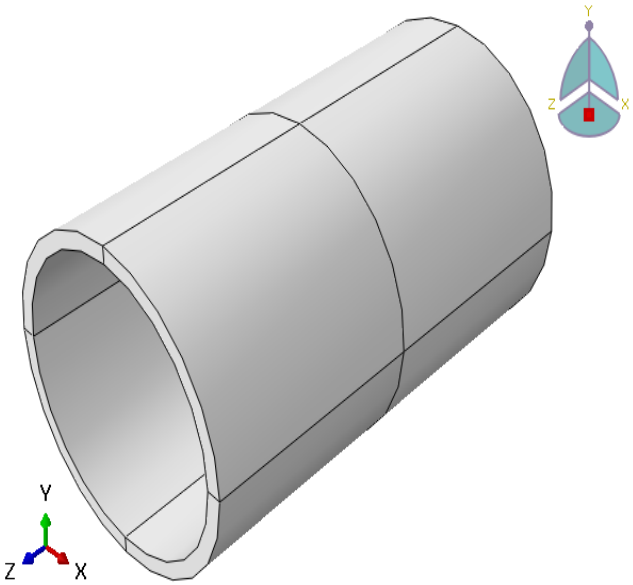

Bamboo fiber tube (t=12mm)

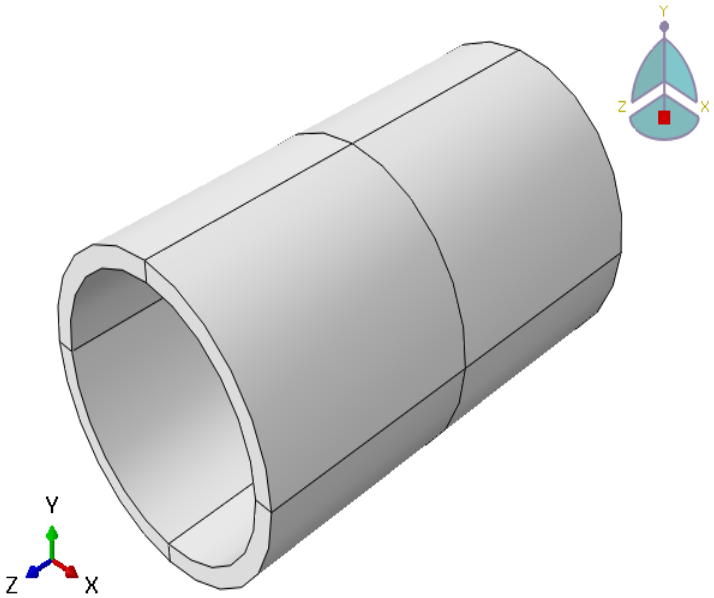

Support and Loading Steel Plate

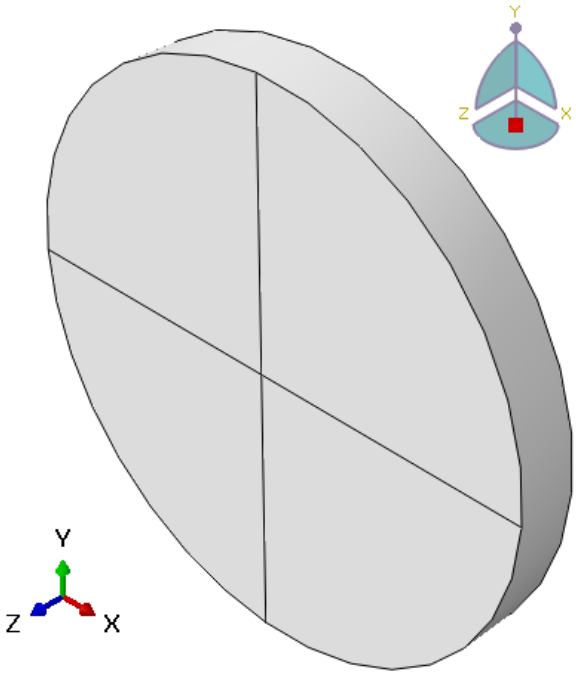

Assembly of plain concrete and BST-5(5.8mm)

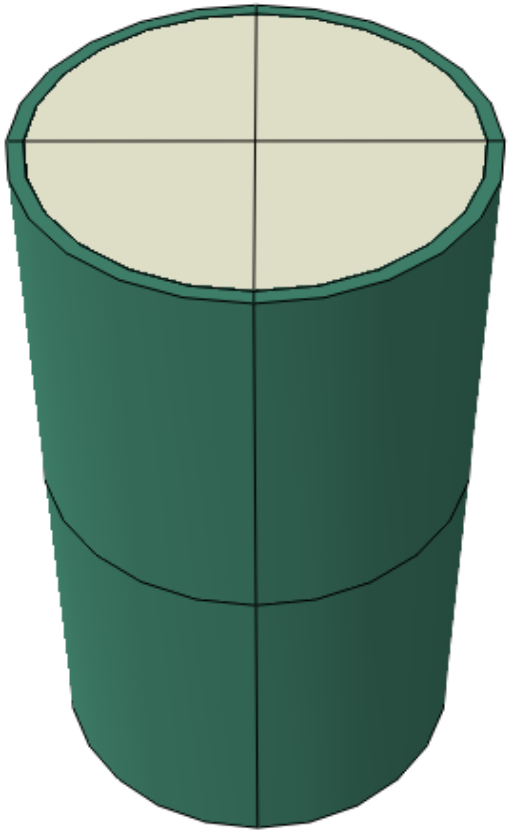

Assembly of plain concrete and BST-5 (9.5mm)

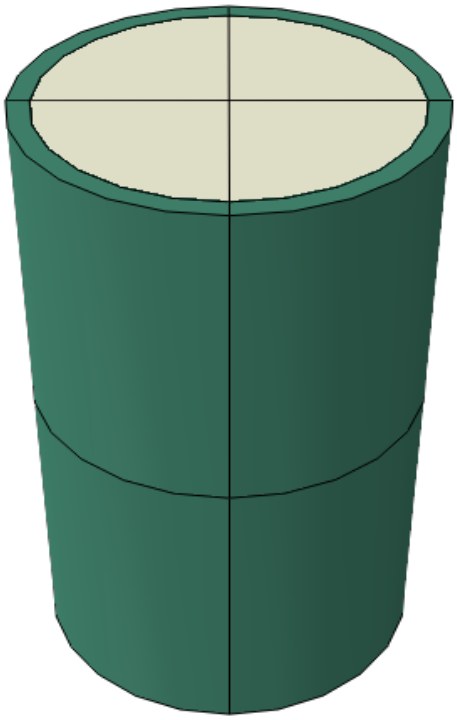

Assembly of plain concrete and BST-5 (12mm)

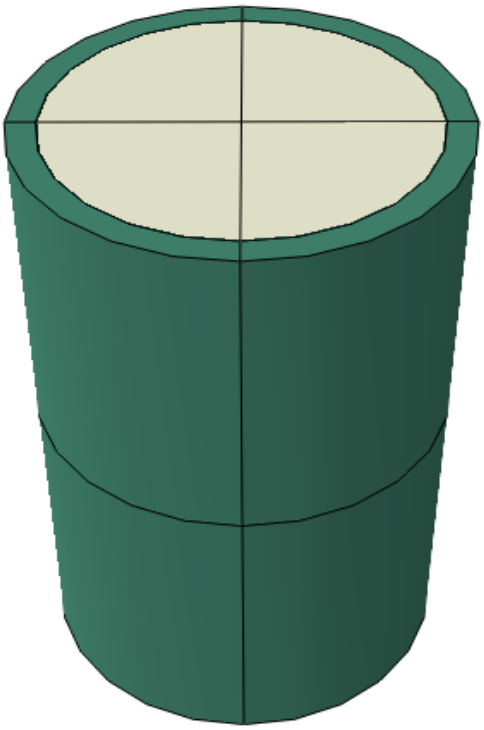

Composite material modeling in ABAQUS 2023 for BST-5 (5.8mm)

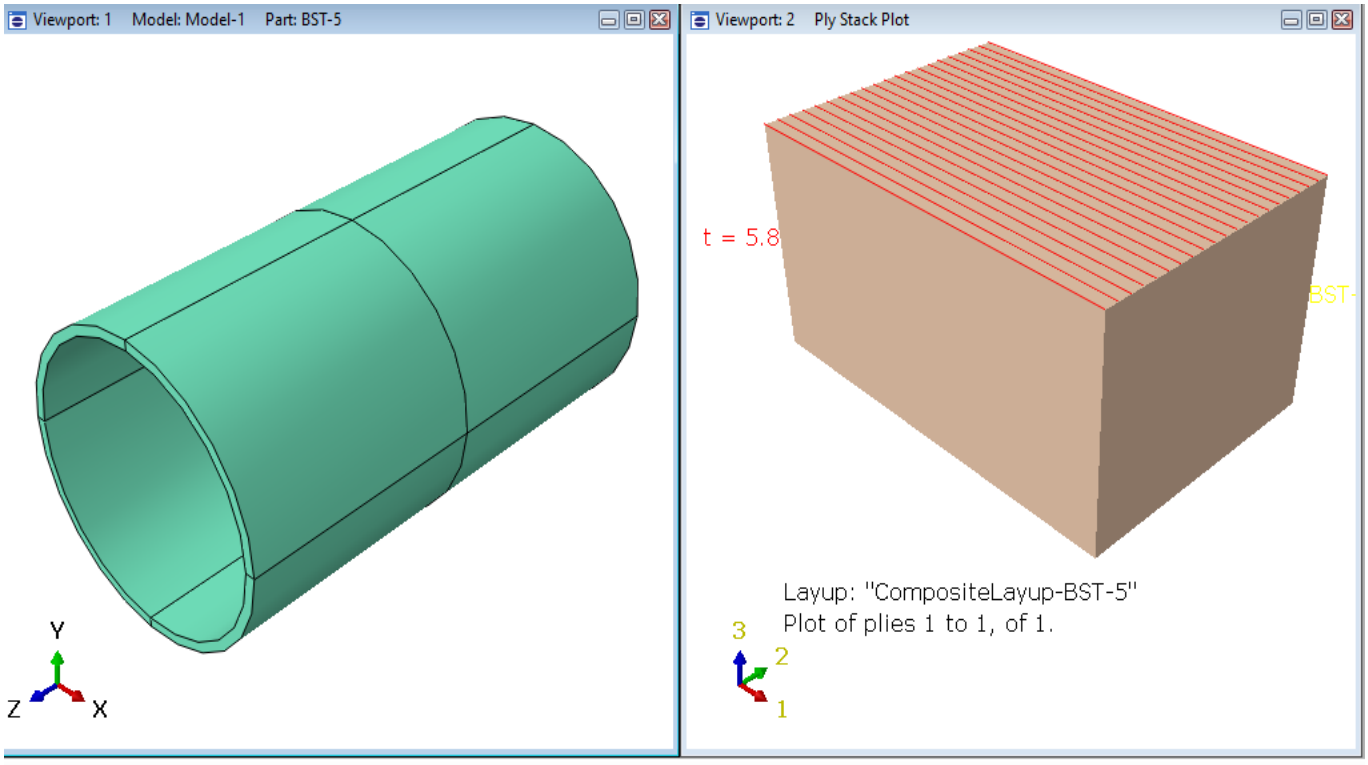

Composite material modeling in ABAQUS 2023 for BST-5 (9.5mm)

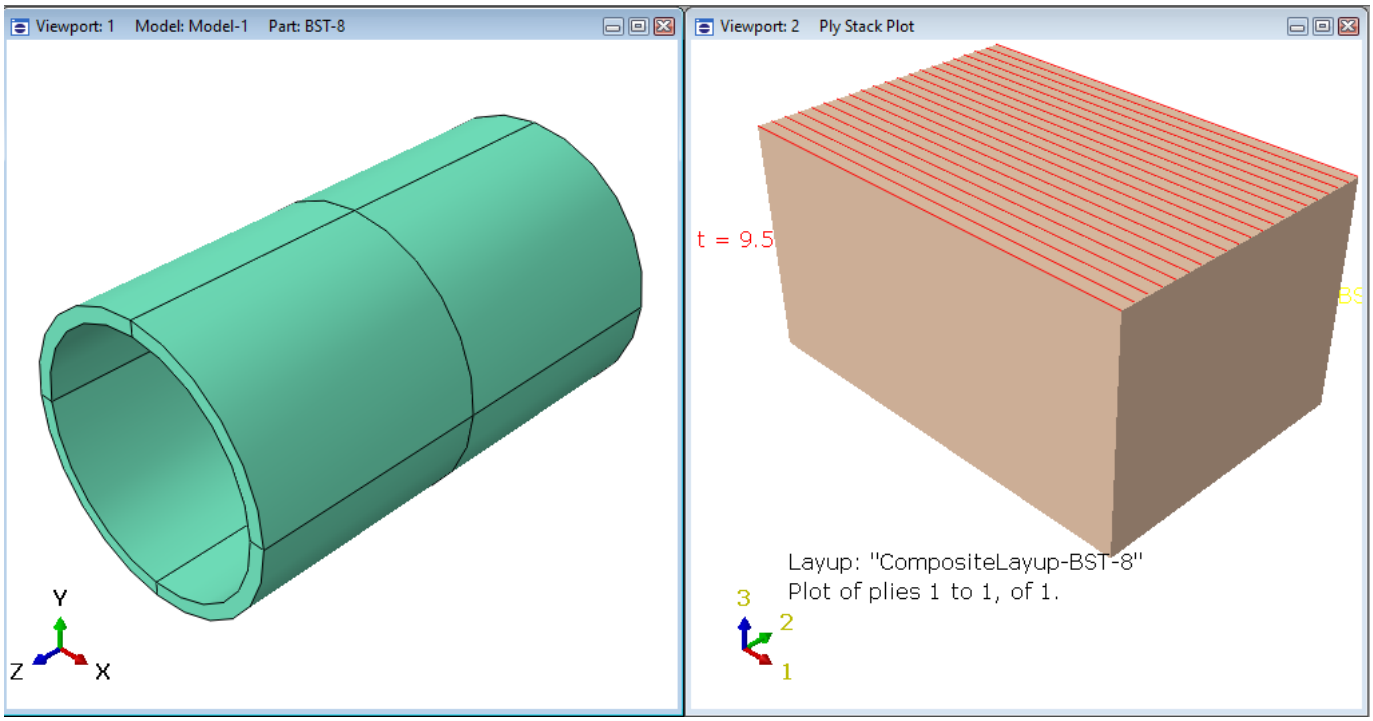

Composite material modeling in ABAQUS 2023 for BST-5 (12mm)

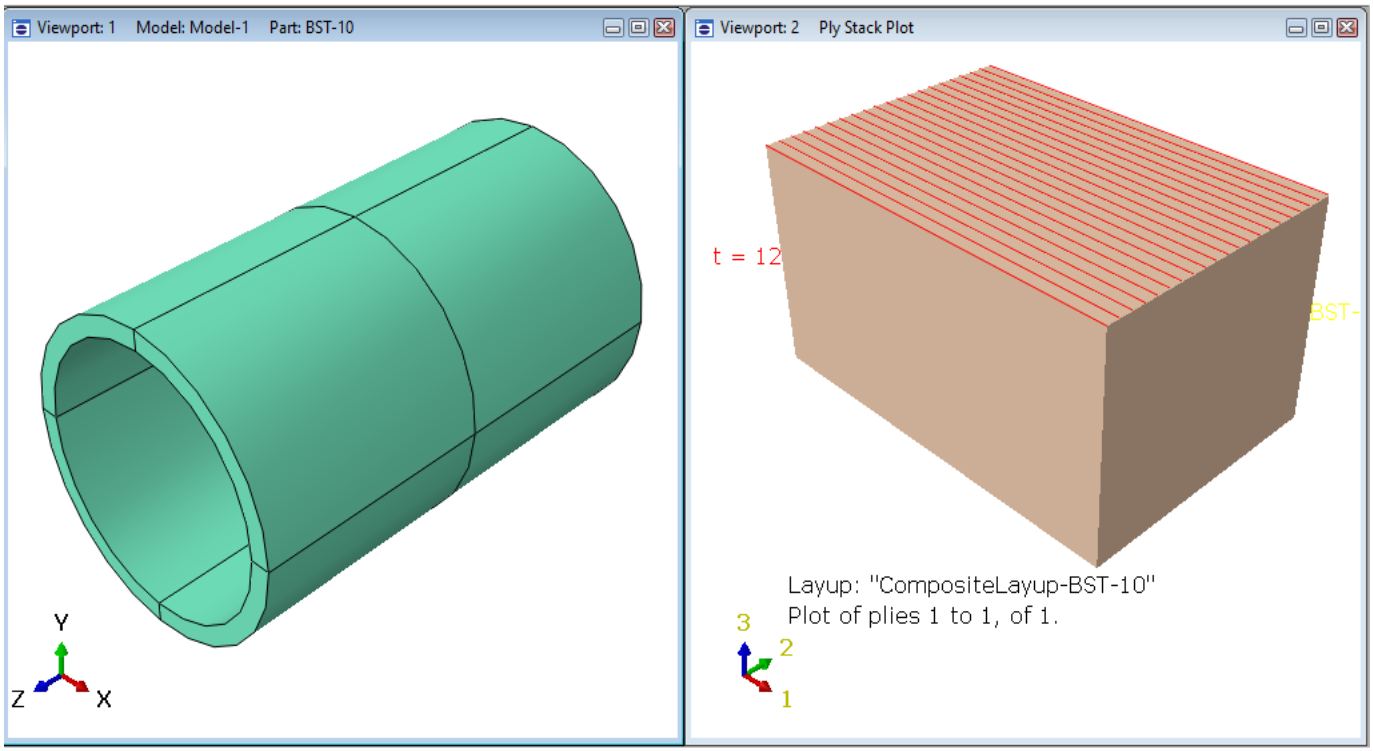

End boundary conditions (fixed support) at the bottom columns.

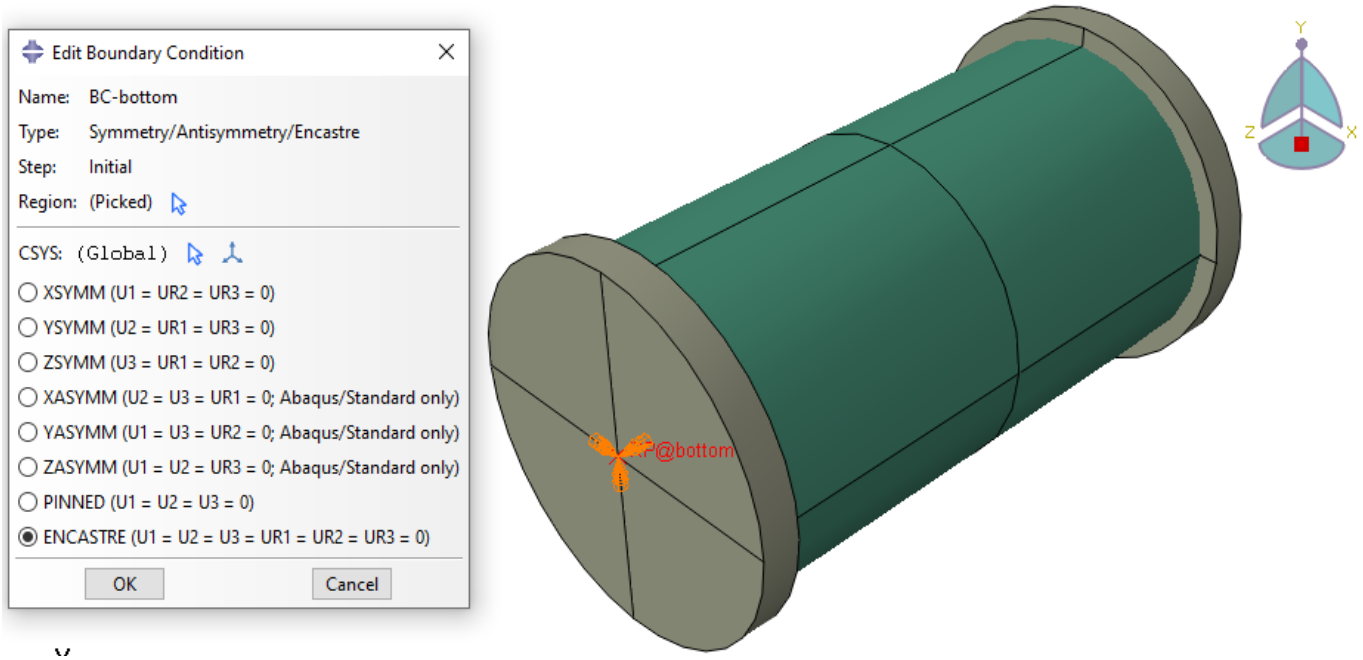

concentric and eccentric loading at the top columns (e=0, e=10mm and e=20mm).

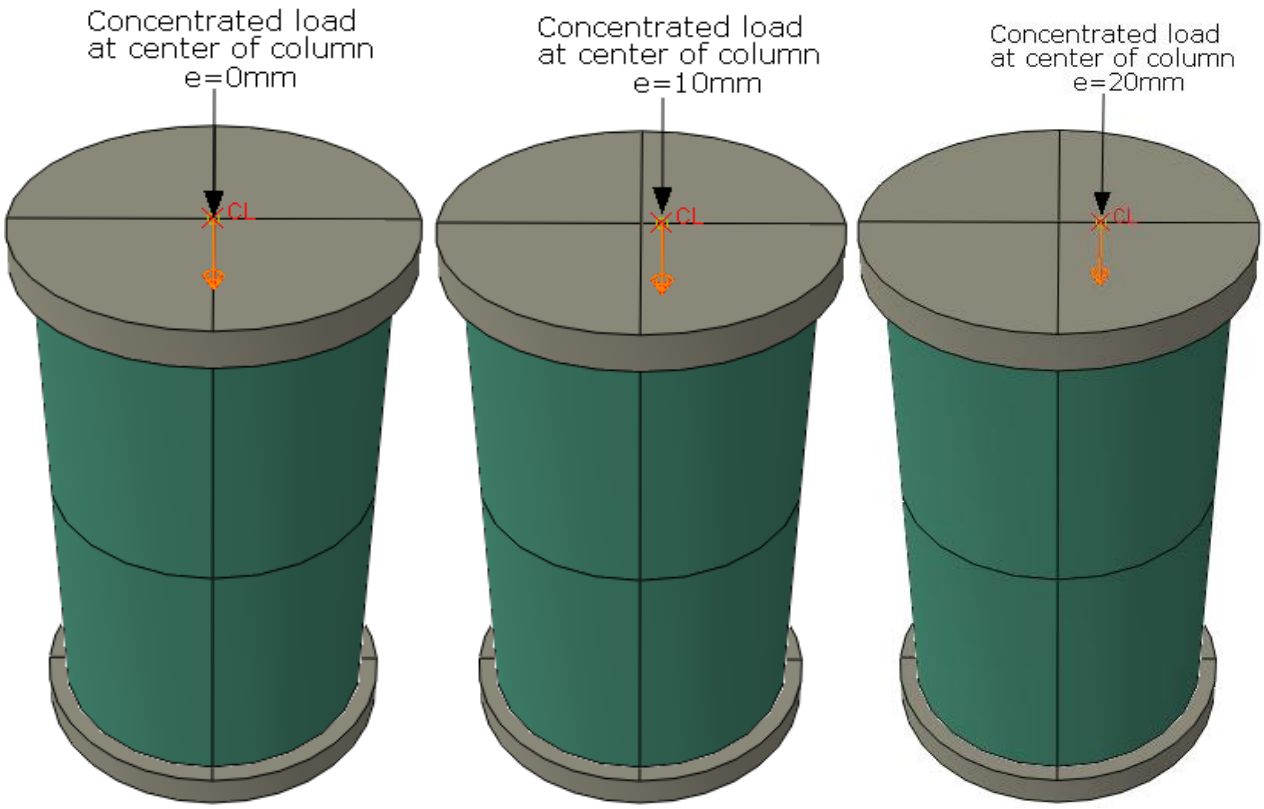

Bamboo fiber tube(5.8mm) plain concrete composite column (BCC-5)

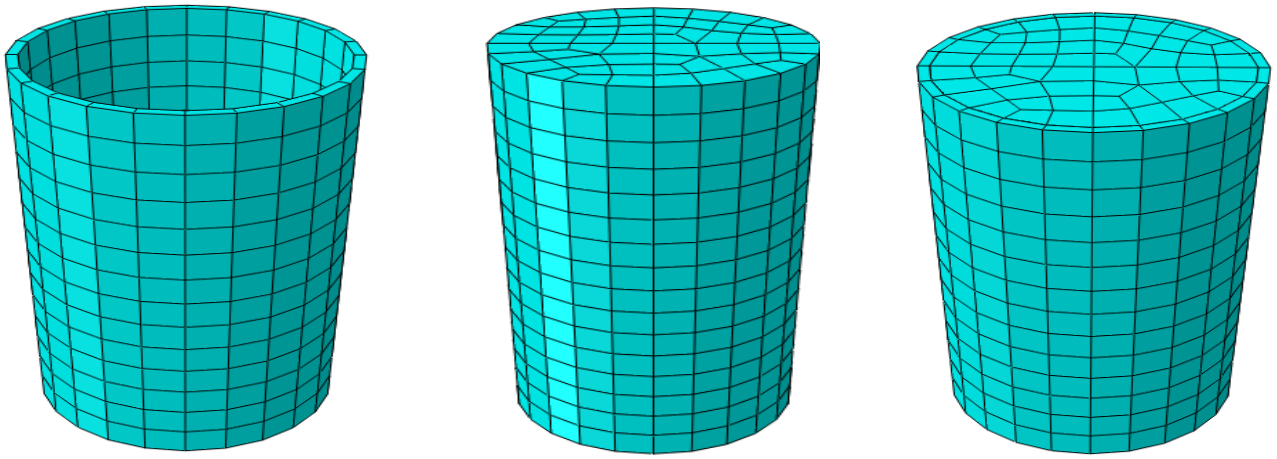

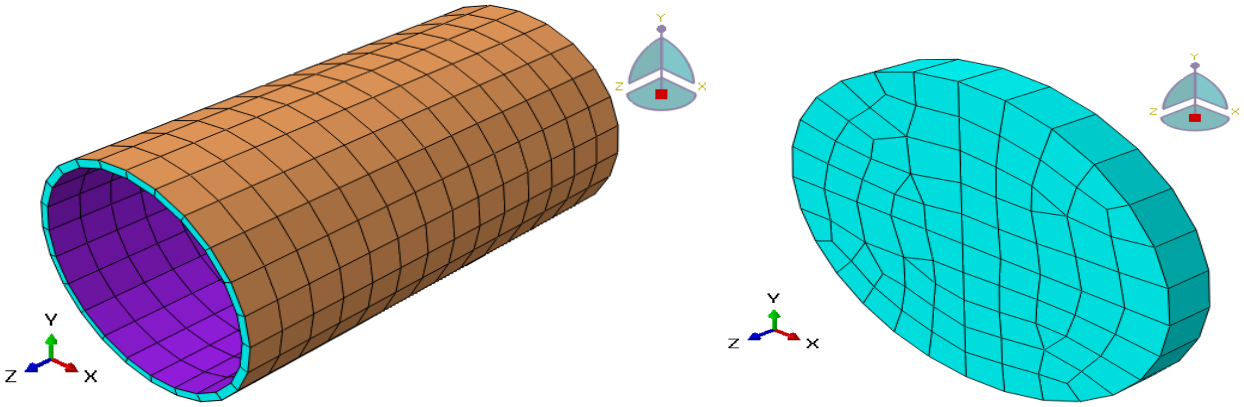

Assign stack direction for bamboo fiber tube Meshing Loading plate

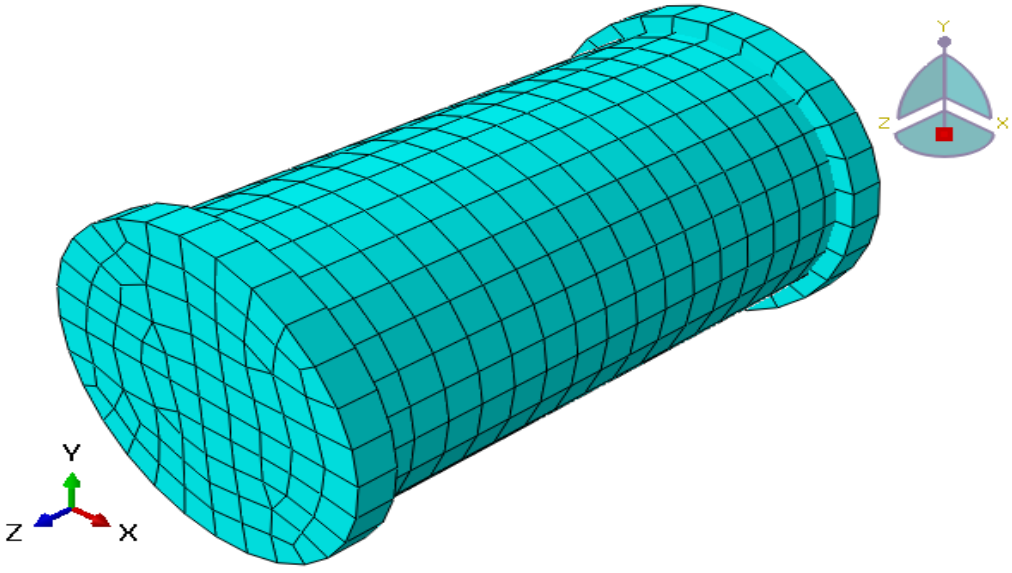

Meshing of Bamboo fiber tube concrete-filled composite column

Figure B.2: Finite element modeling column under study from geometry up to meshing.

C. OUT PUT OF ANALYSIS

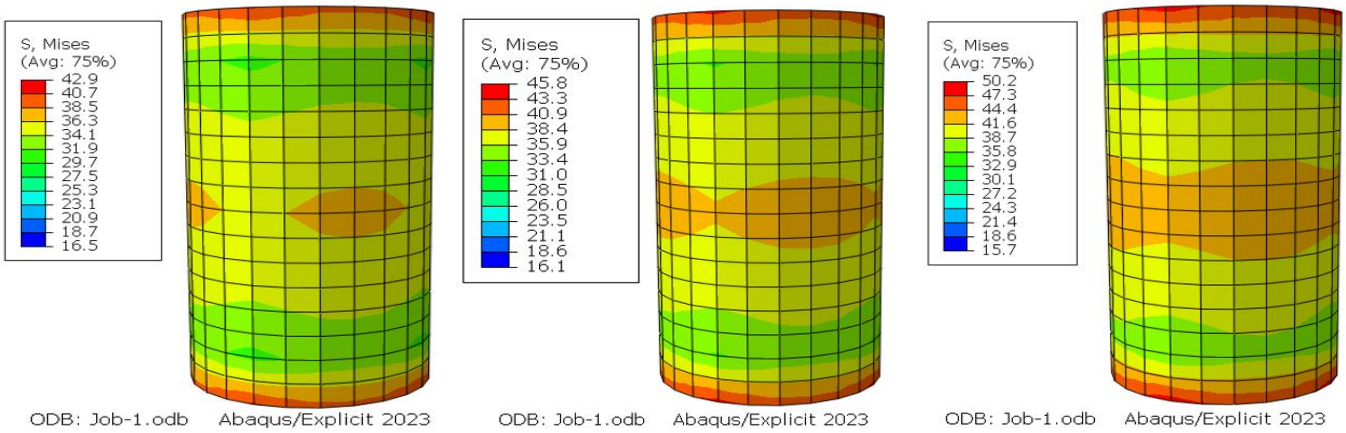

Core concrete of BCC-5 Core concrete of BCC-8 Core concrete of BCC-10

Axial stress contour compression failure of core concrete for BCC-5, BCC-8, BCC-10

a) Eccentricity

Concentric loading (e=0) Eccentric loading (e=5mm) Eccentric loading (e=10mm)

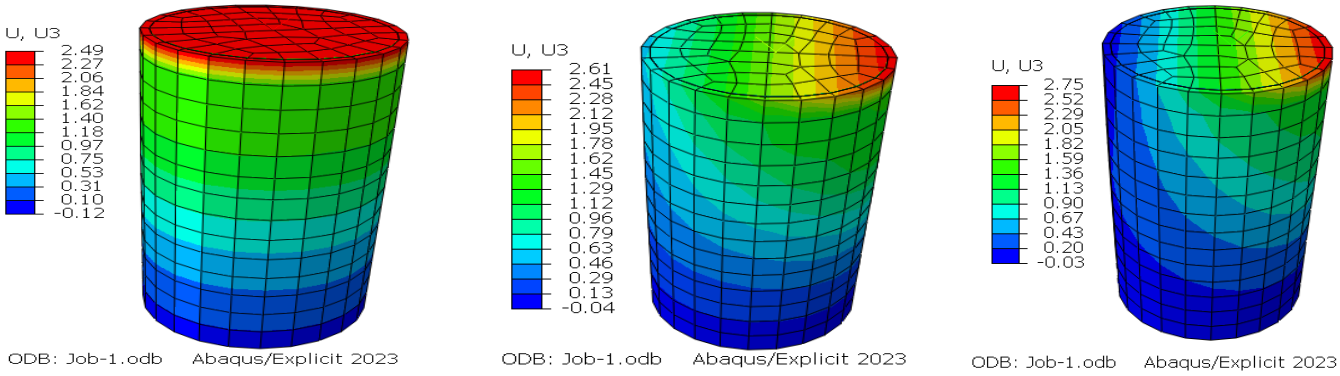

Axial displacement contour with varying eccentricity at failure for BCC-5

Concentric loading (e=0) Eccentric loading (e=5mm) Eccentric loading (e=10mm)

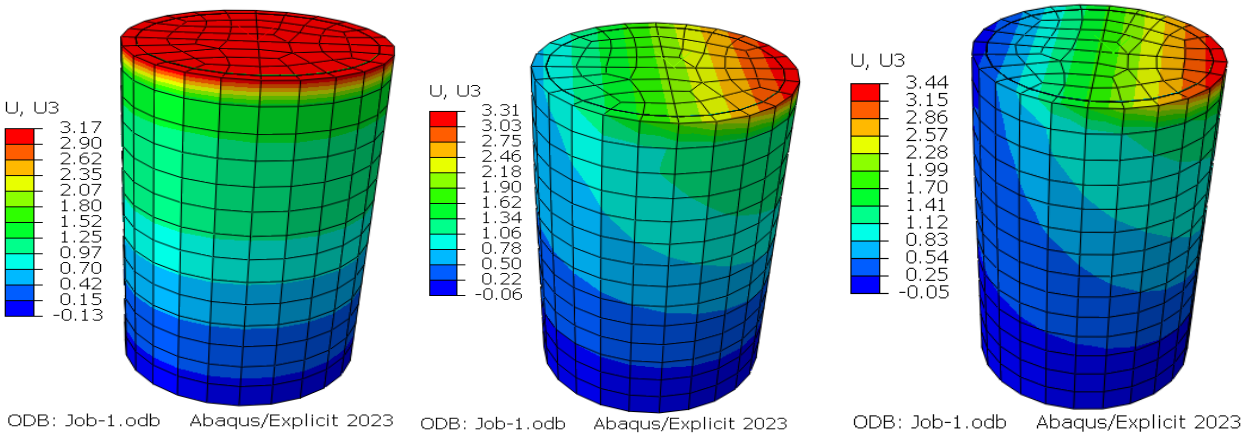

Eccentric loading (e=15)

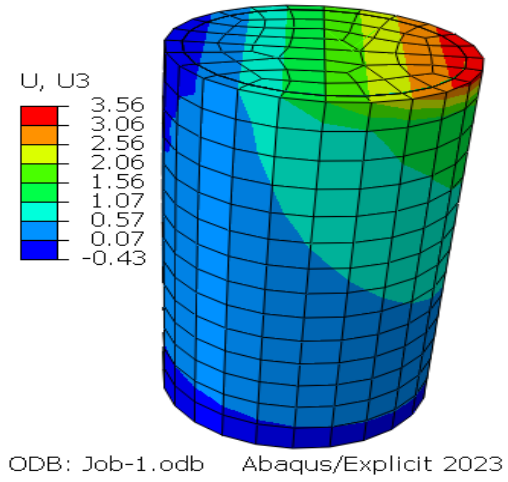

Eccentric loading (e=20mm)

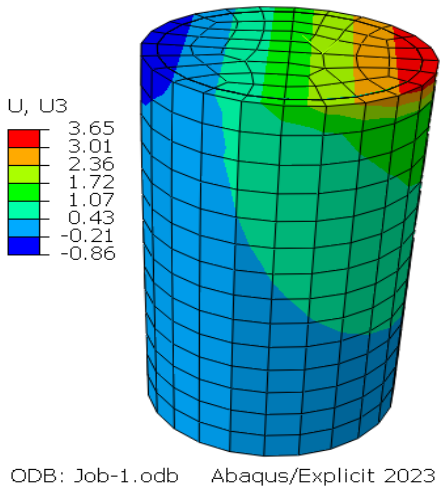

Axial displacement contour with varying eccentricity at failure for BCC-8

Concentric loading (e=0)

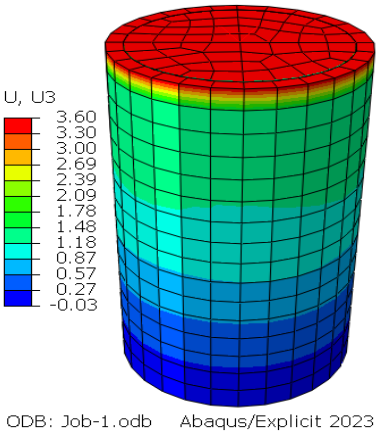

Eccentric loading (e=5mm)

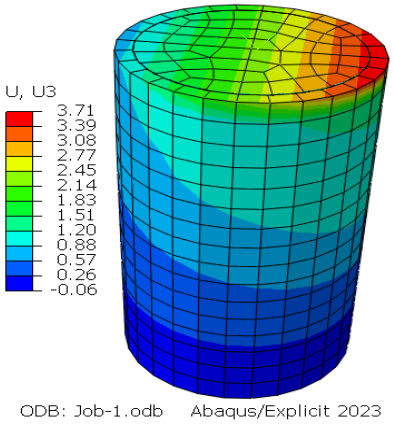

Eccentric loading (e=10mm)

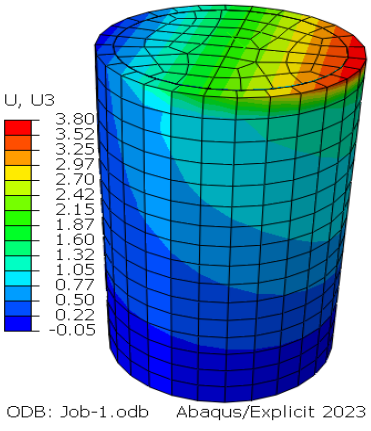

Eccentric loading (e=15)

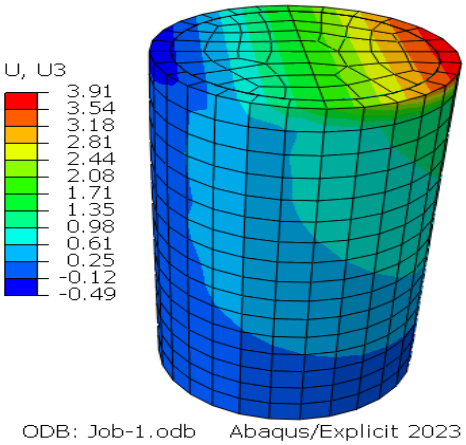

Eccentric loading (e=20mm)

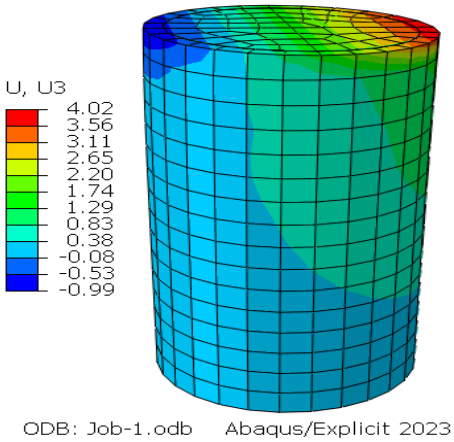

Axial displacement contour with varying eccentricity at failure for BCC-10

D. ANALIYSIS OUT PUT FROM ABAQUS PROGRAM (SAMPLE)

```
Abaqus 2023                                    Date 22-Jan-2024   Time 21:58:12
For use by WhiteDeath under license from Dassault Systemes or its subsidiary.


                    The Abaqus Software is a product of:

                      Dassault Systemes SIMULIA Corp.
                      1301 Atwood Avenue, Suite 101W
                         Johnston, RI 02919, USA


                The Abaqus Software is available only under license
                from Dassault Systemes or its subsidiary and may be
                used or reproduced only in accordance with the terms
                of such license.

                       On machine MULETA
                       you are authorized to run
                       Abaqus/Explicit until 31-Dec-2055

                       Your site id is:


                 For assistance or any other information you may
                 obtain contact information for your local office
                 from the world wide web at:

                   http://www.3ds.com/products/simulia/locations/

          * * * * * * * * * * * * * * * * * * * * * * * * * * * * * * * * *
          *                                                               *
          *                    ******************                         *
          *                    *  N O T I C E  *                         *
          *                    ******************                         *
          *                                                               *
          *                                                               *
          *                        Abaqus 2023                            *
          *                                                               *
          *           BUILD ID: 2022_09_28-21.11.55 183150                *
          *                                                               *
          *                                                               *
          *  Please make sure you are using                               *
          *  release Abaqus 2023 manuals                                  *
          *  plus the notes accompanying this release.                    *
          *                                                               *
          *                                                               *
          *                                                               *
          *                                                               *
          * * * * * * * * * * * * * * * * * * * * * * * * * * * * * * * * *


  PROCESSING PART, INSTANCE, AND ASSEMBLY INFORMATION
*************************************************************

  END PROCESSING PART, INSTANCE, AND ASSEMBLY INFORMATION
*************************************************************


  OPTIONS BEING PROCESSED
****************************
```

```
*Heading
*Node
*Element, type=SC8R
*Nset, nset=ASSEMBLY_BST-5-1__PICKEDSET7
*Elset, elset=ASSEMBLY_BST-5-1_COMPOSITE-BST-5-1
*Elset, elset=ASSEMBLY_BST-5-1__PICKEDSET7
*Elset, elset=ASSEMBLY_BST-5-1___PICKEDSURF6_S2
*distribution, name=ASSEMBLY_BST-5-1_ORI-1-DISCORIENT, location=ELEMENT, table=ORI-1-DISCORIENT_TABLE
*Node
*Element, type=C3D8R
*Nset, nset="ASSEMBLY_C-32,7-1__PICKEDSET5"
*Elset, elset="ASSEMBLY_C-32,7-1__PICKEDSET5"
*Node
*Nset, nset=ASSEMBLY__PICKEDSET10
*Nset, nset=ASSEMBLY__PICKEDSET11
*Nset, nset=ASSEMBLY__PICKEDSET14
*Nset, nset=ASSEMBLY__PICKEDSET15
*Nset, nset=ASSEMBLY__PICKEDSET16
*Nset, nset=ASSEMBLY__PICKEDSET8
*Nset, nset=ASSEMBLY__PICKEDSET9
*Elset, elset=ASSEMBLY__PICKEDSET11
*Elset, elset=ASSEMBLY__PICKEDSET9
*material, name=BST
*damageinitiation, criterion=HASHIN
*damageevolution, type=ENERGY
*density
*elastic, type=ENGINEERINGCONSTANTS
*material, name="C-32,7"
*density
*elastic
*concretedamagedplasticity
*concretecompressionhardening
*concretetensionstiffening
*concretecompressiondamage
*concretetensiondamage
*concretefailure, type=STRAIN
*orientation, name=ASSEMBLY_BST-5-1_ORI-1, system=RECTANGULAR
*solidsection, elset="ASSEMBLY_C-32,7-1__PICKEDSET5", controls=EC-1, material="C-32,7"
*shellsection, elset=ASSEMBLY_BST-5-1_COMPOSITE-BST-5-1, layup=COMPOSITE-BST-5, composite, orientation=ASSEMBLY_BST-5-1
*sectioncontrols, name=EC-1, elementdeletion=YES
*solidsection, elset="ASSEMBLY_C-32,7-1__PICKEDSET5", controls=EC-1, material="C-32,7"
*shellsection, elset=ASSEMBLY_BST-5-1_COMPOSITE-BST-5-1, layup=COMPOSITE-BST-5, composite, orientation=ASSEMBLY_BST-5-1
*rigidbody, refnode=ASSEMBLY__PICKEDSET8, tienset=ASSEMBLY__PICKEDSET9
*rigidbody, refnode=ASSEMBLY__PICKEDSET10, tienset=ASSEMBLY__PICKEDSET11
*rigidbody, refnode=ASSEMBLY__PICKEDSET8, tienset=ASSEMBLY__PICKEDSET9
*rigidbody, refnode=ASSEMBLY__PICKEDSET10, tienset=ASSEMBLY__PICKEDSET11
*rigidbody, refnode=ASSEMBLY__PICKEDSET8, tienset=ASSEMBLY__PICKEDSET9
*rigidbody, refnode=ASSEMBLY__PICKEDSET10, tienset=ASSEMBLY__PICKEDSET11
*rigidbody, refnode=ASSEMBLY__PICKEDSET8, tienset=ASSEMBLY__PICKEDSET9
*rigidbody, refnode=ASSEMBLY__PICKEDSET10, tienset=ASSEMBLY__PICKEDSET11
*surface, type=ELEMENT, name=ASSEMBLY_BST-5-1__PICKEDSURF6
*surface, type=ELEMENT, name=ASSEMBLY_BST-5-1__PICKEDSURF6
*rigidbody, refnode=ASSEMBLY__PICKEDSET8, tienset=ASSEMBLY__PICKEDSET9
*rigidbody, refnode=ASSEMBLY__PICKEDSET10, tienset=ASSEMBLY__PICKEDSET11
*surfaceinteraction, name=INTPROP-1
*friction
*rigidbody, refnode=ASSEMBLY__PICKEDSET8, tienset=ASSEMBLY__PICKEDSET9
*rigidbody, refnode=ASSEMBLY__PICKEDSET10, tienset=ASSEMBLY__PICKEDSET11
*rigidbody, refnode=ASSEMBLY__PICKEDSET8, tienset=ASSEMBLY__PICKEDSET9
*rigidbody, refnode=ASSEMBLY__PICKEDSET10, tienset=ASSEMBLY__PICKEDSET11
*boundary
*boundary
*solidsection, elset="ASSEMBLY_C-32,7-1__PICKEDSET5", controls=EC-1, material="C-32,7"
*rigidbody, refnode=ASSEMBLY__PICKEDSET8, tienset=ASSEMBLY__PICKEDSET9
*rigidbody, refnode=ASSEMBLY__PICKEDSET10, tienset=ASSEMBLY__PICKEDSET11
*friction
*elementoutput, directions=YES
*output, field, timeinterval=0.01
*output, history, variable=PRESELECT
*Step, name=Step-1, nlgeom=YES
*Step, name=Step-1, nlgeom=YES
*dynamic, explicit
*output, field, timeinterval=0.01
*elementoutput, directions=YES
*output, history, variable=PRESELECT
*endstep
```

```
*surface, type=ELEMENT, name=ASSEMBLY_BST-5-1__PICKEDSURF6
*surfaceinteraction, name=INTPROP-1
*friction
*surfacebehavior, pressure-overclosure=HARD
*boundary
*boundary
*Step, name=Step-1, nlgeom=YES
*dynamic, explicit
*cload, amplitude=AMP-1
*contact, op=NEW
*contactinclusions, allexterior
*contactpropertyassignment
*endstep
```

P R O B L E M S I Z E

```
NUMBER OF ELEMENTS IS                                          1392
NUMBER OF NODES IS                                             2161
NUMBER OF NODES DEFINED BY THE USER                            2161
TOTAL NUMBER OF VARIABLES IN THE MODEL                         6489
(DEGREES OF FREEDOM PLUS MAX NO. OF ANY LAGRANGE MULTIPLIER
 VARIABLES. INCLUDE *PRINT,SOLVE=YES TO GET THE ACTUAL NUMBER.)
```

END OF USER INPUT PROCESSING

```
JOB TIME SUMMARY
  USER TIME (SEC)      =      0.20
  SYSTEM TIME (SEC)    =       0.0
  TOTAL CPU TIME (SEC) =      0.20
  WALLCLOCK TIME (SEC) =             1
```

```
Abaqus 2023                                    Date 22-Jan-2024   Time 21:58:12
For use by WhiteDeath under license from Dassault Systemes or its subsidiary.
```

DOMAIN DECOMPOSITION INFORMATION

DOMAIN 1 HAS 696 ELEMENTS AND 1144 NODES with WEIGHT 50.018

DOMAIN 2 HAS 696 ELEMENTS AND 1144 NODES with WEIGHT 49.982

MODEL INFORMATION (IN GLOBAL X-Y COORDINATES)

Total mass in model = 1.45772E-02
Center of mass of model = (-2.524260E-03, 2.520289E-03, 1.500000E+02)

Moments of Inertia :

	About Center of Mass	About Origin
I(XX)	1.345873E+02	4.625734E+02
I(YY)	1.345875E+02	4.625735E+02
I(ZZ)	4.880915E+01	4.880915E+01
I(XY)	-2.979430E-03	-2.979337E-03
I(YZ)	-6.283370E-06	-5.517082E-03
I(ZX)	1.188525E-04	5.638333E-03

STABLE TIME INCREMENT INFORMATION

The stable time increment estimate for each element is based on
linearization about the initial state.

```
 Initial time increment = 1.32173E-06

 Statistics for all elements:
    Mean = 2.59774E-06
    Standard deviation = 9.13990E-07

 Most critical elements:
  Element number   Rank    Time increment   Increment ratio
  (Instance name)
 ---------------------------------------------------------
       106          1       1.321726E-06      1.000000E+00
  BST-5-1
       113          2       1.321726E-06      1.000000E+00
  BST-5-1
       120          3       1.321726E-06      1.000000E+00
  BST-5-1
       127          4       1.321726E-06      1.000000E+00
  BST-5-1
       378          5       1.321726E-06      1.000000E+00
  BST-5-1
       385          6       1.321726E-06      1.000000E+00
  BST-5-1
       392          7       1.321726E-06      1.000000E+00
  BST-5-1
       399          8       1.321726E-06      1.000000E+00
  BST-5-1
       406          9       1.321726E-06      1.000000E+00
  BST-5-1
       413         10       1.321726E-06      1.000000E+00
  BST-5-1


 Instance name for the most critical element will be printed if the critical
 element changes or at the beginning of a new page.


-------------------------------------------------------------------------------

 INFORMATION REGARDING INITIAL CONTACT OVERCLOSURES FOR NEWLY DEFINED GENERAL
 CONTACT INTERACTIONS IN STEP 1

-------------------------------------------------------------------------------

  Abaqus/Explicit will attempt to resolve 480 initial node-face overclosure(s).


  Maximum initial overclosure for node-face contact is 0.48145 at node 625 of
  instance C-32,7-1 and face S1 of element 373 of instance BST-5-1.


  No initial edge-edge overclosures found.


  Maximum initial contact adjustment is: 0.49674 at node 433 of instance
  C-32,7-1.


  30 node-face overclosure(s) left unresolved and will be stored as offsets.
  To help identify the nodes involved in the overclosures a node set
  InfoNodeUnresolvInitOver has been created. Check the message file for more
  detailed information.


  Maximum unresolved overclosure is 0.40229 at node 89 of instance C-32,7-1
  and face S1 of element 53 of instance BST-5-1.


  No edge-edge overclosures left unresolved.


  More detailed information on initial overclosures can be found in the
  message (.msg) file.
```

```
Abaqus 2023                                                Date 22-Jan-2024   Time 21:58:12
For use by WhiteDeath under license from Dassault Systemes or its subsidiary.

The model has been decomposed into 2 domains.
Domain level parallelization will be used with 2 processors.

--------------------------------------------------------------------------------
 SOLUTION PROGRESS
--------------------------------------------------------------------------------

 STEP 1  ORIGIN 0.0000

  Total memory used for step 1 is approximately 14.6 megabytes.
  Element by element stable time estimation algorithm will be used.
  Scaling factor:  1.0000
             STEP      TOTAL      WALL      STABLE    CRITICAL    KINETIC      TOTAL
INCREMENT     TIME       TIME      TIME   INCREMENT     ELEMENT     ENERGY     ENERGY
        0  0.000E+00 0.000E+00  00:00:00 1.260E-06         406  0.000E+00  0.000E+00
INSTANCE WITH CRITICAL ELEMENT: BST-5-1
Output Field Frame Number   0, with time interval 1.000E-02, at step time 0.000E+00 of 1.000E+00
     7936  1.000E-02 1.000E-02  00:00:18 1.260E-06         156  1.425E-03  1.519E-01
INSTANCE WITH CRITICAL ELEMENT: BST-5-1
Output Field Frame Number   1, with time interval 1.000E-02, at step time 1.000E-02 of 1.000E+00
    15871  2.000E-02 2.000E-02  00:00:38 1.260E-06         212  7.224E-04  6.068E-01
INSTANCE WITH CRITICAL ELEMENT: BST-5-1
Output Field Frame Number   2, with time interval 1.000E-02, at step time 2.000E-02 of 1.000E+00
    23806  3.000E-02 3.000E-02  00:00:57 1.260E-06         156  8.530E-04  1.369E+00
INSTANCE WITH CRITICAL ELEMENT: BST-5-1
Output Field Frame Number   3, with time interval 1.000E-02, at step time 3.000E-02 of 1.000E+00
    31741  4.000E-02 4.000E-02  00:01:27 1.260E-06         317  7.019E-04  2.430E+00
INSTANCE WITH CRITICAL ELEMENT: BST-5-1
Output Field Frame Number   4, with time interval 1.000E-02, at step time 4.000E-02 of 1.000E+00
    39676  5.000E-02 5.000E-02  00:01:50 1.260E-06         157  5.106E-04  3.798E+00
INSTANCE WITH CRITICAL ELEMENT: BST-5-1
Output Field Frame Number   5, with time interval 1.000E-02, at step time 5.000E-02 of 1.000E+00
    47610  6.000E-02 6.000E-02  00:02:13 1.260E-06         317  9.524E-04  5.467E+00
INSTANCE WITH CRITICAL ELEMENT: BST-5-1
Output Field Frame Number   6, with time interval 1.000E-02, at step time 6.000E-02 of 1.000E+00
    55545  7.000E-02 7.000E-02  00:02:32 1.260E-06         317  6.015E-04  7.442E+00
INSTANCE WITH CRITICAL ELEMENT: BST-5-1
Output Field Frame Number   7, with time interval 1.000E-02, at step time 7.000E-02 of 1.000E+00
    63480  8.000E-02 8.000E-02  00:02:55 1.260E-06         157  8.128E-04  9.721E+00
INSTANCE WITH CRITICAL ELEMENT: BST-5-1
Output Field Frame Number   8, with time interval 1.000E-02, at step time 8.000E-02 of 1.000E+00
    71414  9.000E-02 9.000E-02  00:03:14 1.260E-06         213  6.344E-04  1.230E+01
INSTANCE WITH CRITICAL ELEMENT: BST-5-1
Output Field Frame Number   9, with time interval 1.000E-02, at step time 9.000E-02 of 1.000E+00
    79349  1.000E-01 1.000E-01  00:03:38 1.260E-06         157  7.195E-04  1.519E+01
INSTANCE WITH CRITICAL ELEMENT: BST-5-1
Output Field Frame Number  10, with time interval 1.000E-02, at step time 1.000E-01 of 1.000E+00
    87284  1.100E-01 1.100E-01  00:04:01 1.260E-06         213  7.409E-04  1.838E+01
INSTANCE WITH CRITICAL ELEMENT: BST-5-1
Output Field Frame Number  11, with time interval 1.000E-02, at step time 1.100E-01 of 1.000E+00
    95218  1.200E-01 1.200E-01  00:04:21 1.260E-06         157  6.797E-04  2.187E+01
INSTANCE WITH CRITICAL ELEMENT: BST-5-1
Output Field Frame Number  12, with time interval 1.000E-02, at step time 1.200E-01 of 1.000E+00
   103153  1.300E-01 1.300E-01  00:04:42 1.260E-06         157  7.418E-04  2.566E+01
INSTANCE WITH CRITICAL ELEMENT: BST-5-1
Output Field Frame Number  13, with time interval 1.000E-02, at step time 1.300E-01 of 1.000E+00
   111087  1.400E-01 1.400E-01  00:05:05 1.260E-06         157  6.772E-04  2.976E+01
INSTANCE WITH CRITICAL ELEMENT: BST-5-1
Output Field Frame Number  14, with time interval 1.000E-02, at step time 1.400E-01 of 1.000E+00
   119021  1.500E-01 1.500E-01  00:05:26 1.260E-06         157  7.308E-04  3.417E+01
INSTANCE WITH CRITICAL ELEMENT: BST-5-1
Output Field Frame Number  15, with time interval 1.000E-02, at step time 1.500E-01 of 1.000E+00
   126955  1.600E-01 1.600E-01  00:05:46 1.260E-06         157  7.025E-04  3.887E+01
INSTANCE WITH CRITICAL ELEMENT: BST-5-1
Output Field Frame Number  16, with time interval 1.000E-02, at step time 1.600E-01 of 1.000E+00
   134890  1.700E-01 1.700E-01  00:06:08 1.260E-06         157  7.086E-04  4.388E+01
INSTANCE WITH CRITICAL ELEMENT: BST-5-1
Output Field Frame Number  17, with time interval 1.000E-02, at step time 1.700E-01 of 1.000E+00
   142824  1.800E-01 1.800E-01  00:06:28 1.260E-06         157  7.133E-04  4.920E+01
INSTANCE WITH CRITICAL ELEMENT: BST-5-1
Output Field Frame Number  18, with time interval 1.000E-02, at step time 1.800E-01 of 1.000E+00
   150758  1.900E-01 1.900E-01  00:06:51 1.260E-06         157  7.017E-04  5.482E+01
INSTANCE WITH CRITICAL ELEMENT: BST-5-1
Output Field Frame Number  19, with time interval 1.000E-02, at step time 1.900E-01 of 1.000E+00
   158692  2.000E-01 2.000E-01  00:07:12 1.260E-06         157  7.170E-04  6.074E+01
INSTANCE WITH CRITICAL ELEMENT: BST-5-1
Output Field Frame Number  20, with time interval 1.000E-02, at step time 2.000E-01 of 1.000E+00
   166626  2.100E-01 2.100E-01  00:07:32 1.260E-06         157  7.027E-04  6.696E+01
INSTANCE WITH CRITICAL ELEMENT: BST-5-1
Output Field Frame Number  21, with time interval 1.000E-02, at step time 2.100E-01 of 1.000E+00
   174560  2.200E-01 2.200E-01  00:07:51 1.260E-06         157  7.121E-04  7.349E+01
INSTANCE WITH CRITICAL ELEMENT: BST-5-1
Output Field Frame Number  22, with time interval 1.000E-02, at step time 2.200E-01 of 1.000E+00
```

```
 STEP 1  ORIGIN 0.0000

             STEP      TOTAL      WALL      STABLE    CRITICAL    KINETIC      TOTAL
INCREMENT     TIME       TIME      TIME   INCREMENT     ELEMENT     ENERGY     ENERGY
   815479  7.700E-01 7.700E-01  00:42:50 1.192E-06         181  5.795E+12  1.095E+06
INSTANCE WITH CRITICAL ELEMENT: BST-5-1
Output Field Frame Number  77, with time interval 1.000E-02, at step time 7.700E-01 of 1.000E+00
   823872  7.800E-01 7.800E-01  00:43:18 1.193E-06         181  7.097E+12  1.096E+06
INSTANCE WITH CRITICAL ELEMENT: BST-5-1
Output Field Frame Number  78, with time interval 1.000E-02, at step time 7.800E-01 of 1.000E+00
   832262  7.900E-01 7.900E-01  00:43:45 1.201E-06         181  8.550E+12  1.097E+06
INSTANCE WITH CRITICAL ELEMENT: BST-5-1
Output Field Frame Number  79, with time interval 1.000E-02, at step time 7.900E-01 of 1.000E+00
   840395  8.000E-01 8.000E-01  00:44:11 1.246E-06         180  1.016E+13  1.155E+06
INSTANCE WITH CRITICAL ELEMENT: BST-5-1
Output Field Frame Number  80, with time interval 1.000E-02, at step time 8.000E-01 of 1.000E+00
   848438  8.100E-01 8.100E-01  00:44:38 1.242E-06         180  1.193E+13  1.186E+06
INSTANCE WITH CRITICAL ELEMENT: BST-5-1
Output Field Frame Number  81, with time interval 1.000E-02, at step time 8.100E-01 of 1.000E+00
   856487  8.200E-01 8.200E-01  00:45:04 1.235E-06         188  1.387E+13  1.263E+06
INSTANCE WITH CRITICAL ELEMENT: BST-5-1
Output Field Frame Number  82, with time interval 1.000E-02, at step time 8.200E-01 of 1.000E+00
   864537  8.300E-01 8.300E-01  00:45:31 1.246E-06         202  1.598E+13  1.417E+06
INSTANCE WITH CRITICAL ELEMENT: BST-5-1
Output Field Frame Number  83, with time interval 1.000E-02, at step time 8.300E-01 of 1.000E+00
   872673  8.400E-01 8.400E-01  00:45:58 1.201E-06         187  1.827E+13  1.425E+06
INSTANCE WITH CRITICAL ELEMENT: BST-5-1
Output Field Frame Number  84, with time interval 1.000E-02, at step time 8.400E-01 of 1.000E+00
   880970  8.500E-01 8.500E-01  00:46:25 1.241E-06         187  2.074E+13  1.498E+06
INSTANCE WITH CRITICAL ELEMENT: BST-5-1
Output Field Frame Number  85, with time interval 1.000E-02, at step time 8.500E-01 of 1.000E+00
   889122  8.600E-01 8.600E-01  00:46:52 1.240E-06         194  2.340E+13  1.646E+06
INSTANCE WITH CRITICAL ELEMENT: BST-5-1
Output Field Frame Number  86, with time interval 1.000E-02, at step time 8.600E-01 of 1.000E+00
   897254  8.700E-01 8.700E-01  00:47:19 1.233E-06         193  2.625E+13  1.817E+06
INSTANCE WITH CRITICAL ELEMENT: BST-5-1
Output Field Frame Number  89, with time interval 1.000E-02, at step time 8.900E-01 of 1.000E+00
   921459  9.000E-01 9.000E-01  00:48:38 1.244E-06         183  3.604E+13  1.851E+06
INSTANCE WITH CRITICAL ELEMENT: BST-5-1
Output Field Frame Number  90, with time interval 1.000E-02, at step time 9.000E-01 of 1.000E+00
   929501  9.100E-01 9.100E-01  00:49:02 1.244E-06         183  3.973E+13  1.851E+06
INSTANCE WITH CRITICAL ELEMENT: BST-5-1
Output Field Frame Number  91, with time interval 1.000E-02, at step time 9.100E-01 of 1.000E+00
   937540  9.200E-01 9.200E-01  00:49:27 1.245E-06         183  4.365E+13  1.852E+06
INSTANCE WITH CRITICAL ELEMENT: BST-5-1
Output Field Frame Number  92, with time interval 1.000E-02, at step time 9.200E-01 of 1.000E+00
   945587  9.300E-01 9.300E-01  00:49:53 1.243E-06         183  4.779E+13  1.851E+06
INSTANCE WITH CRITICAL ELEMENT: BST-5-1
Output Field Frame Number  93, with time interval 1.000E-02, at step time 9.300E-01 of 1.000E+00
   953667  9.400E-01 9.400E-01  00:50:19 1.216E-06         183  5.217E+13  1.852E+06
INSTANCE WITH CRITICAL ELEMENT: BST-5-1
Output Field Frame Number  94, with time interval 1.000E-02, at step time 9.400E-01 of 1.000E+00
   961852  9.500E-01 9.500E-01  00:50:47 1.248E-06         213  5.679E+13  1.837E+06
INSTANCE WITH CRITICAL ELEMENT: BST-5-1
Output Field Frame Number  95, with time interval 1.000E-02, at step time 9.500E-01 of 1.000E+00
   969869  9.600E-01 9.600E-01  00:51:12 1.250E-06         318  6.166E+13  1.839E+06
INSTANCE WITH CRITICAL ELEMENT: BST-5-1
Output Field Frame Number  96, with time interval 1.000E-02, at step time 9.600E-01 of 1.000E+00
   977886  9.700E-01 9.700E-01  00:51:38 1.251E-06         318  6.678E+13  1.840E+06
INSTANCE WITH CRITICAL ELEMENT: BST-5-1
Output Field Frame Number  97, with time interval 1.000E-02, at step time 9.700E-01 of 1.000E+00
   985946  9.800E-01 9.800E-01  00:52:03 1.212E-06         183  7.216E+13  1.840E+06
INSTANCE WITH CRITICAL ELEMENT: BST-5-1
Output Field Frame Number  98, with time interval 1.000E-02, at step time 9.800E-01 of 1.000E+00
   994028  9.900E-01 9.900E-01  00:52:38 1.247E-06         183  7.782E+13  1.841E+06
INSTANCE WITH CRITICAL ELEMENT: BST-5-1
Output Field Frame Number  99, with time interval 1.000E-02, at step time 9.900E-01 of 1.000E+00
  1002118  1.000E+00 1.000E+00  00:53:07 1.240E-06         183  8.374E+13  1.841E+06
INSTANCE WITH CRITICAL ELEMENT: BST-5-1
Restart Number  1 at 1.0000
Output Field Frame Number 100, with time interval 1.000E-02, at step time 1.000E+00 of 1.000E+00

SUMMARY FOR STEP 1

 EXPLICIT EXECUTABLE TIME SUMMARY
      USER TIME (SEC)      =   2885.7
      SYSTEM TIME (SEC)    =   173.80
      WALLCLOCK TIME (SEC) =         3187
             INIT (SEC) =           0
             MAIN (SEC) =        3187

 THE ANALYSIS HAS COMPLETED SUCCESSFULLY
```